NONDESTRUCTIVE EVALUATION OF WOOD PROPERTIES BY STRESS WAVE SPECTRAL ANALYSIS

Stephen M. Shaler

Jozsef Bodig

Michael B. Histand

Structural Research Report No. 43
Civil Engineering Department
Colorado State University
Fort Collins, Colorado 80523

November 1982

NONDESTRUCTIVE EVALUATION OF WOOD PROPERTIES BY STRESS WAVE SPECTRAL ANALYSIS

Stephen M. Shaler

Jozsef Bodig

Michael B. Hlstand

Structural Research Report No. 43
Civil Engineering Department
Colorado State University
Fort Collins, Colorado 80523

November 1982

ABSTRACT OF THESIS

NONDESTRUCTIVE EVALUATION OF WOOD PROPERTIES BY
STRESS WAVE SPECTRAL ANALYSIS

The influence of selected properties on the propagation of stress waves in wood was investigated. Waveform analysis of the stress waves was performed using spectral analysis techniques developed for stationary random processes. Information analyzed from the stress waves included wave velocity, energy spectra, and the frequency response function. Three wood properties investigated as to their influence on stress waves propagation were grain angle, moisture content, and weight loss caused by decay.

Significant relationships between grain angle and the wave properties of velocity, amplitude gain, and total gain were obtained. Significant damping of the stress waves was observed at large grain angles and moisture content values above the fiber saturation point. No significant equations were found for consistent prediction of moisture content. The results of the decay study showed that as weight loss increased, the ratio of energy of the stress wave to that input to the specimen decreased for the perpendicular to grain case.

Two approaches toward prediction of wood strength were investigated. The first method employed prediction of wood properties from the stress wave spectral characteristics. Known relationships between these wood properties and strength were then utilized. The second approach involved direct correlation of the stress wave

spectral properties with strength. Significant correlations with strength were obtained using both approaches. Application of basic results are discussed as to their applicability toward development of an nondestructive evaluation (NDE) procedure for wood poles used in transmission line structures.

ACKNOWLEDGEMENTS

This report represents a portion of the work accomplished as part of RP-1352-2, "Reliability-Based Design of Transmission Line Structures", which is supported by the Electric Power Research Institute, Palo Alto, California, Mr. Phillip G. Landers, Project Manager.

TABLE OF CONTENTS

Chapter		Page
1	INTRODUCTION	1
2	REVIEW OF LITERATURE	4
	2.1 INTRODUCTION	4
	2.2 ECONOMIC IMPORTANCE OF NDE	4
	2.3 TRADITIONAL NDE APPROACHES	5
	2.3.1 NDE of Stiffness	6
	2.3.2 Relationship between Strength and Stiffness of Wood	9
	2.4 WOOD CHARACTERISTICS RELATED TO STRENGTH	10
	2.4.1 Effect of Decay on Wood Strength and Stiffness	13
	2.4.2 Pole Inspection Methods	16
3	THEORY OF PROPAGATION AND ANALYSIS OF STRESS WAVES	21
	3.1 WAVE PROPAGATION IN SOLIDS	21
	3.2 THEORY OF STRESS WAVE PROPAGATION	21
	3.3 WAVE PROPAGATION IN VISCO-ELASTIC MATERIALS	33
	3.4 WAVE PROPAGATION IN WOOD	36
	3.5 NATURE OF WAVEFORM DATA	39
	3.6 CHARACTERIZATION OF SYSTEM RESPONSE	42
	3.6.1 Time Domain Analysis	44
	3.6.2 Frequency Domain Analysis	48
	3.7 SYSTEM DYNAMICS	51
4	EXPERIMENTAL PROCEDURE	62
	4.1 EXPERIMENTAL DESIGN	62
	4.2 MATERIAL SELECTION	63
	4.3 SPECIMEN PREPARATION	63
	4.3.1 Moisture Conditioning	67
	4.3.2 Decaying of Specimens	69
	4.4 NONDESTRUCTIVE EVALUATION (NDE) PROCEDURE	71
	4.4.1 Instrumentating the Specimen	71
	4.4.2 Testing Frame	73
	4.4.3 Data Collection Procedure	78
	4.4.4 Analyzing Equipment	79
	4.4.5 Nondestructive Wave Parameters	84
	4.5 DESTRUCTIVE TESTING	84
5	DATA REDUCTION	87
	5.1 MEASUREMENT OF WAVEFORM PARAMETERS	87
	5.2 DESTRUCTIVE PARAMETERS	95

Chapter		Page
6	PREDICTION OF SELECTED WOOD PROPERTIES	98
	6.1 OVERVIEW	98
	6.2 PREDICTION OF GRAIN ANGLE	98
	6.3 PREDICTION OF MOISTURE CONTENT	107
	6.4 PREDICTION OF WEIGHT LOSS	113
	6.5 PREDICTION OF MOR AND MOE	116
	6.5.1 MOR and MOE with Constant Moisture Content	116
	6.5.2 MOR and MOE with Constant Grain Angle	117
	6.5.3 MOR and MOE with Varying Grain Angle and Moisture Content	121
7	WAVE PROPAGATION ANALYSIS AS AN NDE TECHNIQUE	132
	7.1 INTRODUCTION	132
	7.2 INFLUENCE OF WOOD PROPERTIES ON WAVE PROPAGATION	132
	7.3 PREDICTION OF WOOD STRENGTH NDE PROCEDURES	137
	7.3.1 Prediction of Strength from Measured Material Properties	138
	7.3.2 Prediction of Strength through Measured Moisture Content and Predicted Grain Angle	141
	7.3.3 Prediction of Strength by Direct Correlation with NDE Parameters	142
	7.4 COMPARISON OF NDE PREDICTION TECHNIQUES	149
8	SUMMARY AND CONCLUSIONS	155
	8.1 RELATIONSHIPS OF WOOD PROPERTIES WITH STRESS WAVE SPECTRA CHARACERISTICS	155
	8.2 PREDICTION OF STRENGTH FROM NDE STRESS WAVE CHARACTERISTICS	157
	8.3 RECOMMENDATIONS FOR FURTHER RESEARCH	158
	8.4 APPLICATIONS OF RESULTS TO A POLE NDE TECHNIQUE	159
	LITERATURE CITED	162
APPENDICES		
A	LISTING OF ACRONYMS FOR NDE PARAMETERS	169
B	FREQUENCY RESPONSE FUNCTION VALUES FRFREQ[1/], FRAMP[2/], FRINT[3/], and TRANSIT TIME VALUES TTIME[4/] FOR GRAIN ANGLE-MOISTURE CONTENT STUDY SPECIMENS	175
C	ENERGY SPECTRUM VALUES ENGAMP[1/], INTFENG[2/], ENG1AMP[3/] AND INT1ENG[4/] FOR GRAIN ANGLE-MOISTURE CONTENT STUDY SPECIMENS	178

Chapter		Page
D	ENERGY SPECTRUM VALUES ENG2AMP[1/], INT1ENG[2/], ENGIMP[3/] and ENGINT[4/] FOR GRAIN ANGLE-MOISTURE STUDY SPECIMENS	181
E	ENERGY SPECTRUM VALUES ENGINPD[1/], ENGIND[2/], ENGINTPD[3/], AND ENGINTD[4/] FOR DECAY STUDY SPECIMENS .	184
F	ENERGY SPECTRUM VALUES ENGAMPPD[1/], ENGAMPD[2/], INTENGPD[3/], AND INTENGD[4/] DECAY STUDY SPECIMENS . . .	186
G	FREQUENCY RESPONSE FUNCTION VALUES FRFREQ[1/] AND FRINT[2/] FOR DECAY STUDY SPECIMENS AFTER EXPOSURE TO DECAY	188
H	SUMMARY OF MATERIAL PROPERTIES FOR GRAIN ANGLE-MOISTURE CONTENT STUDY SPECIMENS	190
I	SUMMARY OF MATERIAL PROPERTIES FOR DECAY STUDY SPECIMENS	193
J	REGRESSION ANALYSIS STATISTICS	196
K	SUMMARY OF MEASURED AND PREDICTED MOR VALUES	201

LIST OF TABLES

Table		Page
2.1	Frequency coefficients of beam equation for various support configurations	8
3.1	Units of amplitude for spectral analysis functions (from HP 5423A Structural Dynamics Analyser User's Guide Manual, Volume 1)	46
4.1	Specimens and parameters for DEC study	64
4.2	Specifications for Columbia Model 3021 accelerometer	75
4.3	Measurement state one for time domain analysis	82
4.4	Measurement state two for frequency domain analysis	83
6.1	Specimen groupings of constant moisture content for grain angle study	100
6.2	Summary of best predictive equations for grain angle at various moisture contents	106
6.3	Specimen groupings of constant grain angle for moisture content prediction	108
6.4	Summary of regression statistics for prediction of weight loss (percent) in 90 degree specimens	114
6.5	Summary of best predictive equations for MOR at various moisture content values	118
6.6	Summary of best predictive equations for MOE at various moisture content values	119
7.1	Average FRAMP values above and below the fiber saturation point at five grain angles	136
7.2	Summary of equations for prediction of grain angle when moisture content is known	143

Table		Page
7.3	Summary of regression statistics for prediction of MOR	144
7.4	Average errors of predicted MOR values as a function of grain angle	153

LIST OF FIGURES

Figure		Page
2.1	MOR versus dynamic MOE minimum for lodgepole pine (2 by 4, 2 by 6)(57)	11
2.2	Relationship of MOE with grain angle by Hankinson's formula and tensor transformation for Douglas-fir, coastal variety	14
2.3	Frequency response of a sound pole (35)	19
2.4	Frequency response of pole with extensive internal decay (35)	20
3.1	One-dimensional propagation of an energy disturbance at a) initial condition, and b) time t	23
3.2	Particle motion associated with passage of a dilatation wave	25
3.3	Particle motion associated with passage of a distortion wave	26
3.4	Reflection of a compressive dilatation wave normal to a free surface	29
3.5	Reflection of a dilatation wave impinging obliquely on a plane free surface	30
3.6	Reflection and refraction of an incident dilatation wave at a plane interface of two dissimilar materials .	32
3.7	Wave propagation in wood exhibiting high-frequency damping	35
3.8	Relationship of logarithmic decrement to moisture content (15)	38
3.9	Relationship of stress wave velocity to moisture content in Sweetgum (21)	38
3.10	Ensemble of sample functions forming a random process .	41

Figure		Page
3.11	Representation of wave propagation in wood as a "black box" system	43
3.12	Time record of a stress wave in wood	45
3.13	Autocorrelation function plots (autocorrelograms): a) Sine wave, b) Sine wave plus random noise, c) Narrow-band random noise, d) Wide-band random noise	47
3.14	Energy spectral density of time record in Figure 3.12 .	50
3.15	Flow chart of spectral analysis procedures for calculation of frequency response function	52
3.16	Heuristic mechanical vibratory system	54
3.17	Hypothetical frequency response function	56
3.18	Cross-correlogram of two waveforms	58
4.1	Material selection from a log for the GAMC study	65
4.2	Specimen selection from wood slabs	66
4.3	Specimen locations for DEC study	68
4.4	Final specimen dimensions	68
4.5	Decay bin for specimens	70
4.6	Accelerometer holder	72
4.7	Specimen preparation frame	74
4.8	Fully instrumented specimen	74
4.9	Nondestructive evaluation test frame	77
4.10	HP5423A structural dynamics analyzer, Metriguard stress wave timer, and HP7225A Plotter	80
4.11	Test frame for specimens in flexure	86
5.1	Time record of stress wave in a) 90 degree specimen at 160% moisture content b) 0 degree specimen at 7% moisture content	89

Figure		Page
5.2	Energy spectral density of a) 90 degree specimen at 160% moisture content and b) 0 degree specimen at 7% moisture content	90
5.3	Frequency response function of a) 90 degree specimen at 160% moisture content and b) 0 degree specimen at 7% moisture content	91
5.4	Use of cursor capability to identify maximum gain factor and attendant frequency	92
5.5	Plot of a) energy spectral density and b) integration of energy spectrum	94
5.6	Example of invalid test due to base attachment of accelerometer holder	96
6.1	Scatter diagram of grain angle (degress) versus FRFREQ (Hz) for group CMC3 exhibiting curvilinear behavior	102
6.2	Plot of TTIME regression equations for grain angle prediction at various moisture contents	103
6.3	Plot of FRINT parabolic regression equations for grain angle prediction at various moisture contents	104
6.4	Scatter diagram of moisture content (percent) versus FRFREQ (Hz) for group CGA7 exhibiting curvilinear behavior	111
6.5	Scatter diagram of weight loss (percent) versus NNINTENGD for 90 degree DEC specimens	115
6.6	Plot of FRFREQ straight-line regressions for MOR prediction at various moisture content values	120
6.7	Plot of TTIME straight-line regression equations for MOR prediction at various grain angles	122
6.8	Scatter diagram of MOR versus FRFREQ (Hz) for all specimens	123
6.9	Scatter diagram of MOE versus FRFREQ (Hz) for all specimens	124
6.10	Scatter diagram of MOR versus FRINT for all specimens	125
6.11	Scatter diagram of MOE versus FRINT for all specimens	126

Figure		Page
6.12	Scatter diagram of MOR versus TTIME for all specimens	128
6.13	Scatter diagram of MOE versus TTIME for all specimens	129
6.14	Scatter diagram of MOE versus E_d for all specimens . .	130
7.1	Scatter diagram of MOR_{act} versus MOR_{pred1} as predicted from measured material properties	140
7.2	Scatter diagram of MOR_{act} versus MOR_{pred2} as predicted from measured moisture content and grain angle predicted from Eq. 6.3	145
7.3	Scatter diagram of MOR_{act} versus MOR_{pred3} as predicted from measured moisture content and grain angle predicted from Eq. 6.4	146
7.4	Scatter diagram of MOR_{act} versus MOR_{pred4} as predicted from measured moisture content and grain angle predicted from TTIME equations in Table 7.2.	147
7.5	Scatter diagram of MOR_{act} versus MOR_{pred5} as predicted from measured moisture content and grain angle predicted from FRINT equations in Table 7.2	148
7.6	Scatter diagram of MOR_{act} versus MOR_{pred6} as predicted from measured NDE variable FRFREQ and Eq. 6.5	150
7.7	Scatter diagram of MOR_{act} versus MOR_{pred7} as predicted from measured NDE variable TTIME and Eq. 6.7	151

Chapter 1

INTRODUCTION

The large degree of variability in strength properties of wood results largely from its biological nature. Design values assigned to wood components are quite conservative because of this variability. Current research at Colorado State University (CSU), supported by the Electric Power Research Institute (EPRI)*, is attempting to better account for this variability in the design of wood transmission structures by incorporating it directly into the design procedure. This probabilistic design procedure models the statistical variability of loads and strength to determine the level of reliability for an entire pole line.

Implementation of the design methodology requires the distributions of strength and stiffness values for the poles comprising the transmission line in question. A method developed by Mulheren (54) and others at CSU under a previous EPRI project has been used successfully to obtain this information. In addition to the above, the strength of an individual pole often needs to be known. The ability to predict the strength of an individual wood pole would enable designers to preselect poles for maximum design efficiency as

---

*EPRI Project RP-1342-2. Reliability-Based Design of Transmission Line Structures.

well as remove low strength poles from an existing line. No method with sufficient accuracy is currently available for this purpose.

The nondestructive evaluation (NDE) procedure developed by Mulheren involves the measurement of velocity of a stress wave induced into the pole. The basis for wave velocity studies is the principle of wave propagation in solids. This phenomenon is complex and little understood in a material as diverse as wood. The measurement of velocity utilizes on a part of the information available in stress wave propagation. Techniques available in the field of waveform spectral analysis enable researchers to extract a large amount of information beyond that of velocity. To date, few research results are available on the spectral properties of stress waves in wood. However, the general field of wave propagation analysis in other materials is rapidly gaining acceptance as a valuable tool for the investigation of material behavior.

The purpose of this research was to investigate potentially useful characterisitcs of stress waves as a function of the material properties of wood. For such an exploratory research, careful experimental procedures must be developed as well as analysis techniques of the stress wave. Correlation of the wave parameters to wood properties and thus to the strength of the wood was attempted. Through such knowledge of wave behavior in wood, prediction of the condition of the wood should be possible. Once the material characteristics are known, fundamental relationships between strength and those properties should enable the prediction of wood strength on a piece by piece basis. The final goal is that of obtaining an easy, quick procedure for NDE of the strength of wood with greater accuracy than available with current

procedures. The exploratory nature of this work should be emphasized as the first step toward the final goal of a reliable wood pole strength prediction technique.

Chapter 2

REVIEW OF LITERATURE

2.1 INTRODUCTION

The literature review briefly covers the traditional concepts of nondestructive evaluation (NDE) as applied to solid wood and wood composites. An economic motivation for an efficient NDE process is given along with limitations of present techniques, especially as related to inspection of wood poles.

2.2 ECONOMIC IMPORTANCE OF NDE

Economics is a pervasive factor in the use of any product including wood. Increasing stumpage prices for timber from federal land as well as increasing labor, energy, and production costs have all contributed to increased cost to consumers of wood products. With the demise of low cost wood products, significant economic benefits may be derived from an accurate knowledge of wood properties obtained through NDE. The savings arise from several areas including more efficient utilization and design, higher reliability of wood structures, and increased safety.

The first NDE wood pole maintenance program appears to have been initiated by Detroit Power and Light in the late 1970s. The procedure utilized the Pole-Tek device in conjunction with increment bases. This program was credited with decreasing maintenance costs from $16.00 to $2.60 per pole (13). The NDE technique for wood poles is

especially important in view of EPRI (Electric Power Research Institute) projections that,

> "during the next 20 years, more than 40 million poles worth more than twenty-billion dollars (in 1980 dollars) will be used in the construction and maintenance of transmission and distribution lines" (19).

Due to the magnitude of these costs, even small increases in efficiency resulting from an effective NDE procedure will translate into a multimillion dollar saving.

2.3 TRADITIONAL NDE APPROACHES

NDE is any process by which one or more characteristics of a material are evaluated without altering these characteristics. Using the above definition, it can be recognized that the first form of NDE used with wood products was a visual inspection. While grading through visual examination is widely used in the wood industry, its subjectivity is well recognized. The primary objective of developing new NDE procedures for wood products is to improve the prediction of a given property for a group or an individual member.

The effectiveness of an NDE procedure can best be examined by the "selection efficiency" concept. The ideal NDE would not only reject all material of insufficient quality, but at the same time also ensure the retention of all adequate material. Selection efficiency, as defined by Miller (51, 52), is the percentage of material of acceptable strength which is actually recovered after rejection of the low quality pieces has been ensured. Thus, if all inferior material, but no acceptable material is rejected by an NDE, the selection efficiency is 100 percent. In practice, however, an NDE which assures detection of all defective material also rejects acceptable material, thereby creating a lower selection efficiency.

Two criteria of most interest in an NDE assessment of wood products for structural uses are the stiffness and strength. Presently used NDE procedures for both properties and their interrelationships are discussed in the following sections.

2.3.1 NDE of Stiffness

The stiffness of wood products is a primary concern for structural applications. The majority of NDE techniques have concentrated on prediction of modulus of elasticity (MOE) through application of fundamental knowledge assuming linear elastic and often homogeneous material behavior. Though wood often violates these assumptions, several acceptable predictive procedures exist.

Perhaps the simplest NDE technique of MOE determination is through static bending. For example, the deflection of a center-loaded, simply supported beam is defined by Equation (2.1) as,

$$\Delta = P\ell^3/48EI \qquad (2.1)$$

where: Δ = maximum deflection at mid-span,

P = applied vertical load,

ℓ = span,

I = moment of inertia about the horizontal neutral plane,

E = modulus of elasticity, often designated as MOE due to the inclusion of shear deflection in Eq. (2.1).

This may be rearranged to allow calculation of MOE by knowledge of the applied load, resulting deflection, and dimensions of the member.

The static bending principle is employed in the machine stress rating of lumber. Most grading machines either apply a set load and measure the deflection or monitor the load required to obtain a predetermined deflection (9, 44). Research on such a 'stiffness' tester

was conducted as early as 1960 by Hoyle (31, 32). As of the mid-1970s over 80 machine stress rating (MSR) graders of various manufacture were in use throughout the world (62).

Another approach widely used for determination of lumber stiffness is transverse vibration. From classical vibration theory, the natural frequency of vibration for a prismatic beam is given by Eq. (2.2)(72),

$$\omega_n = \beta_n^2 \left(\frac{EI}{\rho}\right)^{\frac{1}{2}} = (\beta_n \ell)^2 \left(\frac{EI}{\rho \ell^4}\right)^{\frac{1}{2}} \qquad (2.2)$$

where: β_n = constant depending on boundary conditions,

ρ = density,

ℓ = span,

E = dynamic modulus of elasticity,

I = moment of inertia,

ω_n = natural frequency,

n = mode number.

Values for $(\beta_n \ell)^2$ with typical end conditions are given in Table 2.1 (72).

Equation (2.2) may be rearranged to calculate the dynamic modulus of elasticity, E_d, given the natural frequency.

$$E_d = \omega_n^2 \rho / \beta_n^4 I \qquad (2.3)$$

The natural frequency may be determined by either free or forced vibration. Employing a free vibration scheme for structural lumber, Pellerin (61) obtained a coefficient of determination (r^2) of 96 percent between static MOE determined from destructive testing and

Table 2.1. Frequency coefficients of beam equation for various support configurations.

Beam Configuration	$(\beta_1 \ell)^2$ Fundamental	$(\beta_2 \ell)^2$ Second Mode	$(\beta_3 \ell)^2$ Third Mode
Simply supported	9.87	39.5	88.9
Cantilever	3.52	22.4	61.7
Free-free	22.4	61.7	121.0
Clamped-hinged	15.4	50.0	104.0
Hinged-free	0.0	15.4	50.0

E_d. Miller (53) tested 219 jack pine and white spruce 2 in. x 6 in. x 12 ft joists. The MOE was determined by measuring the natural frequency in free vibration. Standard error of the estimate (SEE) for prediction of MOR was 3600 psi. Hearmon (27) obtained an r^2 of 0.49 in predicting load at failure from the square of the natural frequency for fifty-one 2 in. x 4 in. joists. Difficulties arose in the measurement of member vibration when loaded as a joist, thus the natural frequency was obtained from vibration as a plank.

The use of static deflection and transverse vibration methods for MOE determination, while theoretically sound, have problems in certain applications. Static deflection measurements are difficult for certain products such as utility poles in service, where the physical problems of bending a pole with line are prohibitive.

The "E-computer " produced by Metriguard Inc., employs transverse vibration techniques for determination of the MOE of lumber and laminated beams (47). No transverse technique is currently in use for standing poles due in part to the handling, instrumentation, and boundary value problems.

Another NDE technique is stress wave timing. This procedure involves measurement of the velocity of wave propagation. The relationship between E_d and stress wave velocity is given in Eq. (2.4),

$$E_d = c^2\rho \tag{2.4}$$

where: E_d = dynamic modulus of elasticity,

ρ = density,

c = velocity of wave propagation.

Commercial devices for measurement of the wave velocity are produced in the U.S. by James Electronics (34) and Metriguard Inc. (48). The James V-meter employs ultrasonic frequencies while the Metriguard stress wave timer works in the sonic frequency range. Gerhards (22) found no difference in results obtained by the two instruments. Dunlop (16) measured wave velocity in particle board through the thickness and in the plane of the panel. Prediction of the panel MOE using Eq. (2.4) and inplane velocity yielded an r^2 value of 53 percent. Galligan and Courteau (20) found an r^2 of 92 percent between static MOE and E_d determined by wave velocity for structural lumber. Use of either vibration or wave velocity for predicting E_d yields similar results. Comparison between E_d, determined from transverse vibration, and that by wave propagation yielded an r^2 of 93 percent. Aspects of the theory of stress wave propagation and some governing equations are dealt with in Chapter 3.

2.3.2 Relationship between Strength and Stiffness of Wood

Prediction of strength through NDE procedures has been primarily accomplished through a correlation with some measure of stiffness (18, 42, 53, 57, 61). A common analysis is the prediction of MOR from MOE

(MOR/MOE). A typical scatter diagram of an MOR/MOE regression is shown in Figure 2.1 (57). The strength of a material has no theoretical relationship with its elastic parameters (28) yet they are positively correlated. This correlation is from the mutual dependence of strength and stiffness on such intrinsic wood characteristics as density, grain angle, and moisture content. Since the relationship is empirical a degree of uncertainty arises when predicting strength from stiffness as is indicated by the scatter about the regression equation. The amount of scatter is influenced by the presence of defects and their location. Miller (53) used E_d from flexural vibration to predict MOR. Typical scatter about the regression equation was approximately ± 10,000 psi. Kramer (42) employed a similar technique with southern pine lumber. The relationship between MOR and E_d had an r^2 value of 77 percent with actual values ranging as much as ± 4000 psi from predicted values.

2.4 WOOD CHARACTERISTICS RELATED TO STRENGTH

The limited accuracy in the prediction of a single member's strength from a measure of its stiffness has motivated interest in alternate approaches. Wave propagation and fracture mechanics are two such disciplines currently receiving attention. As mentioned, prediction of strength through an MOR/MOE regression has no theoretical basis. A more accurate prediction of strength of wood with no defects is possible through knowledge of the material characteristics (i.e., density, moisture content).

The most important wood characteristic to predict strength of clear wood is reported to be specific gravity (60). The general

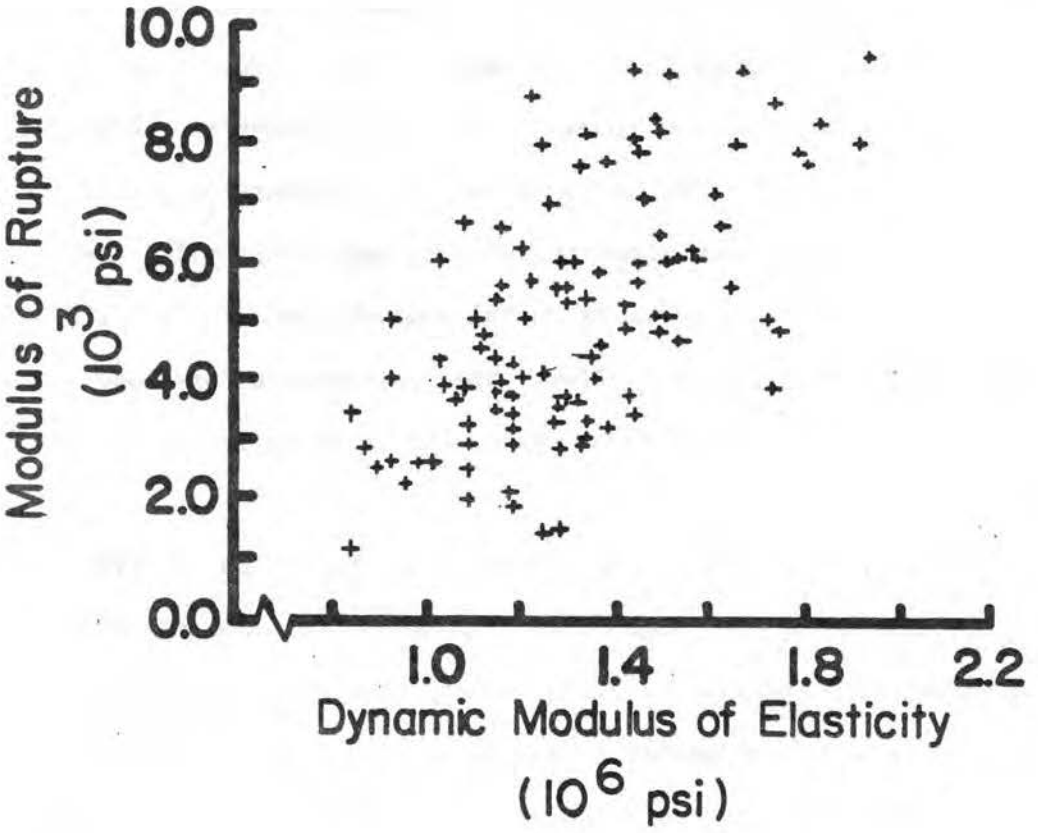

Figure 2.1. MOR versus dynamic MOE minimum for lodgepole pine (2 by 4, 2 by 6)(57).

relationship between specific gravity and strength is given by Eq. (2.6)(74).

$$S = KG^n \tag{2.6}$$

where: S = strength property of interest,

K = constant, depends on strength property,

G = specific gravity,

n = exponent, depends on strength property.

Moisture content below the fiber saturation point affects the strength and elastic properties to a large extent. Typical magnitudes of influence per one percent change of moisture content are; 2 percent for MOE, 4 percent for MOR, and 6 percent for compression parallel to grain (74). Environmental factors such as temperature (11), chemical degradation (77), and especially fungal degradation (14, 30, 39, 76, 79, 80) may significantly affect the performance of wood. The influence of fungal decay will be dealt with in depth in the following section.

All the influences listed above are based on analysis of knot-free specimens. A significant influence on strength is cross grain, especially local cross grain around knots. Strength properties are sensitive to cross grain; a large reduction can occur with grain angles as low as 15 degrees relative to the longitudinal axis. Local characteristics such as knots may control the strength of the entire member.

A well-known empirical formula for determining change in strength with grain angle is knownas Hankinson's formula, Eq. (2.7),

$$N = PQ/\{P\sin^2\theta + Q\cos^2\theta\} \tag{2.7}$$

where: N = strength at grain angle θ,

P = strength parallel to grain,

Q = strength perpendicular to grain,

θ = grain angle, measured from the longitudinal axis.

The effect of cross grain on elastic parameters for wood may also be determined according to the laws of tensor transformation. For the case of E in the LT-plane, Eq. (2.8) gives the governing relationship,

$$E_\theta = 1/\{\frac{1}{E_L}\cos^4\theta + \frac{1}{E_T}\sin^4\theta + [\frac{1}{G_{LT}} - \frac{2\nu_{TL}}{E_T}]\cos^2\theta \sin^2\theta\} \quad (2.8)$$

where: E_L = modulus of elasticity in the L direction,

E_T = modulus of elasticity in the T direction,

G_{LT} = modulus of rigidity in LT plane,

ν_{TL} = poisson ratio for passive strain in the T direction over active strain in L direction.

A typical example of variation in MOE with grain angle is shown in Figure 2.2.

2.4.1 Effect of Decay on Strength and Stiffness

To quantify the effect of decay on strength and stiffness some measure of its presence is necessary. Harltey (25) and others have concluded that weight loss of wood is the best basis on which to judge the degree of decay influences. Difficulties arise due to the different influence of fungal type (i.e., brown vs. white rot) as well as variation in species resistance to decay. Further complications arise since the various physical properties of wood are not equally sensitive to decay. Nevertheless, some guidelines do exist for categorizing the influence of decay on properties.

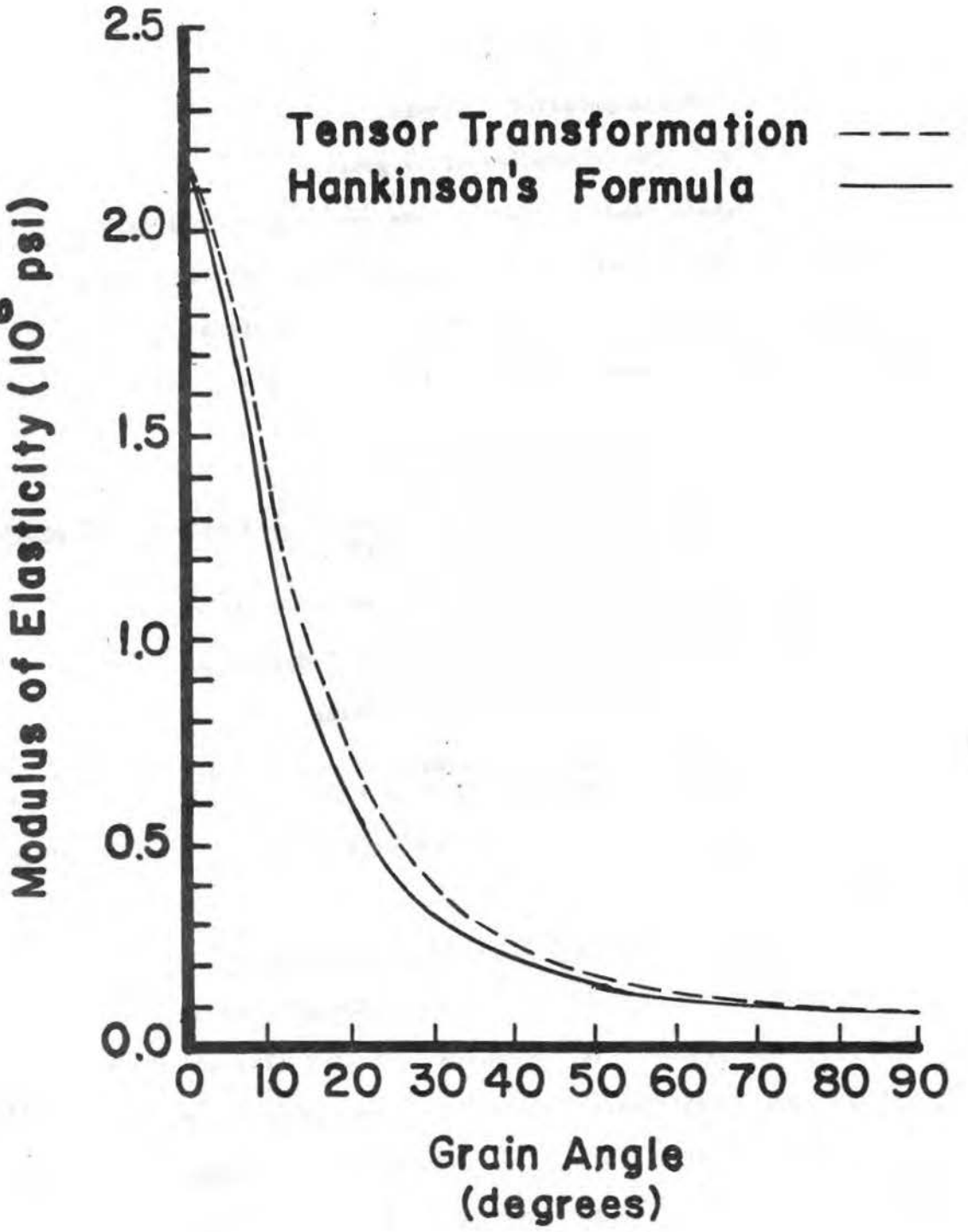

Figure 2.2. Relationship of MOE with grain angle by Hankinson's formula and tensor transformation for Douglas-fir, coastal variety.

The mechanical property most sensitive to decay is toughness, with up to 50 percent reduction observed for a 1 percent weight loss (80). Toughness is a measure of the energy absorbed to failure of a specimen by impact. Work to failure is the second most sensitive parameter to dacay. Kennedy (39) working with tropical hardwoods found that brown rot had a greater effect on work to maximum load in bending than did white rot. Brown rot primarily affect the cellulosic structures whereas white rots decompose all components of the wood (7). Cartwright et al. (10), found that softwoods exposed to brown rot exhibited a greater reduction in MOE than in MOR. For a 2 percent weight loss, MOR was reduced 50 percent and MOE 55 percent. For a 2 percent reduction in specific gravity in softwoods exposed to white rot, MOR was affected more (14 percent reduction) than MOE (4 percent reduction)(64).

Decay is difficult to detect at levels of weight loss less than 10 percent. Yet strength values at this weight loss are in some instances reduced by half (80). For wood poles, these levels of decay are not as influential on strength, especially when present in the interior.

The deleterious effect of decay fungi on strength is especially important to users of wood poles. Due to contact with soil conditions for decay are favorable. Even with preservative treatments, decay will eventually occur and is a prime cause for pole replacement. A survey of treated transmission poles in the northeast U.S. found decay located primarily in the untreated heartwood (82). The majority of decay fungi isolated were white rot type. Henningsson et al. (29), studied the effect of soft rot on salt-treated poles in Sweden. The

Scots pine (Pinus silvestris) poles studied had been in service from 21 to 35 years. They found reductions in pole bending strength of 29 to 85 percent. It should be noted that soft rots attacked the outer portion of poles, the portions with the greatest influence on section modulus and thus bending strength. Wang et al. (76), measured the free vibration natural frequency of small white pine (Pinus strobus L.) cantilever beam specimens with no defects before and after various levels of decay. They found significant reduction (1 percent significance level) in natural frequency as decay increased. A 41 percent reduction in natural frequency occurred for a 14 percent weight loss.

2.4.2 Pole Inspection Methods

Numerous techniques are in use today for the detection of decay in wood poles. However, the only completely reliable method of detecting decay is microscopic examination and culturing of samples, usually obtained from increment bores (24). A simple method for detecting internal decay is sounding with a hammer. An undecayed pole has a sharp sound while a decayed pole has a hollow sound (24). Suspect poles still must be examined using cores from an increment borer.

Numerous other pole testing devices are in use, among them the Shigometer, Pilodyn, and Pol-Tek (68, 81, 71). The Shigometer uses the phenomenon of decreasing resistance to a pulsed electric current as decay increases. The Pilodyn tester is an impact hammer which measures the depth of penetration of a probe for a fixed impact energy. Pole-Tek uses wave velocity measurements and is able to detect advanced decay (i.e., voids in the interior) in Douglas-fir poles. Each method is only partially successful in detecting

incipient decay and usually requires a subsequent increment core and culturing of suspected poles. None of the above devices give any direct indication of the strength and stiffness of the pole.

Miller et al. (50), and Breeze et al. (8), investigated the use of wave velocity through the diameter of a pole to determine decay. Miller stated that the method was efficient at detecting poles with interior voids caused by decay. The measured velocity was 10 to 40 percent greater in western red cedar poles when voids were absent. The presence of ring shake in southern pine poles resulted in higher velocities. Breeze employed a similar technique to estimate the crushing strength resistance of poles by comparing velocity through sound portions of the poles with velocity through a section containing a void. With this information, the size of the void was calculated assuming a linear relationship. The crushing strength was then predicted as a function of cross-sectional area. For the case of a predicted decrease in crushing strength of 30 percent, actual decreases ranged from 5 to 70 percent. This magnitude of error was consistent throughout the study. Measurement of velocity through the length of a pole was conducted by Dunlop (17). He concluded that this method may not be useful in detecting decay. The approach also presented the logistical problem of inducing the wave at the top of a standing pole.

Shaw (67, 68) has developed a pole inspection device, known as the Resotest, currently in commercial use in Australia. Measurements of vibration amplitudes below 400 Hz are used to determine the presence of interior voids. No subsequent core bores are used with this apparatus. The device is calibrated only for use on Eucalyptus

species at this time. Work by Jensen (35) indicated that Douglas-fir poles without internal voids exhibit a natural frequency between 2100 and 2500 Hz, as shown in Figure 2.3. Voids in the pole interior resulted in the natural frequency shifting to approximately 1500 Hz, see Figure 2.4. No commercial device evolved from this research to date. Kaiserlik (37) conducted a survey of NDE methods possibly applicable for predicting strength losses in treated pilings used for docks. His recommendation was to evaluate stress wave energy, hardness, and E_d determined from stress wave velocity.

NDE of the strength of wood material without defects may be accomplished by vibrational or stress wave techniques. It appears that the stress wave approach is better suited for work with poles. Before attempting stress wave studies in a complex structure such as a pole, fundamental research in small clear specimens with no defects is necessary. Basic concepts of stress waves and waveform analysis necessary for this investigation is presented in the following chapter.

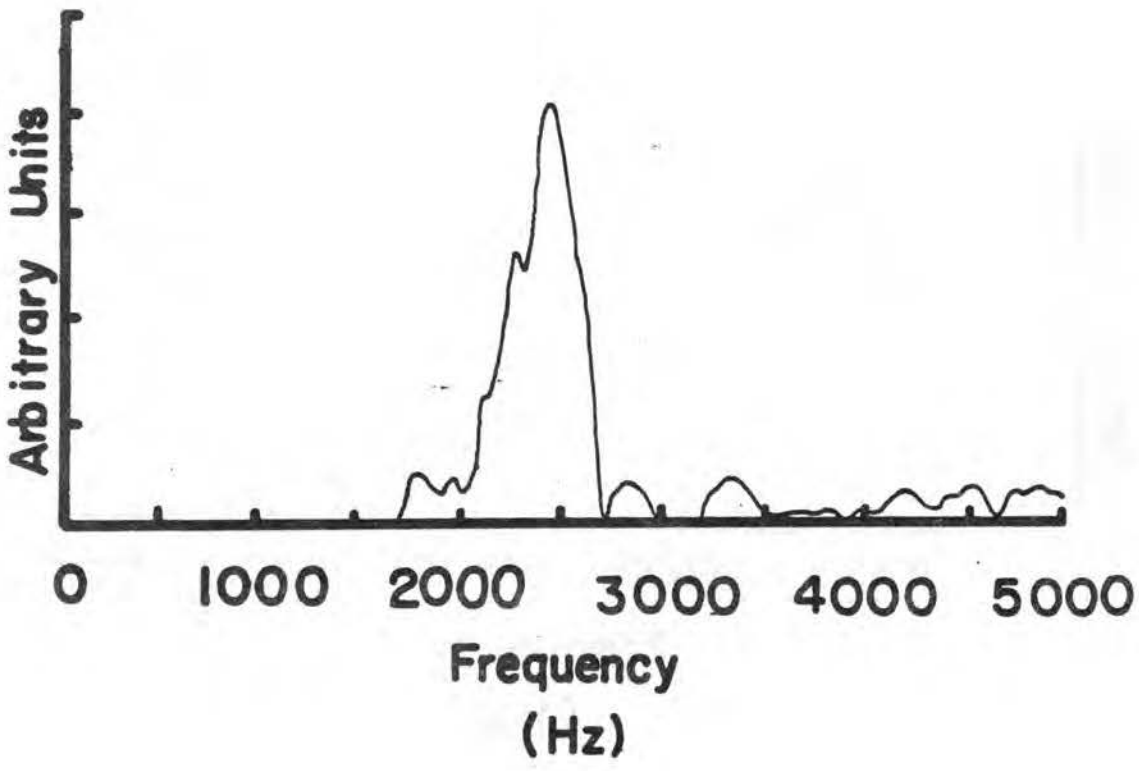

Figure 2.3. Frequency response of a sound pole (35).

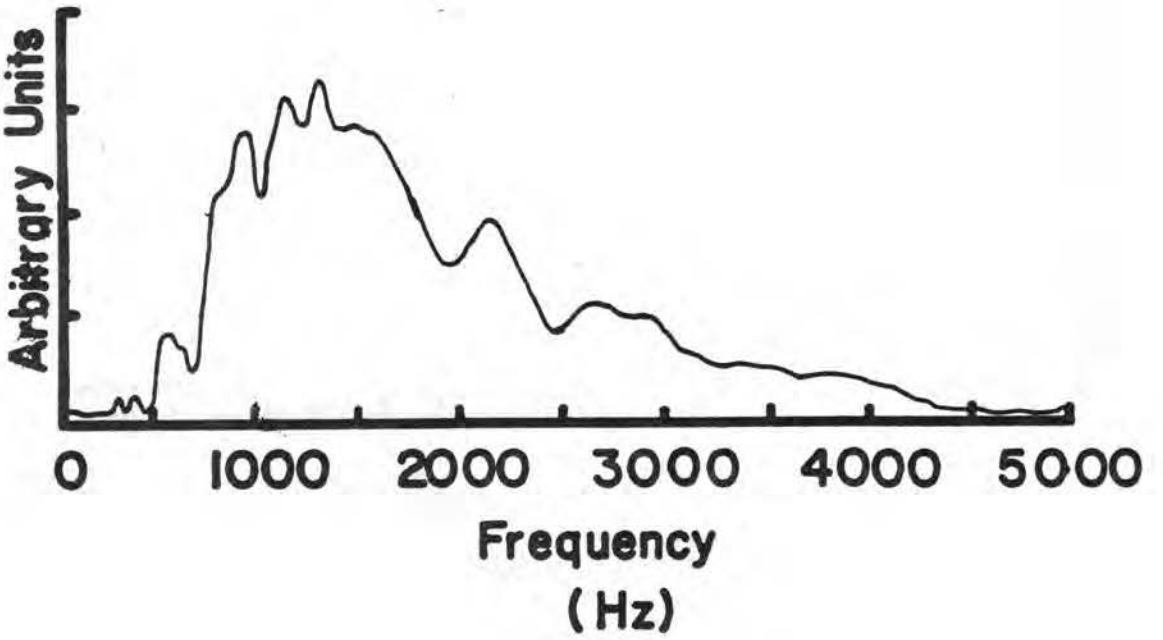

Figure 2.4. Frequency response of pole with extensive internal decay (35).

Chapter 3

THEORY OF PROPAGATION AND ANALYSIS OF STRESS WAVES

3.1 WAVE PROPAGATION IN SOLIDS

Stress wave propagation refers to the transmission of energy through a solid (78). The mode of transmission involves the disturbance of elements within the solid from their equilibrium position, as opposed to a translation of the solid as a whole. An earthquake is a common example of an environmental stress wave. Stress waves become important in engineering design consideration when applied forces are changing rapidly or of short duration (40). Traditional mechanics of materials and rigid body dynamics equations are insufficient to describe the nonequilibrium conditions characteristic of stress waves. Stress wave propagation through all materials have many common characteristics. However, an inhomogeneous anisotropic solid such as wood introduces further conditions which must be considered to describe the energy transmission involved. A brief discussion of common characteristics of stress waves are given before introducing the more advanced concepts necessary for describing stress wave propagation in wood.

3.2 THEORY OF STRESS WAVE PROPAGATION

Although not all aspects of wave propagation are of interest for this investigation, a knowledge of some fundamentals is needed for interpretations of the research and the analysis later described. The

nature of stress wave propagation is dependent on the degree of material inhomogeneity, geometry, boundary conditions, and applied forces (5). The simplest example involves an isotropic, homogeneous, elastic material of infinte dimensions in which a plane wave propagates in a uniaxial direction. The governing equation derived from the one-dimensional stress wave theory is, a hyperbolic partial differential wave equation given by,

$$\frac{\partial^2 \mu}{\partial t^2} = c^2 \frac{\partial^2 \mu}{\partial x^2} \tag{3.1}$$

where: μ = particle displacement,

t = time,

x = position on the propagation axis,

c = wave velocity.

A solution of Eq. (3.1) which is known as the D'Alembert solution, is of the form (38),

$$\mu(x, t) = \tfrac{1}{2}\{f(x + ct) + f(x - ct)\} \tag{3.2}$$

where: $f(x)$ = initial displacement

Physically, the D'Alembert solution describes the translation of the initial conditions in both the positive and negative directions as shown in Figure 3.1. The distance the wave travels in a given time, t, is dependent on the wave velocity, c. The solution requires that the amplitude of the progressive waves be one-half of the initial amplitude. This characteristic implies that the intersection of waves follow the concept of superposition. No damping or distortion of the wave is assumed.

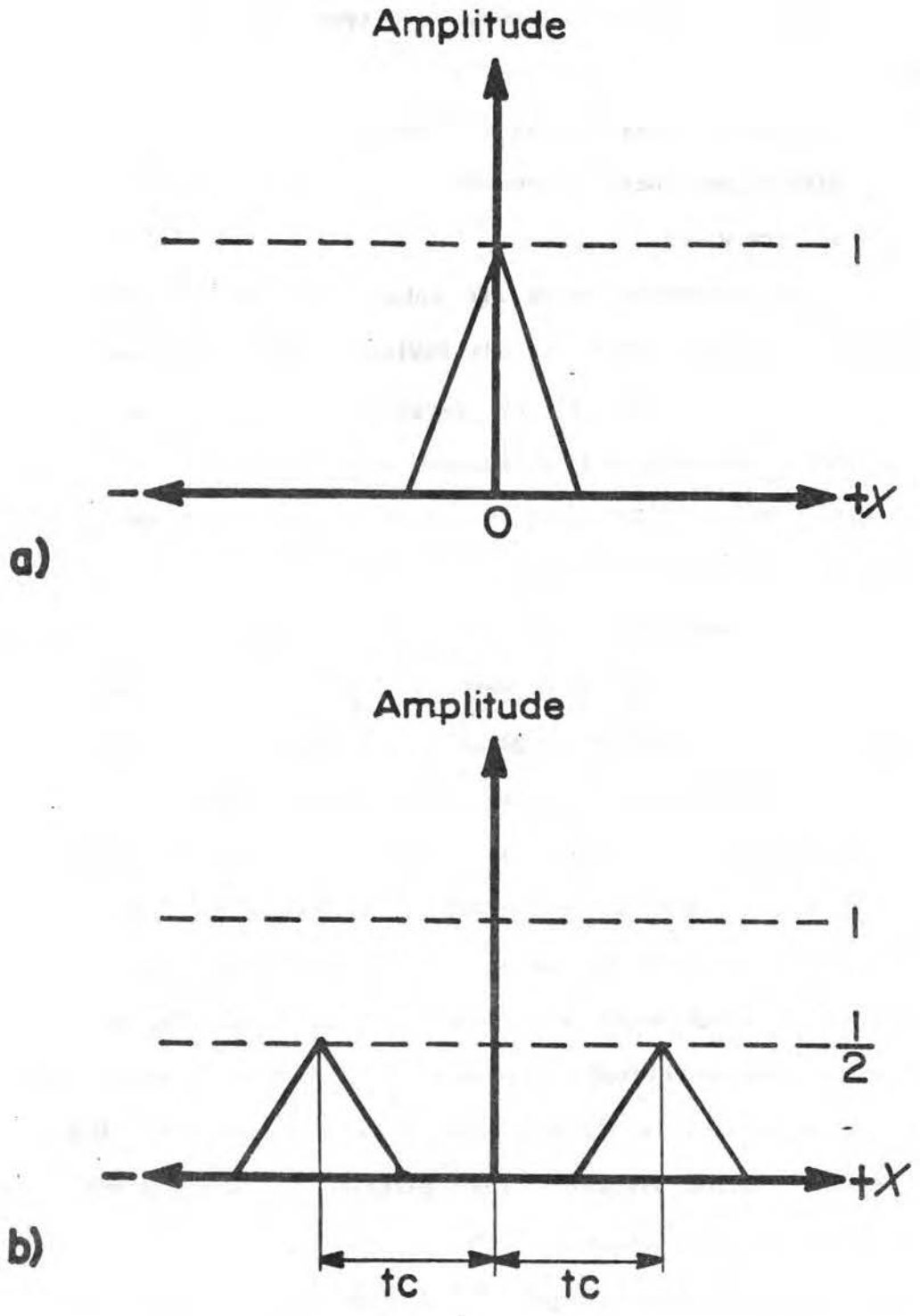

Figure 3.1. One-dimensional propagation of an energy disturbance at a) initial condition, and b) time t.

In elastic solids, three fundamental types of waves may occur, namely:

1. dilatation (longitudinal or P-waves),
2. distortion (shear or S-waves),
3. surface waves.

Dilatation and distortion waves are subsets of the group known as plane waves. Surface waves include Rayleigh, Lamb, and Love waves (49). Only Rayleigh waves will be discussed here, since they represent the most significant type of surface wave (40).

To differentiate between wave types it is helpful to consider the motion of discrete elements (particles) within a solid. The particle motion for all described wave types occur about an equilibrium position (40). In a dilatation wave, particle motion is coincident with the direction of energy propagation. As depicted in Figure 3.2, this particle movement about equilibrium follows the same axis as that of the propagating wave. In contrast, particle motion in a distortion wave is at right angles to the direction of propagation. This vertical motion for a laterally moving distortion wave is illustrated in Figure 3.3. Rayleigh waves may occur only on a material surface. Amplitudes of the associated particle motion diminishes exponentailly for particles located in the material, away from surfaces. Due to this, particle motion associated with passage of a Rayleigh wave is negligible in the interior of a solid.

Propagation velocity is dependent upon the type of wave, material geometry, and mechanical properties of the material. In an infinite material two velocities are possible. These two velocities, C_ℓ and C_s represent the dilatation wave and distortion wave, respectively.

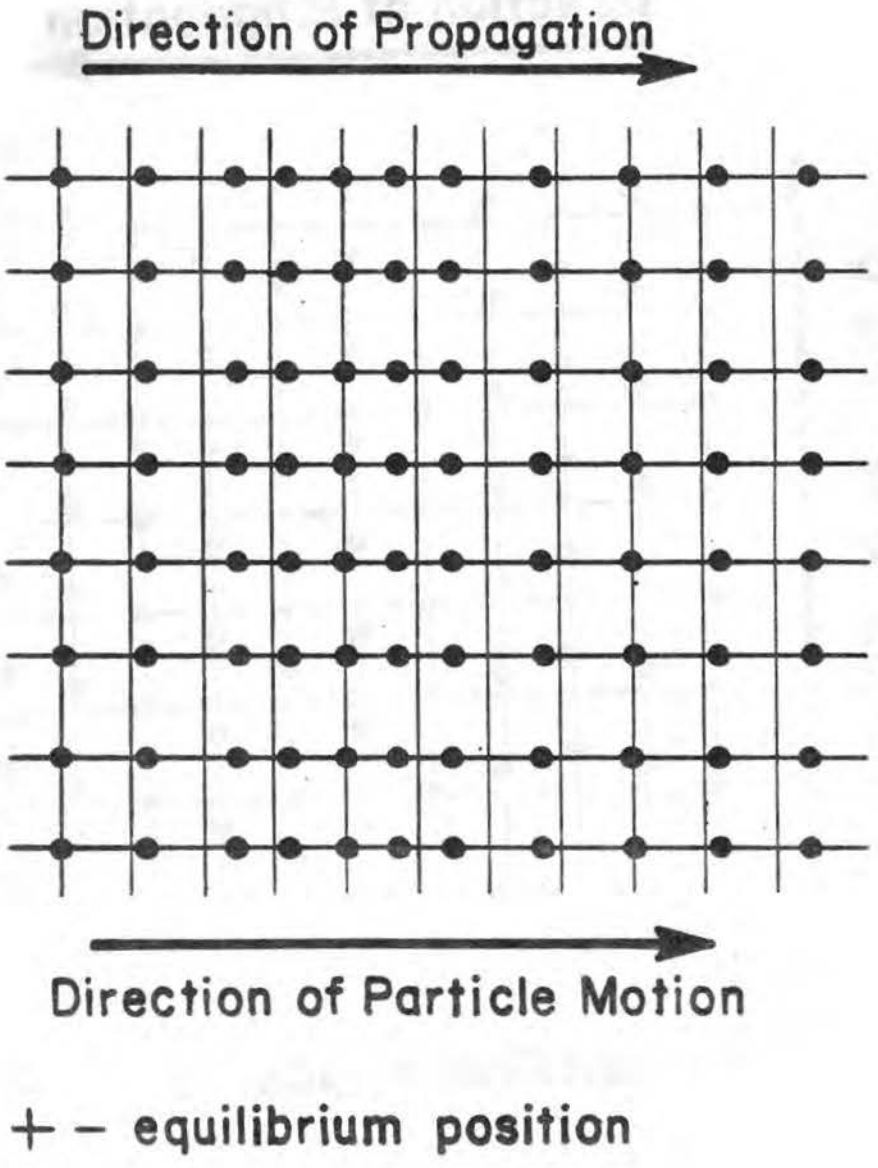

Figure 3.2. Particle motion associated with passage of a dilatation wave.

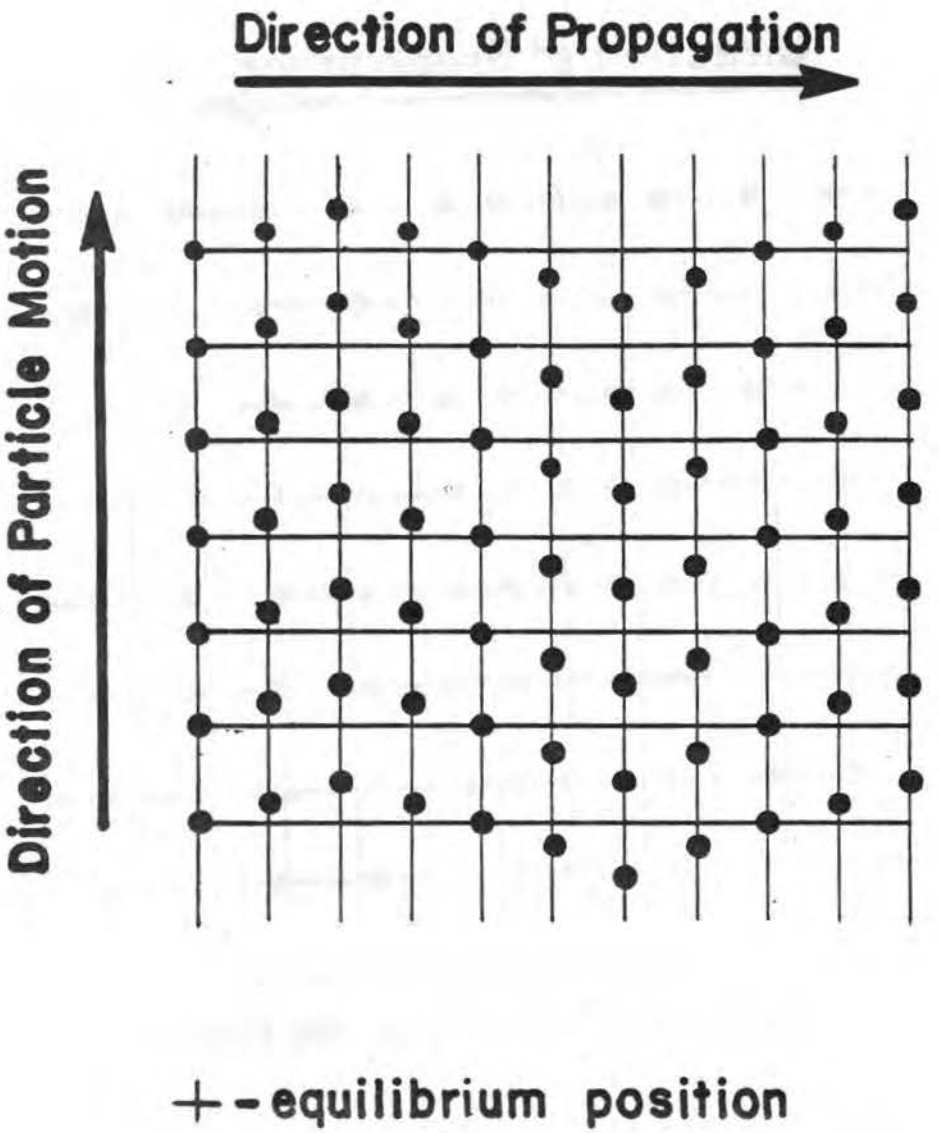

Figure 3.3. Particle motion associated with passage of a distortion wave.

For isotropic homogeneous materials, the velocity of a dilatation wave is given by Eq. (3.3) and that for a distortion wave by Eq. (3.4).

$$C_\ell = \left[\frac{\lambda + 2G}{\rho}\right]^{\frac{1}{2}} \tag{3.3}$$

$$C_s = \left[\frac{G}{\rho}\right]^{\frac{1}{2}} \tag{3.4}$$

where: C_ℓ = velocity of a dilatation wave,

C_s = velocity of a distortion wave,

ρ = bulk density of material,

G = modulus of rigidity,

λ = Lame's constant.

The modulus of elasticity, E, and the poisson ratio, ν, of an isotropic solid are related to the Lame' constant, λ, and the modulus of rigidity, G, by the following equations,

$$E = \frac{G(3\lambda + 2G)}{\lambda + G} \tag{3.5}$$

$$\nu = \frac{\lambda}{2(\lambda + G)} \tag{3.6}$$

For the case of a circular rod with its lateral dimensions small compared to the wavelength of the stress wave, lateral strains may be ignored and the velocity of a dilatation wave is given by,

$$c_\ell = \left[\frac{E}{\rho}\right]^{\frac{1}{2}} \tag{3.7}$$

The expression for velocity given by Eqs. (2.4) and (3.7) are mathematically equivalent often used in investigations of material behavior (3, 5, 12, 21, 41).

An important consideration is the reflection and refraction of waves at material boundaries. The four reflection cases considered for elastic waves are:

1. reflection at a free boundary--normal incidence,
2. reflection at a free boundary--oblique incidence,
3. reflection and refraction at a plane interface,
4. reflection and refraction at curved surfaces.

Incidence of a wave at a free boundary results in total reflection of wave energy back into the material. One-dimensional stress wave theory assumes that the angle of incidence is always normal to the free surface. If the incident wave is dilatational (Figure 3.4 (a)) with a given sense, i.e., compressive or tensile, then the reflected wave must also be dilatational but with an opposite sense (Figure 3.4 (c)). By the same reasoning an incident distortion wave upon reflection will retain its distortion character.

Typically the incident wave does not impinge on a surface at right angles. Reflection of a pure dilatational or distortion wave under this condition generates a disturbance which is a mixture of both wave types. The case of an incident dilatation wave is shown in Figure 3.5. The energies of the reflected dilatation, A_{LR}, and distortion, A_{SR}, waves are always less than the amplitude of the incident wave, A_{LI}. In a conservative medium the sum of the reflected wave energies equals that of the incident wave. Their relative magnitude depends upon the impingement angle, α_{LI}, and the elastic constants of the material. In general, the following relationships hold for isotropic, homogeneous materials:

1. $\alpha_{LI} = \alpha_{LR}$
2. $\beta_{SR} < \alpha_{LR}$
3. $A_{LR} < A_{LI}$
4. $A_{SR} < A_{LI}$

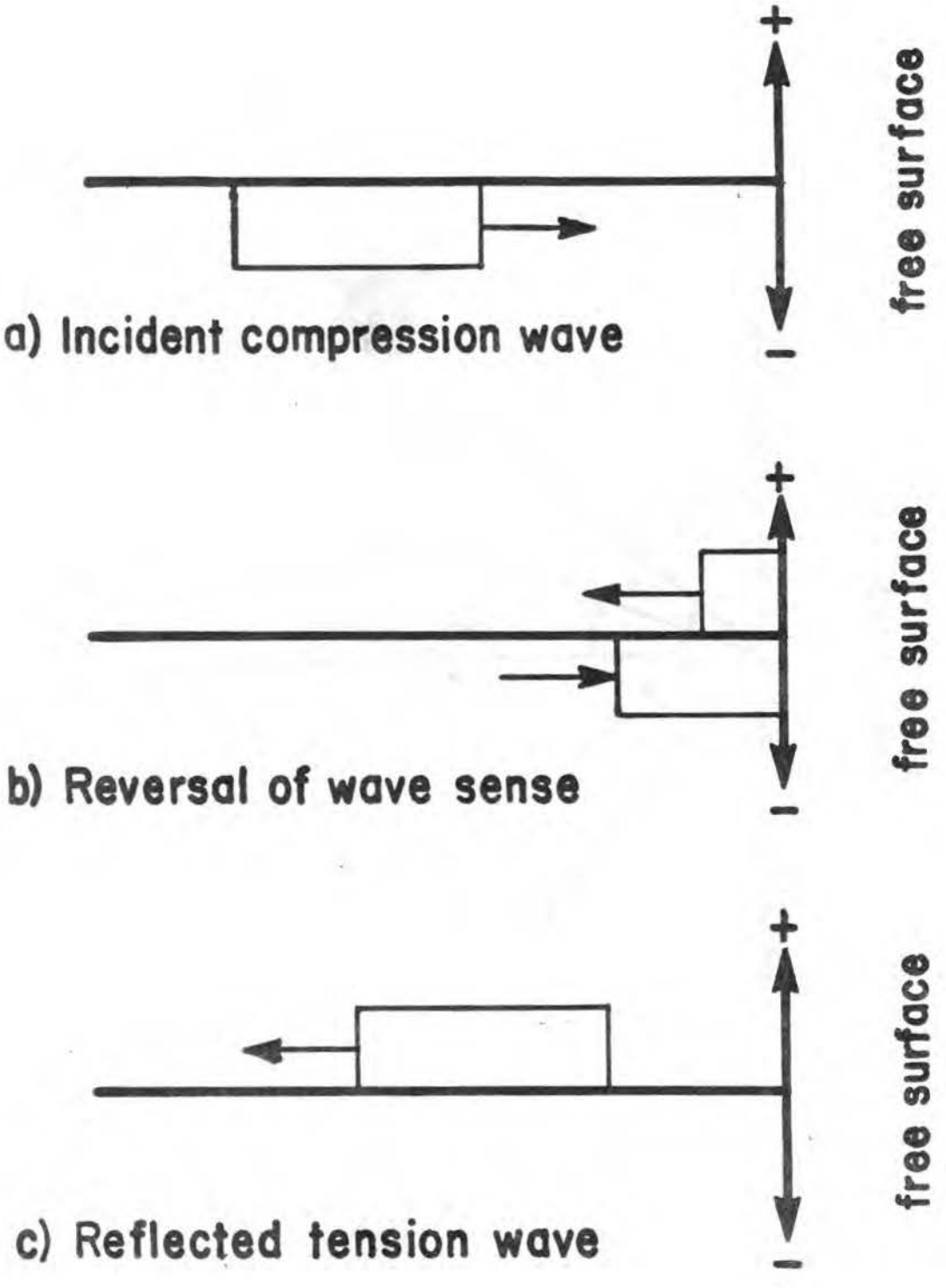

Figure 3.4. Reflection of a compressive dilatation wave normal to a free surface.

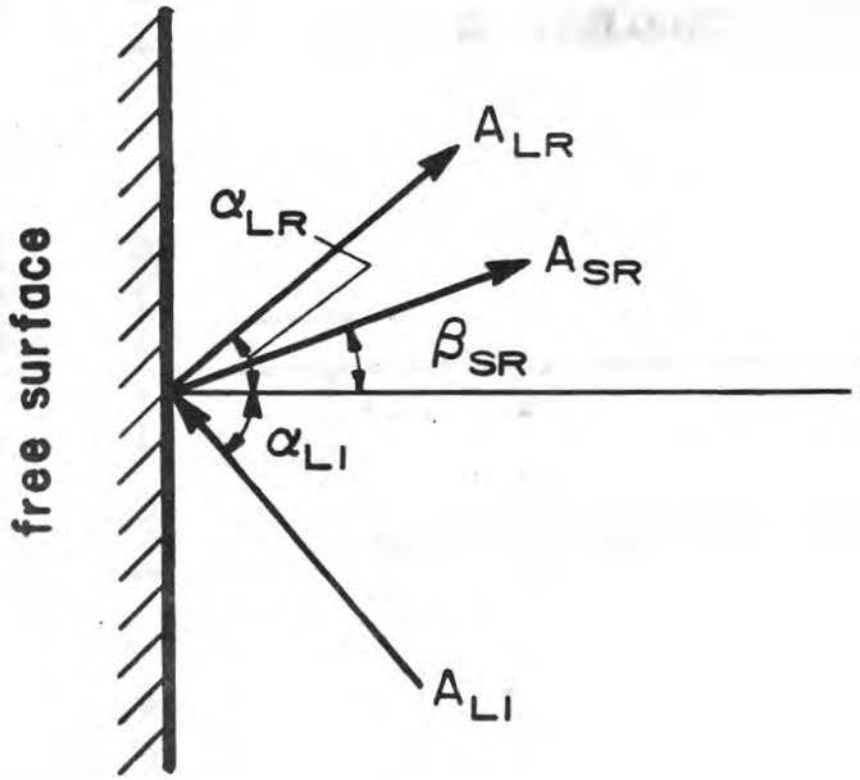

Figure 3.5. Reflection of a dilatation wave impinging obliquely on a plane free surface.

where: β_{SR} = angle of reflected distortion wave

α_{LR} = angle of reflected dilatation wave

These relationships apply for elastic waves of any shape (78).

Incidence of a plane wave at a boundary of two dissimilar materials generates four waves. Two waves, A_{LR}, A_{SR}, are reflected back into the original material as if the interface were a free boundary. Additionally, a dilatation, A'_{LR}, and a distortion wave, A'_{SR}, propagate in the dissimilar material. A schematic representation of this phenomenon is depicted in Figure 3.6. Note that the waves in the dissimilar material are refracted with respect to the angle of incidence.

The amount of energy transmitted through the interface depends on the ratio of the acoustic impedance, Z, of the materials. Acoustic impedance is defined as (59),

$$Z = \rho c \tag{3.8}$$

The ratio of transmitted energy to the energy of the incident wave is given by Eq. (3.9).

$$\frac{I_t}{I_i} = \frac{4Z_1Z_2}{(Z_1 + Z_2)^2} \tag{3.9}$$

where: I_t = intensity of transmitted waves

I_i = intensity of incident wave

Z_1 = impedance of incident wave material

Z_2 = impedance of transmitted wave material

The reflected wave intensity is related to the intensity of the incident wave by Eq. (3.10).

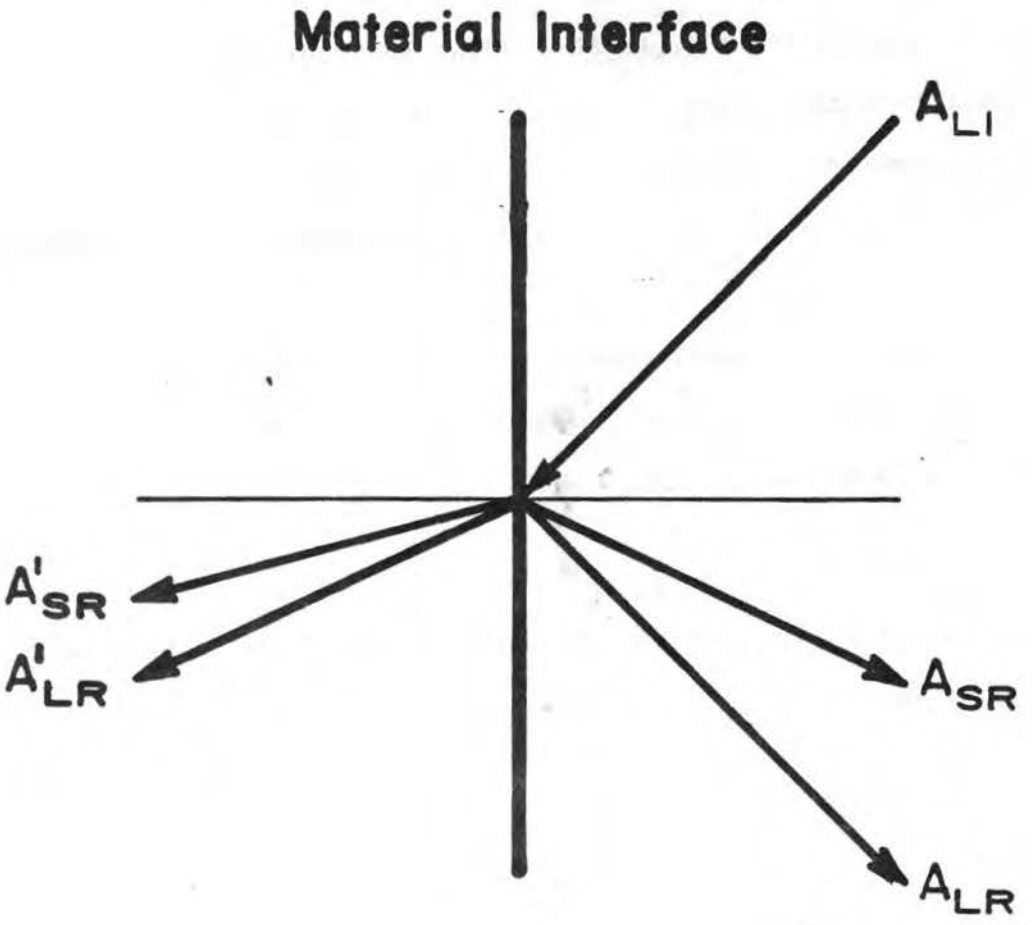

Figure 3.6. Reflection and refraction of an incident dilatation wave at a plane interface of two dissimilar materials.

$$\frac{I_r}{I_i} = \left[\frac{(Z_1 - Z_2)}{(Z_1 + Z_2)}\right]^{\frac{1}{2}} \tag{3.10}$$

where: I_r = intensity of reflected wave.

SI units of Z are kg/m^2sec. Typical values of Z for air, water, and steel are 400, 1.45×10^6, and 3.9×10^7 kg/m^2sec, respectively. Using Eq. (3.9) and the impedance values of air and water the transmitted energy from one material to another is calculated to be 0.11 percent. In general, the larger the difference in impedances between materials, the less the energy that is transmitted.

When the incident wave is nonplanar or the interface is curved the reflection and refraction patterns are complex and not easily identified (49). Description of these patterns, if possible, often require computer algorithms. Such complex phenomenon occur in wood due to ring curvature and anatomical features such as rays and cell cavities. The above is noted to impress upon the reader the complexity of wave propagation in wood and the difficulty of its mathematical description.

3.3 WAVE PROPAGATION IN VISCO-ELASTIC MATERIALS

The preceeding section on wave propagation assumed that the material is linearly elastic, i.e., a Hookean solid. If the material exhibits visco-elastic behavior, additional considerations of the stress wave propagation must be made (78). Stress waves in visco-elastic materials are characterized by strain components which lag in time relative to the varying stress components. This lag depends on a time associated with the interval required for the viscous stress to equalize (stress relaxation)(64).

A stress wave resulting from an impact is composed of a multiple number of frequencies. In a dispersive, visco-elastic material the higher frequency components travel at greater velocities (78), and cause the stress wave to change shape with time, exclusive of any reflections at boundaries.

Additionally, attenuation increases as frequency increases. This attenuation causes an initially nonsinusoidal wave, given sufficient time, to damp to an approximately sinusoidal form (64). Experimental results obtained in this study for wood exhibit this phenomenon (Figure 3.7). The attenuation of stress waves in wood, due to its visco-elastic nature, is said to be a result of internal friction. Internal friction, F, is the result of the mechanical energy of the stress wave being converted to other forms of energy such as sound and heat (36). Internal friction is calculated as,

$$F = 2ac/f \tag{3.11}$$

where: F = internal friction,

a = attenuation (dB),

f = frequency (Hz),

c = velocity at frequency f.

The attenuation, a, is determined using Eq. (3.12).

$$a = \frac{8.6186}{x} \ln \frac{\sigma_o}{\sigma_x} \tag{3.12}$$

where: x = distance between two points in the material

σ_o = stress at initial point

σ_x = stress at final point

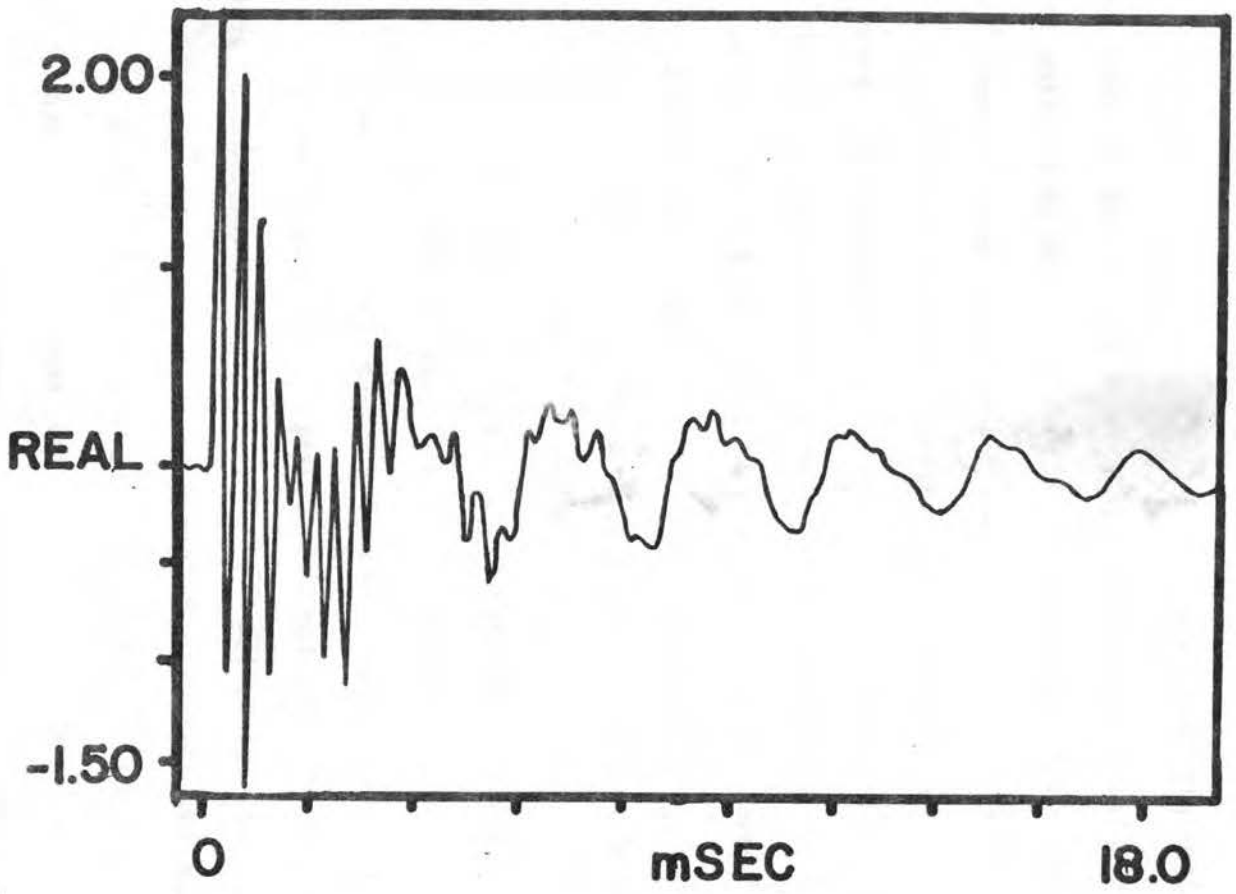

Figure 3.7. Wave propagation in wood exhibiting high-frequency damping.

Vibration damping is often reported as the logrithmic decrement, δ (12, 36, 63). "Log dec," as it is often termed, is one-half the value of internal friction.

$$\delta = \frac{F}{2} \tag{3.13}$$

3.4 WAVE PROPAGATION IN WOOD

Investigations concerning stress wave propagation in wood have primarily dealt with two criteria, the velocity and attenuation of a dialatation wave. Wave frequencies investigated mostly ranged from 100 Hz to 1 KHz. Courteau (12) reported that internal friction is independent of frequency in the range of 2000 to 4000 Hz. Bertholf (5) reported that one-dimensional elastic theory adequately predicted the major components of strain in wood rods caused by impact-induced stress waves. Inconsistencies were possibly due to the visco-elastic nature of wood and by neglecting lateral effects. In Bertholf's study only dilatation waves were considered and reflections were ignored.

Becker (3) use 1 MHz pulsed frequencies to find that attenuation in particle board gave significant indications of the tensile strength perpendicular to the board surface. Dunlop (16) working with sonic frequencies did not find the relationship to be significant for predictive purposes. Kaiserlik and Pellerin (36) used attenuation, gross density, and wave velocity to predict the tensile strength of 1 by 4 inch boards, with a coefficient of determination of 82 percent. Sellevold et al. (66), found that low temperature influenced the internal friction, with maximum damping occurring at a temperature of -96°C at a moisture content of 27 percent. The internal friction generally increased with increased moisture content. The effect of moisture content on internal friction and wave velocity has been

studied extensively (22, 33, 63). Employing flexural vibration, Pentoney (63) found increased internal friction with increased moisture content when the excitation frequency was lower than 500 Hz. James (33) and Dunlop (15) reported similar results employing dilatation waves. Dunlop's results are presented in Figure 3.8. Gerhards (21) found that wave propagation velocity, C_ℓ, decreased with increasing moisture content in a nonlinear fashion (see Figure 3.9).

Grain angle has been shown to be related to wave velocity. Depending on the species, propagation velocities perpendicular to grain are two to four times lower than parallel to grain (43). Typical velocities in Douglas fir range from 4000 to 6000 meters per second in the longitudinal direction. In lumber, the effect of cross grain on the measured velocity is influenced by the placement of the sensors. In the above study, Gerhards (23) found that the highest velocity was resulted when the sensors were placed along the same growth increment, even though this was not the shortest geometrical distance. If the sensors were placed in line with intervening cross grain the velocity was reduced. This is possibly due to a wave-guide effect where the waves are reflected within growth rings.

Konarski and Wazny (41) studied the influence of decay on wave velocity along with strength and elastic properties at oven-dry and 28 percent moisture contents. They discovered that interrelationships exist between rate of velocity change of decayed or undecayed state and such wood properties as density, MOE, tensile strength, and compressive strength.

Mann et al. (46), used the theory of wave propagation in an orthotropic plate to predict the elastic coefficients of milk carton

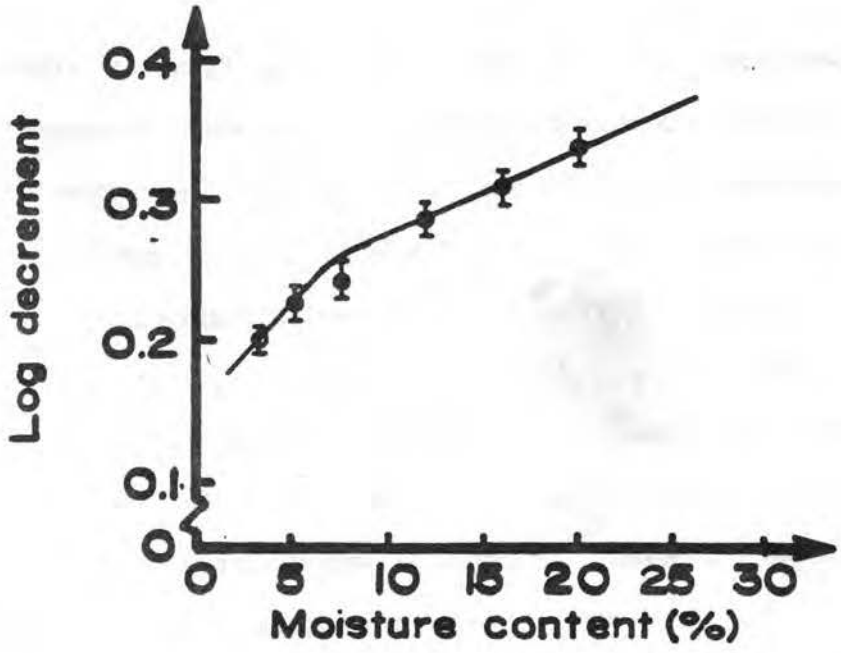

Figure 3.8. Relationship of logarithmic decrement to moisture content (15).

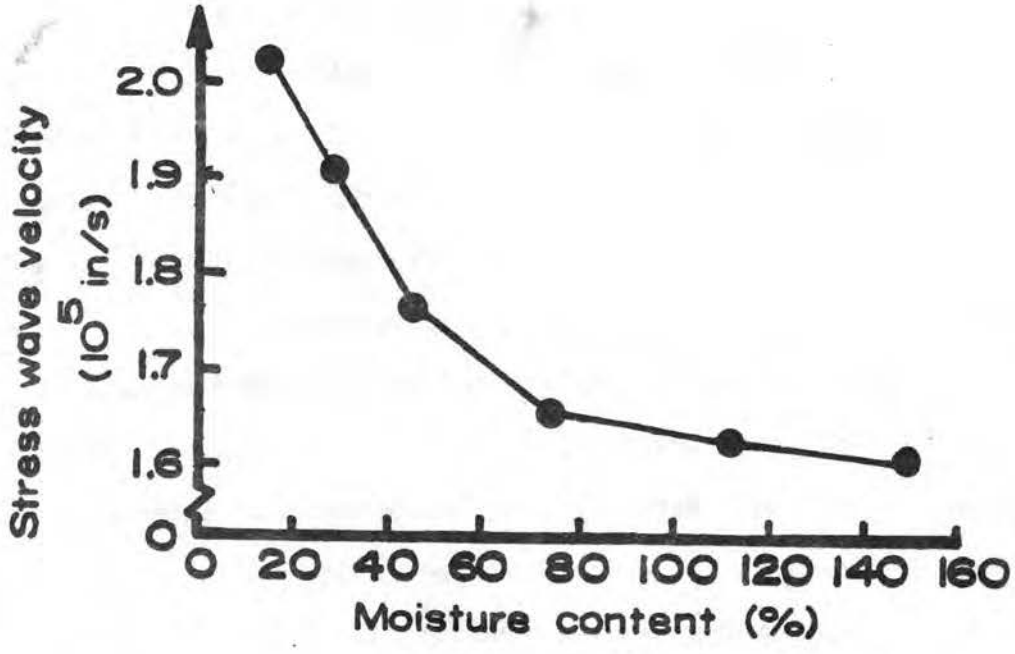

Figure 3.9. Relationship of stress wave velocity to moisture content in Sweetgum (21).

stock. An ultrasonic pulse technique was used and wave velocities at different orientations formed the basis of characterizing the dispersive nature of the material.

In wood, measurements of stress wave velocity and attenuation have been shown to be strongly affected by grain angle, moisture content, and decay. Furthermore, the strength of wood is also dependent on these factors. Unfortunately if only wave velocity and attenuation are measured, the material properties of interest cannot be completely defined. Therefore further measurement methods need to be developed to accurately predict the strength and stiffness of wood.

3.5 NATURE OF WAVEFORM DATA

A description of stress wave propagation in wood is mathematically difficult due to reflection, scattering, superposition of wave types, and the influence of numerous anatomical characteristics. A rigorous mathematical solution has not been obtained even for the simpler case of a three-dimensional finite isotropic elastic bar (5). The absence of a workable mathematical model prevents the prediction of wave characteristics with the needed precision. As a consequence, data representing wave propagation in wood is nondeterministic (random). However, analysis techniques are available to describe such behavior through the use of probability statements and statistical averages.

The analysis procedures for such random data are dependent upon the nature of the data. Various types of data will be described and the wave propagation classified into one of the categories. The appropriate analysis techniques chosen depends on the selected category.

Before the classification of random data the concept of sampling needs to be introduced. A single time history representing a random phenomenon is termed a "sample function." If one only observes the phenomenon for a finite time interval, the time history is termed a "sample record" (4). Theoretically, a random phenomenon could produce an infinite number of sample functions, the collection or ensemble of which is termed a random (stochastic) process, Figure 3.10.

The property of a random process at any instant in time may be theoretically obtained by averaging the values of each sample record of the random process. The collection of sample records is termed an "ensemble." A correlation (R_x) between the values of a random process at two times, t and $(t + \tau)$, may also be computed by multiplying the respective values $x(t)$ with $x(t + \tau)$ and dividing the product by the number of sample records. When the mean value, $\mu(t)$, and the correlation, R_x, between t and $(t + \tau)$ does not appreciably change with different selections of t, the process is defined as being "stationary." A nonstationary random process does not possess the above property. Most stationary processes are ergodic, i.e., the number of sample records used has little significance. Since the statistical properties of each sample do not vary appreciably with time, a stationary ergodic random process may be satisfactorily characterized by a single sample record.

An important type of nonstationary process is a transient. A transient is a process which has a well-defined beginning and end over the length of the sample record. The analysis techniques for stationary processes may be used for transient phenomenon with the additional requirement that several sample records, an ensemble, be observed to increase the accuracy of the prediction.

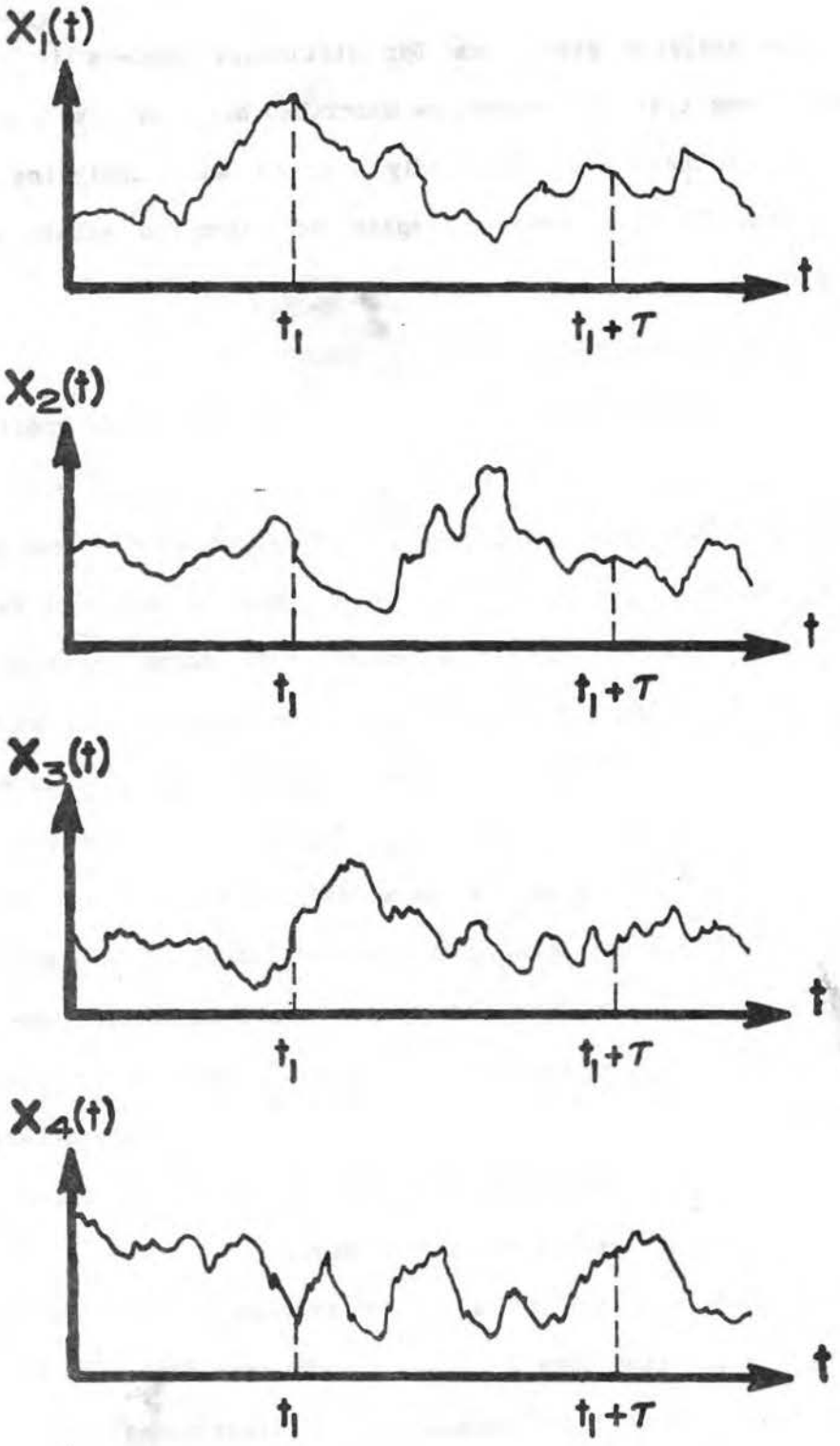

Figure 3.10. Ensemble of sample functions forming a random process.

The analysis procedures for stationary process is considered. Keep in mind that the techniques described here are also applicable to transient phenomenon. The only concern when analyzing transient phenomenon is that enough samples be taken to ensure acceptable accuracy.

3.6 CHARACTERIZATION OF SYSTEM RESPONSE

The propagation of a stress wave requires the application of energy to a solid (e.g., wood). The applied energy will produce a response in the solid which for this research is a stress wave. The relationship of the stress wave to an input is solely a function of the characteristics of the material. By using waveform analysis techniques relating the stress wave to the input one can determine the characteristics of wood as a dynamic system. In this research, the input is an impact transient, the "black box" is the wood, and the response is the stress wave as shown in Figure 3.11. A change in wood properties alters the relationship of the output to the input. Before examining various methods for system characterization one needs to know how to quantify the input and output. Using these principles we can then relate the two processes and obtain the characteristics of the system. In effect, the wood properties are correlated with the propagation parameters of the stress wave.

The sample record of a random process (e.g., stress wave) is measured in the time domain. That is, the dependent variable is time. Alternatively, the time record may be transformed to a frequency domain by use of fourier transforms. Although the above two representations are equivalent in terms of the data they describe, analysis in the frequency domain gives certain descriptive parameters which are

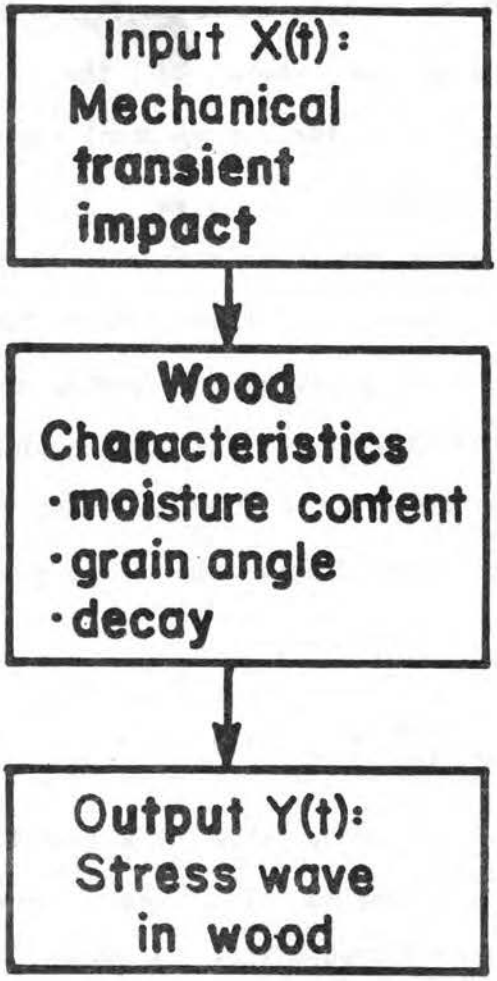

Figure 3.11. Representation of wave propagation in wood as a "black box" system.

often of greater value. The analysis procedures are described next for a time history in both the time domain and frequency domain.

3.6.1. Time Domain Analysis

The basis for all analysis is a time record of the observed phenomenon with an example given in Figure 3.12. Units of the time record correspond to those of the transducer used during experimentation. Units for all spectral analysis functions described are summarized in Table 3.1.

Autocorrelation refers to a measure of the dependence of values at one time to those at another time. The estimate of an autocorrelation value is given by multiplying the values of $x(t)$ and $x(t + \tau)$ and dividing the product by the time record length, T. The autocorrelation function, $R_x(\tau)$, expresses the value of the autocorrelation for values of from zero to the record length. In equation form,

$$R_x(\tau) = \lim_{\tau \to \infty} \frac{1}{\tau} \int_0^{\tau} x(t)\, x(t + \tau) d\tau \qquad (3.14)$$

Commonly, $R_x(\tau)$ is plotted as a function of τ to obtain an autocorrelogram. Examples of autocorrelograms for four types of signals are given in Figure 3.13. A maximum value always occurs at a time lag (τ) of zero. If the data are periodic the autocorrelogram will also be periodic. When noise is present the correlation decreases as the time lag increases. The principal application for an autocorrelogram is the detection of the presence of deterministic data in a signal masked by random noise (4).

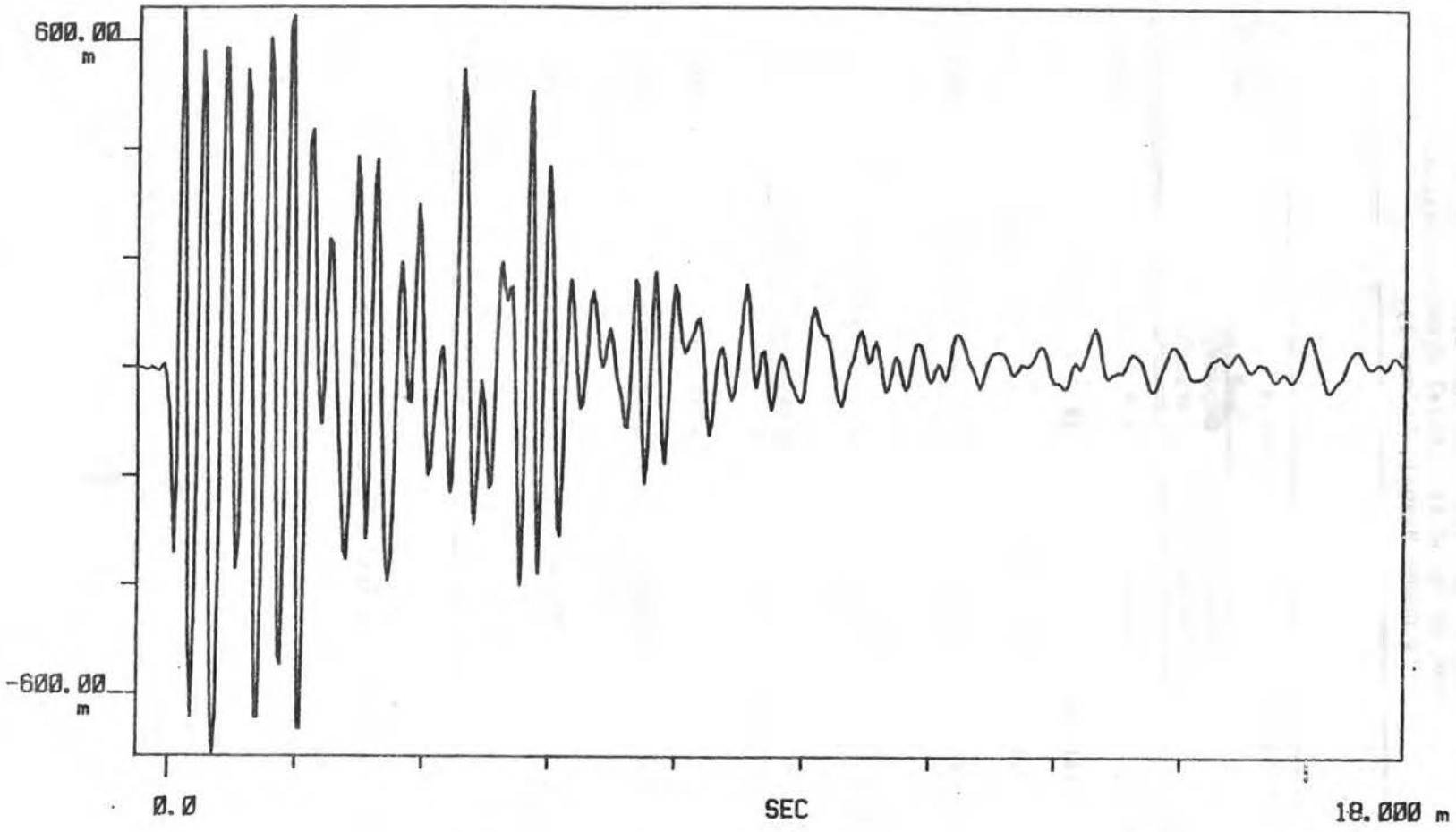

Figure 3.12. Time record of a stress wave in wood.

Table 3.1. Units of amplitude for spectral analysis functions (from HP 5423A Structural Dynamics Analyser User's Guide Manual, Volume 1).

Function	Units		Setting on HP5423A
	Independent Variable	Dependent Variable	
Time Record	Seconds	K * Volts	REAL
Auto-Correlation	Seconds	$(K * Volts)^2$	REAL
Cross-Correlation	Seconds	$K_1 * K_2 * Volts^2$	REAL
Power Spectral Density	Frequency (Hz)	$\left\{ \frac{(K * Volts)^2}{Hz} \right\}^{1/2}$	MAG
Energy Spectral Density	Frequency (Hz)	$\left\{ \frac{(K * Volts)^2 \, sec}{Hz} \right\}^{1/2}$	MAG
Cross-Energy Spectral Density	Frequency (Hz)	$\left\{ \frac{(K_1 * K_2 * Volts^2) sec}{Hz} \right\}^{1/2}$	MAG
		Degrees	PHASE
Conerance Function	Frequency (Hz)	Unit-less	MAG
Frequency Response Function	Frequency (Hz)	K_2 / K_1	MAG
		Degrees	PHASE

K = engineering units per volt output of transducer.

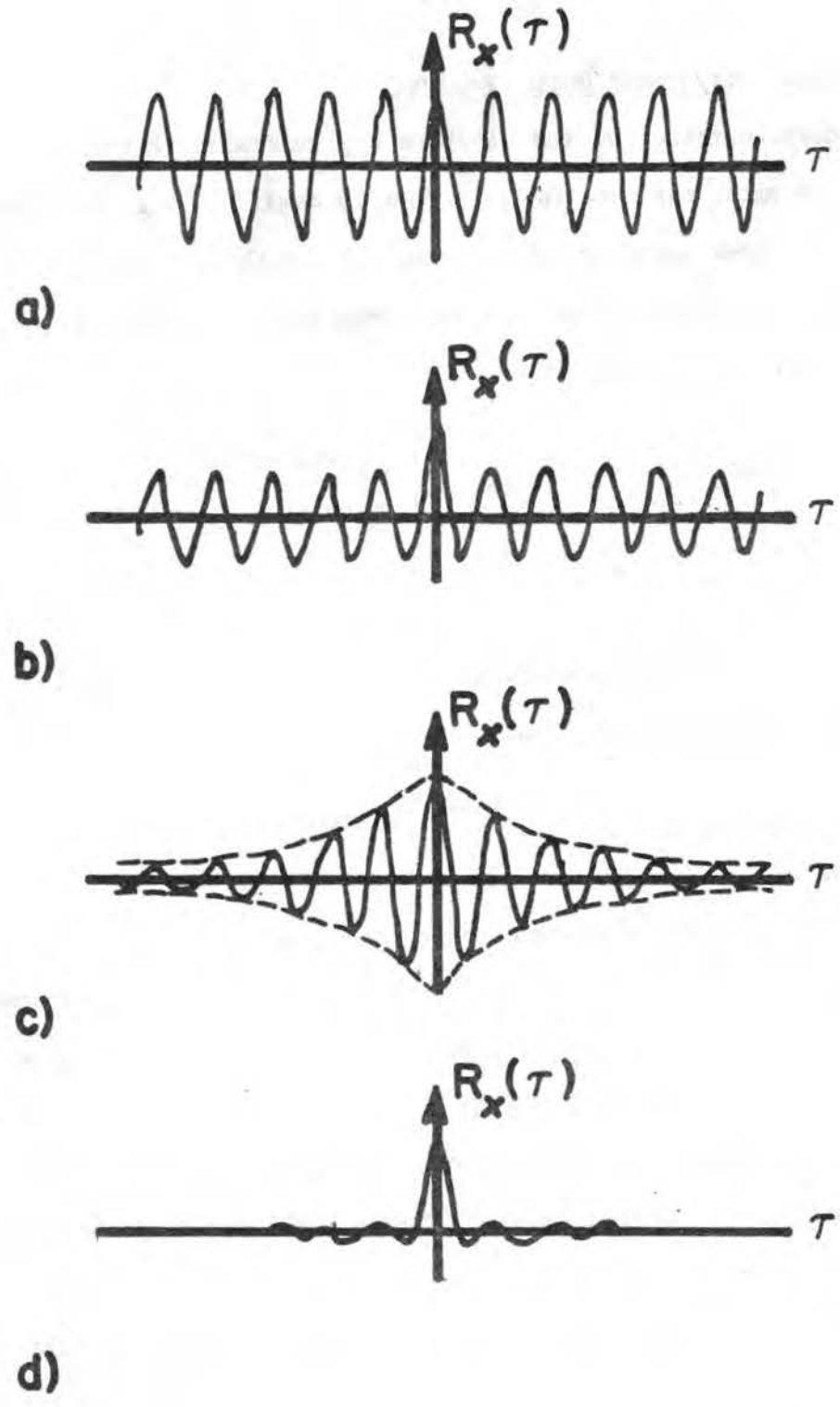

Figure 3.13. Autocorrelation function plots (autocorrelograms):
a) Sine wave,
b) Sine wave plus random noise,
c) Narrow-band random noise,
d) Wide-band random noise.

3.6.2. Frequency Domain Analysis

Characteristics of the waveform are generally better interpreted by transforming the data to the frequency domain. This transformation is accomplished by operating on the data with the discrete Fourier transform. By definition, the discrete Fourier transform, FT, of a sequence of data, $x_i(t)$, is;

$$FT\{x_k(t)\} = \hat{x}_k(f) = \frac{1}{N} \sum_{r=0}^{N-1} x_r e^{-i(2\pi kr/N)} \tag{3.15}$$

where: $k = 0, 1, 2, \ldots, N-1,$

$r = 0, 1, 2, \ldots, N-1,$

x_r = measured dependent value.

It can be shown that the transform pair exists, i.e.,

$$FT\{\hat{x}_k(f)\} = x_k(t) = \sum_{k=0}^{N-1} \hat{x}_r e^{i(2\pi kr/N)} \tag{3.16}$$

where: $\hat{x}_r$ = FT of measured dependent value.

By operating on the time record $x_i(t)$ with the FT, the information is expressed as a function of frequency, $x_i(f)$. On the digital computer the speed of this procedure has been enhanced by the development of the fast fourier transform (FFT) algorithm. Reviews of this procedure are given by Newland (56), Kaplan (38), and Bendat and Piersol (4).

If we apply the FT to the autocorrelation function the Power Spectral Density Function (PSD) is obtained (56). The PSD describes the general frequency data composition in terms of its mean square value. In equation form, the PSD function ($G_x(f)$) is;

$$G_x(f) = 2(\Delta t)[\hat{R}_o + 2 \sum_{r=1}^{m-1} \hat{R}_\tau \cos(\frac{\pi rf}{f_c}) + \hat{R}_m \cos(\frac{\pi mf}{f_c})] \tag{3.17}$$

where: Δt = time interval between samples,

m = maximum lag number,

$\hat{R}_\tau$ = estimate of the autocorrelation function at lag τ,

$\hat{R}_m$ = estimate of autocorrelation function at time lag ($m\tau$),

f_c = $\frac{1}{2}\Delta t$, cutoff frequency.

The PSD is related to the autocorrelation function by the relationship;

$$G_x(f) = 2 \int_{-\tau_m}^{\tau_m} R_x(\tau) \cos(2\pi f\tau) d\tau \qquad (3.18)$$

where: τ_m = maximum time lag value

The Energy Spectral Density Function (ESD) of a waveform is closely related to its PSD. The ESD is commonly used when a transient waveform is analyzed. The ESD ($\hat{G}_x(f)$) can be calcualated from the PSD by;

$$\hat{G}_x(f) = TG_x(f) \qquad (3.19)$$

where: T = entire record length

The predominant frequencies of a system may be determined by inspection of the ESD. Relative energy at a frequency is obtained from a measure of the amplitude at that frequency. The ESD of the time record in Figure 3.12 is shown in Figure 3.14. Note the predominance of frequency content concentrated in a narrow bandwidth at approximately 3000 Hz.

For our purposes, the autocorrelation function and the energy spectral density are tools to help understand the behavior of wave propagation in wood.

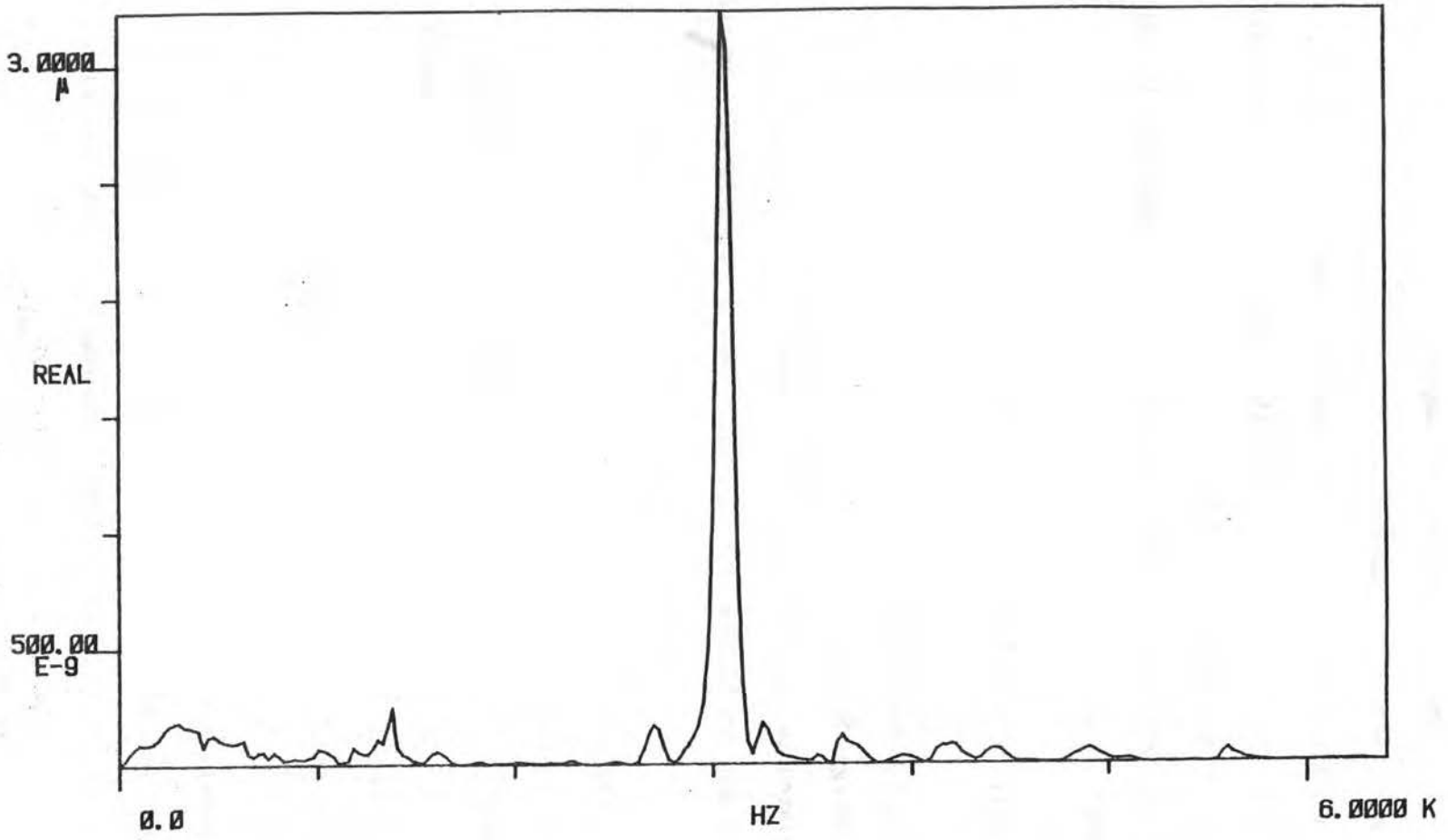

Figure 3.14. Energy spectral density of time record in Figure 3.12.

3.7 SYSTEM DYNAMICS

As mentioned previously, a system is defined by its input-output relationship. The time record, ESD, and autocorrelation function will be used to develop a relationship between the stress wave input and output for wood. A schematic presentation of this development is given in Figure 3.15.

The analysis procedures are based on several assumptions about the characteristics of the system. Schematically, a single input, single output system was shown in Figure 3.11. Three principal assumptions are that the system is represented by constant parameters, it is linear, and the system input $x(t)$ is from a well-defined stationary random process. Constant parameter implies that all system properties are time invariant. Linearity implies the validity of the principle of superposition.

There are several related methods to describe the input-output relationship of a system. The weighting function $h(\tau)$ and the frequency response function $H(f)$ define the relationship in the time and frequency domains respectively. Physically, $h(\tau)$ is the response of a system to a unit impulse applied a time τ before. The unit impluse is of the form;

$$x(t) = I\delta(t) \tag{3.20}$$

where: I = amplitude of input,

$\delta(t)$ = dirac delta function.

The unit impulse is often a sharp impact or hammerblow. Once the response of a system to a unit impulse is known, the response $y(t)$ of the system to an arbitraty input $\beta(t)$ can be determined by use of the convolution integral, i.e.,

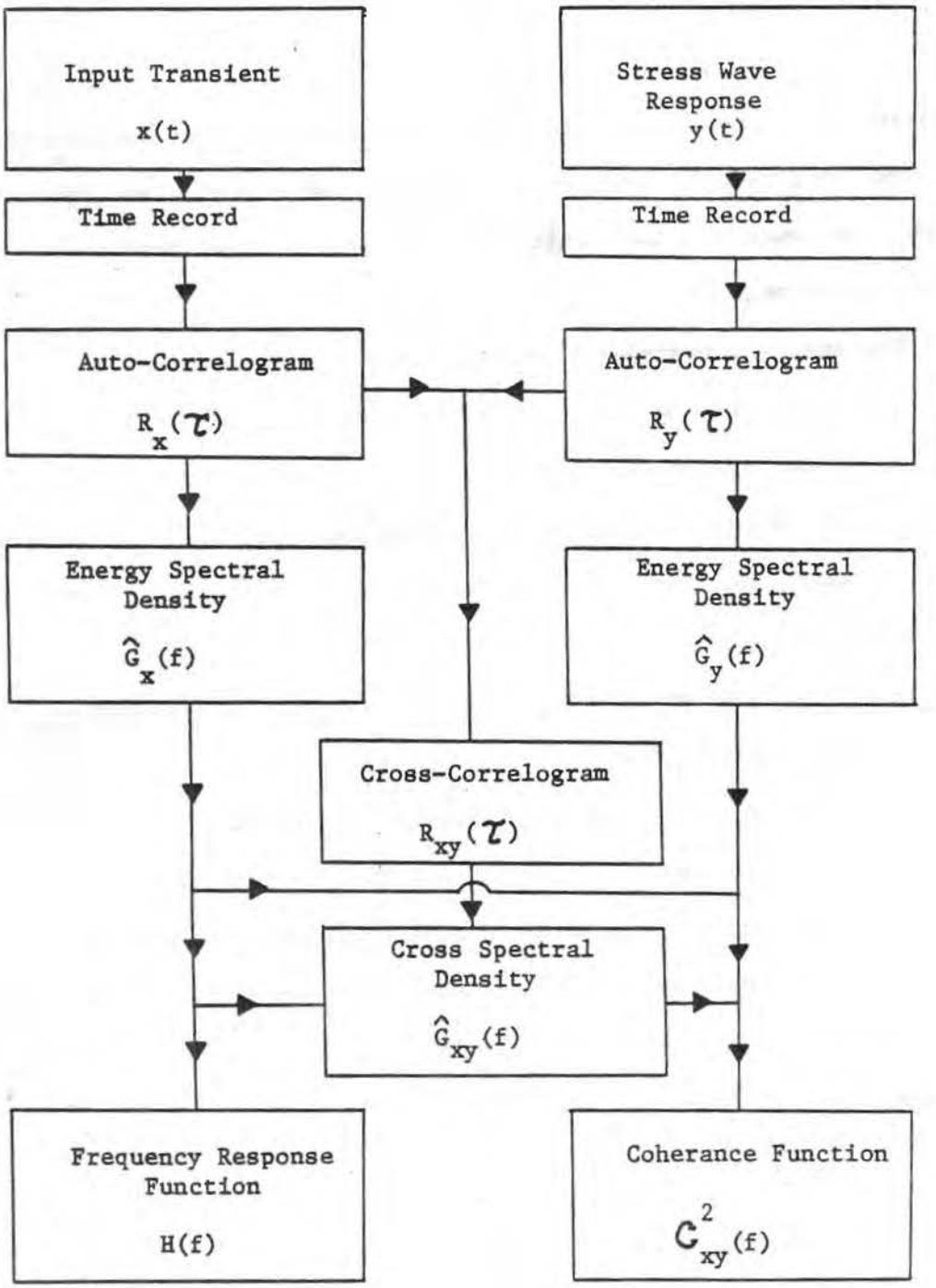

Figure 3.15. Flow chart of spectral analysis procedures for calculation of frequency response function.

$$y(t) = \int_0^\infty h(\tau)\, \beta(t - \tau)d\tau \tag{3.21}$$

The frequency response function, H(f), is the fourier transform of the convolution integral and gives the system response to an arbitrary input in the frequency domain. In equation form, H(f) is given by:

$$H(f) = \int_0^\infty h(\tau)d^{-i(2\pi f\tau)} \tag{3.22}$$

Alternatively, H(f) may be determined if the governing equation for the system is known. Although this is seldom practical, the development of H(f) by this method is instructive for its physical significance. For the mechanical system in Figure 3.16 a), the governing differential equation is:

$$5\ddot{y}(t) + 20\dot{y}(t) + 10y(t) = x(t) \tag{3.23}$$

The applied forcing function x(t) in Figure 3.16 b) is defined as:

$$x(t) = \begin{cases} At & 0 \leq t \leq 1 \\ 0 & t > 1 \end{cases} \tag{3.24}$$

Taking the fourier transform of Eq. (3.23) we obtain:

$$-\omega^2 Y(\omega) + 4i\omega Y(\omega) + 2Y(\omega) = X(\omega) \tag{3.25}$$

where: ω = circular frequency (radians),

$Y(\omega)$ = fourier transform of system response y(t),

$X(\omega)$ = fourier transform of system input x(t).

Equation (3.25) may be arranged to;

$$Y(\omega)(-\omega^2 + 4i\omega + 2) = X(\omega) \tag{3.26}$$

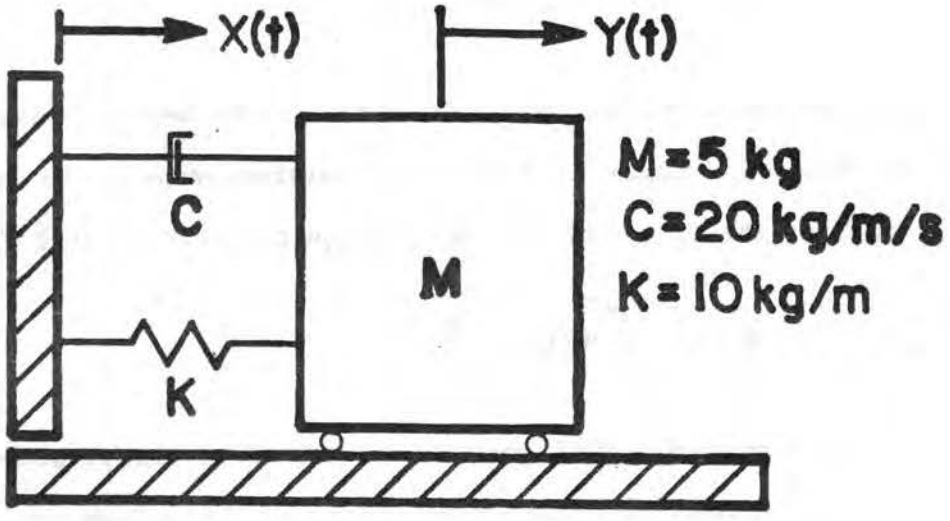

a) Mechanical system

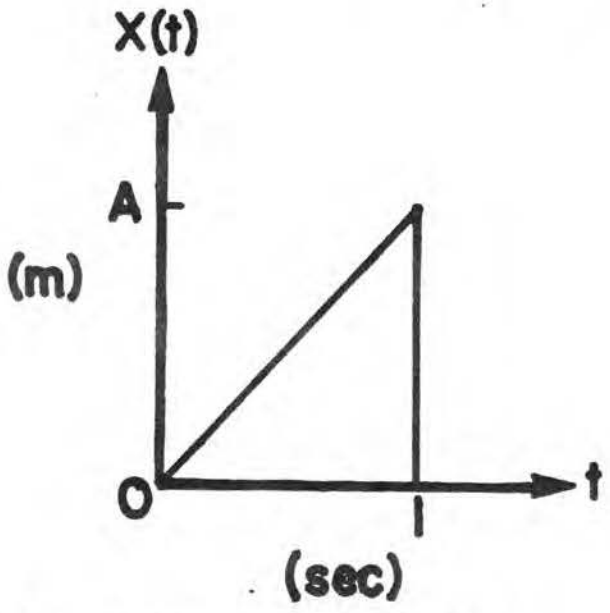

b) System input X(t)

Figure 3.16. Heuristic mechanical vibratory system.

$$Y(\omega) = \frac{1}{-\omega^2 + 4i\omega + 2} X(\omega) \tag{3.27}$$

$$Y(\omega) = H(\omega)X(\omega) \tag{3.28}$$

where: $H(f) = 2\pi H(\omega)$ is the frequency response function.

Thus, the response of a system $y(t)$ to any input $x(t)$ may be determined in the transform space by multiplying the frequency response function $H(\omega)$ by the fourier transform of the input $X(\omega)$ and then taking the inverse transform of their product.

The general form of $H(f)$ in Eq. (3.22), is complex valued. It is often beneficial to write $H(f)$ in polar notation. A complex number of the form;

$$z = a + bi \tag{3.29}$$

may be rewritten as;

$$z = r\, e^{i\theta} \tag{3.30}$$

where: $r = |z| = \sqrt{a^2 + b^2}$

$e^{i\theta} = \cos\theta = i \sin\theta$

In polar notation then, $|H(f)|$ is of the form;

$$H(f) = |H(f)|\ e^{-i\theta(f)} \tag{3.31}$$

where: $|H(f)|$ = amplitude response of system,

$\theta(f)$ = phase response of system.

Let us examine a hypothetical situation where the amplitude response $|H(f)|$ is shown in Figure 3.17 a) and the phase response $\theta(f)$ is given in Figure 3.17 b). Assume that a 1000 Hz sine input with an amplitude of one-half inch is applied to the system. The

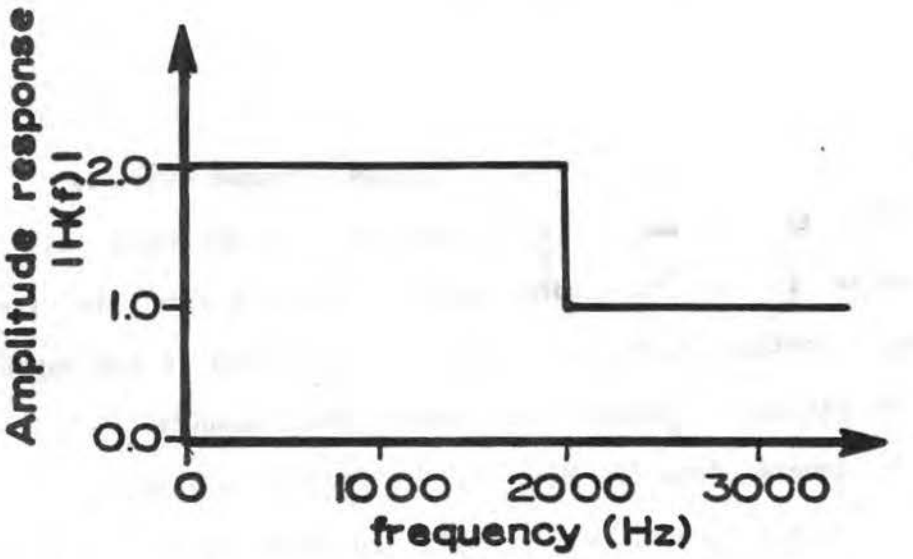

a) System amplitude response

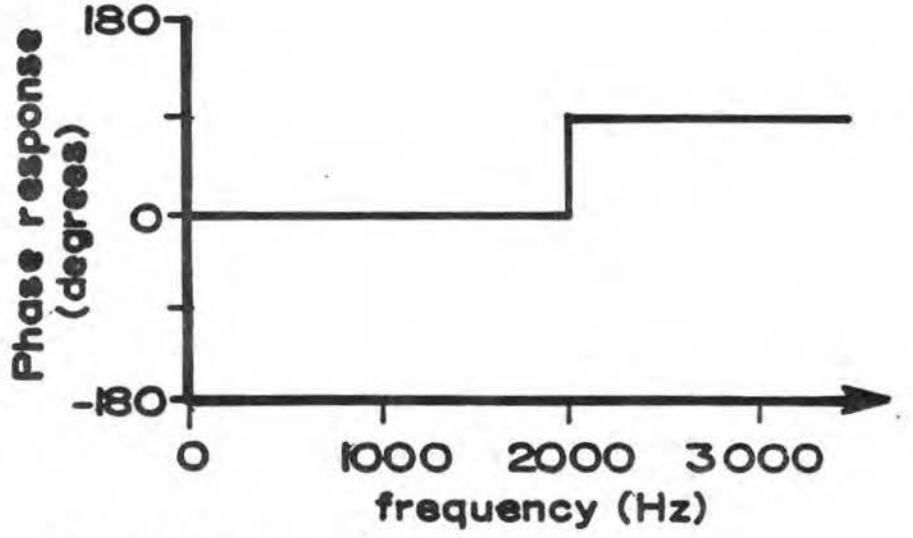

b) System phase response

Figure 3.17. Hypothetical frequency response function.

system would experience a gain of two and a phase shift of zero degrees. Thus, the output would be a 1000 Hz sine wave with a displacement of one inch. A system input $x(t)$ consisting of a 3000 Hz sine wave with a displacement of one-half inch would undergo a gain of one and a phase shift of 90 degrees. The output $y(t)$ would then be a 3000 Hz cosine wave with a one-half inch displacement.

If the frequency response function is known, then the system response for an input $x(t)$ can be predicted. In typical applications we are interested in obtaining $H(f)$. The method used in this research involves the measurement of the input and output and by following the procedures outlined in Figure 3.15 to estimate $H(f)$.

Once the input and output are measured and characterized by their autocorrelation function and ESD, the cross-correlation function, $R_{xy}(\tau)$ can be determined. The $R_{xy}(\tau)$ is defined as the correlation between a value at time t of the input with the value at time $(t + \tau)$ of the output. In equation form;

$$R_{xy}(\tau) = \frac{1}{N - r} \sum_{n=1}^{N-r} x_n y_{n+r} \tag{3.32}$$

where: $r = 0, 1, 2, \ldots, m$,

m = maximum lag number,

N = maximum number of data values.

Cross-correlation is typically plotted as a function of time lag (τ), with the plot termed a cross-correlogram. Consider the cross-correlogram plotted in Figure 3.18. The best correlation between the output and input occurs after a time lag of approximately 9 msec. The periodic nature of $R_{xy}(\tau)$ indicated the input and system response were also periodic.

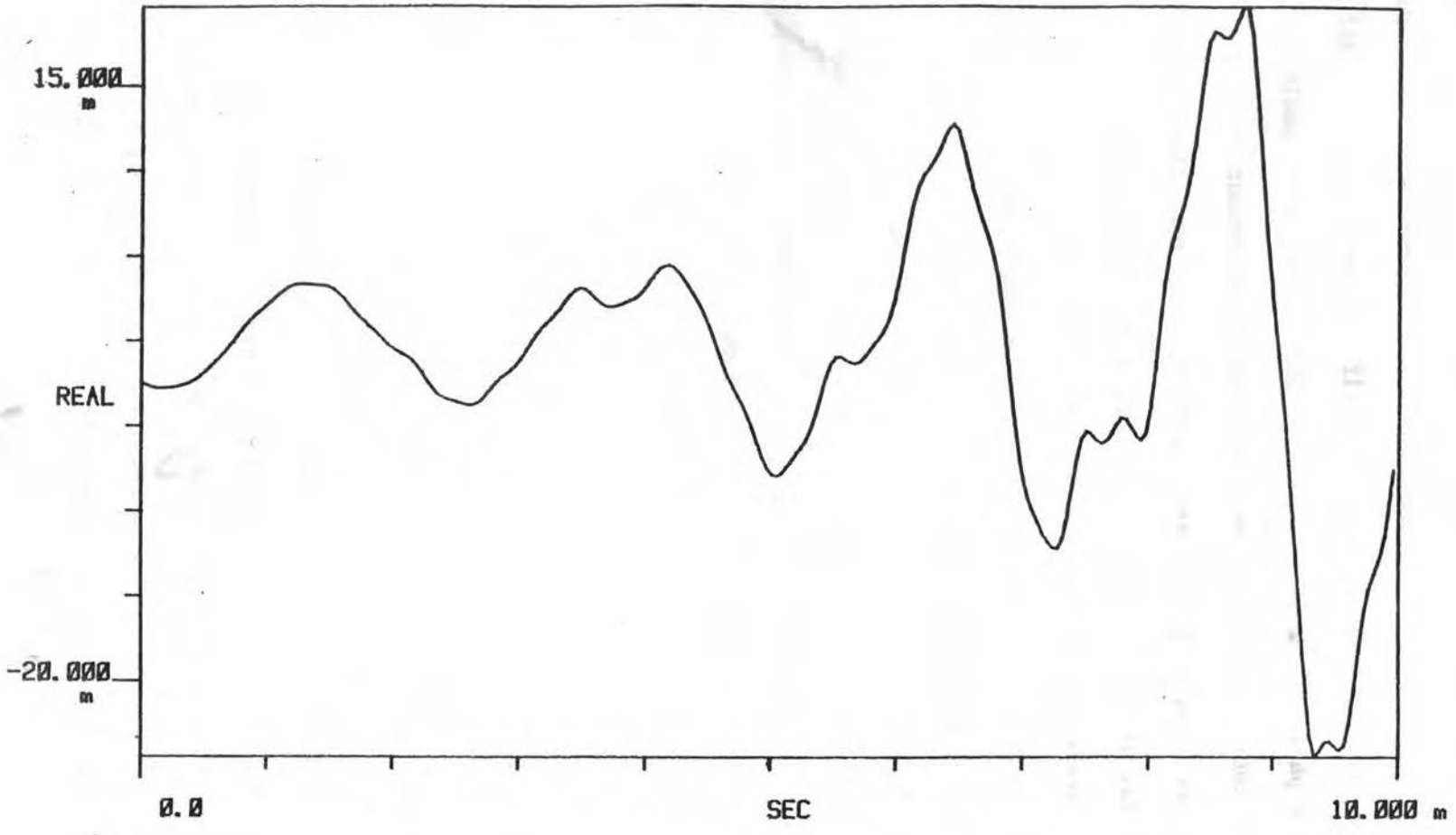

Figure 3.18 Cross-correlogram of two waveforms.

An application for a cross-correlogram is the measurement of time delays. For a linear system, the cross-correlogram will directly determine the time required for propagation. This time corresponds to the maximum average product of the two signals. If the velocity through the system is frequency dependent, a distinct maximum value may not be present in the cross-correlogram. When this occurs use of the cross-spectra yields more useful information.

The cross energy spectral density $\hat{G}_{xy}(f)$, or cross-spectra, is the fourier transform of the cross-correlation function. Since the cross-spectra is complex valued, it may be expressed in terms of real and imaginary components;

$$\hat{G}_{xy}(f) = C_{xy}(f) - iQ_{xy}(f) \tag{3.33}$$

where: $C_{xy}(f)$ = coincident spectral density function,

$Q_{xy}(f)$ = quadrature spectral density function.

Like $H(f)$, $\hat{G}_{xy}(f)$ may be written in complex polar notation such that:

$$\hat{G}_{xy}(f) = \left|G_{xy}(f)\right| e^{-i\theta_{xy}(f)} \tag{3.34}$$

where: $\left|\hat{G}_{xy}(f)\right|$ = cross-spectra gain function,

$\theta_{xy}(f)$ = cross-spectra phase function.

Note that the phase information obtained from the cross-spectra is identical to the phase response $\theta(f)$ determined for the frequency response function. The magnitude $\left|\hat{G}_{xy}(f)\right|$ is related to the energy spectral density of the input and output in the following manner;

$$\left|G_{xy}(f)\right|^2 \leq \hat{G}_x(f)\hat{G}_y(f) \tag{3.35}$$

An important application of the cross-spectrum is the measurement of time delays through a system in which the velocity is frequency

dependent. The propagation delay (τ) through a system at any frequency f is given by;

$$\tau = \theta_{xy}(f)/2\pi f \tag{3.36}$$

where: $\theta_{xy}(f)$ = phase function (radians),

τ = time delay (seconds).

The cross-ESD is related to the frequency response function as shown below;

$$\hat{G}_{xy}(f) = H(f)\hat{G}_{x}(f) \tag{3.37}$$

As indicated by Eq. (3.37), H(f) may be calculated from the quotient of the cross spectrum and input spectrum, i.e.,

$$H(f) = \hat{G}_{xy}(f)/\hat{G}_{x}(f) \tag{3.38}$$

We have shown how the frequency response function may be determined from measurement of the input and output of a system. A logical extension is the determination of the accuracy to which H(f) has been estimated. The measure of the accuracy of H(f) is given by the coherence function ($C^2_{xy}(f)$). Coherence is calculated from the amplitude of the cross-spectra and the ESD of the input and output as follows;

$$C^2_{xy}(f) = \frac{G_{xy}(f)^2}{G_x(f)G_y(f)} \tag{3.39}$$

The coherence function is a measure of the correlation of input and output at some frequency f. Values of $C^2_{xy}(f)$ may range from 0 to 1, and are unitless. A value of zero indicates no correlation while $C^2_{xy}(f) = 1.0$ indicate a perfect correlation, i.e., x(t) and y(t) are fully coherent. Values of $C^2_{xy}(f)$ less than one may be caused by any of three possibilities;

1. Extraneous noise is present in the measurements.
2. The system relating $x(t)$ and $y(t)$ is not linear.
3. $y(t)$ is an output due to an input $x(t)$ as well as other inputs.

The coherance function may be used to give confidence intervals of the estimate of the frequency response function $H(f)$. For a complete presentation of this topic, see Bendat and Piersol (4).

We have seen that the relationship of output to the input of a system is a function of its dynamic characteristics. Use of such spectral analysis procedures as autocorrelation, cross-energy spectral density, and frequency response function allow us to ascertain the system dynamic character from measurement of the input and output.

The above techniques may be applied to wood in which an input has created a stress wave. Other investigators have found the velocity and attenuation of stress waves to be influenced by such wood properties as moisture content, grain angle, and decay. The strength and stiffness of wood is also known to be influenced by these same material characteristics. Unfortunately, the complexity of material organization has prevented a closed form solution to wave propagation in wood. However, by known variation of wood characteristics and analysis of the stress wave output by spectral analysis techniques, an understanding of the influence on dynamic properties may be obtained. Once these relationships are established, further spectral analysis will indicate the characteristics of the wood itself and hence the strength and stiffness of an individual member.

Chapter 4

EXPERIMENTAL PROCEDURE

4.1 EXPERIMENTAL DESIGN

The strength of wood is known to be the result of a complex interaction of such material properties and environmental factors as density, anatomy (i.e., cell types, juvenile vs. mature wood, etc.), rate of loading, inhomogeneities (such as knots, and checks), grain angle, moisture content, decay, and temperature. Moisture content, grain angle, and decay were selected as the major factors for inclusion in this experiment. The choice of variables was based on their relatively major contribution to the strength and stiffness properties of any one species of clear wood.

The experimental design was divided into two phases. Phase one dealt with moisture content and grain angle as the material variables. This portion of the experiment was designated GAMC (Grain Angle-Moisture Content). A total of 9 grain angles were investigated. The desired grain angle values were 0, 3, 6, 10, 15, 20, 30, 60, and 90 degrees. Moisture content varied from an air-dry value of approximately 7 percent to a saturated condition. The seven moisture content groups tested were 7, 15, 20, 25, 30, 50, and saturated conditions. The condition of grain angle and moisture content resulted in 63 specimens.

In the second phase involving studying the influence of decay, it was felt that a variation in wood properties was also desirable. Therefore, three grain angles, 0, 10, and 90 degrees, were used. The moisture content of all specimens was above the fiber saturation point. Sets of specimens from each grain angle group were decayed for a length of time up to 26 weeks. The 53 specimens for this phase, designated DEC (Decay), are given in Table 4.1.

4.2 MATERIAL SELECTION

All specimens were Douglas-fir (Pseudotsuga menziesii, Mirb.). This species was selected due to its economic importance and availability. For the GAMC study, a tree was selected from a stand approximately 40 miles west of Fort Collins, CO, at an elevation of approximately 7500 feet. Only sections from the bottom ten feet of the bole were used for the study. A second Douglas-fir log from the coast of California was provided by Anton Pugel of Arcata Redwood for material used in the DEC study.

4.3 SPECIMEN PREPARATION

Each log section was cut to be 12 to 20 inches in length. The sections were cut with a chain saw along the longitudinal axis into two half-cylinders. A three-inch wide slab was then cut from the pith outward as illustrated in Figure 4.1. These slabs were then squared. Specimens were cut at the nominal grain angle by a table saw, with the grain deviation occurring primarily in the LT plane. As illustrated in Figure 4.2, slabs 1¼ inch wide were cut at the desired grain angle. Each slab was then ripped to the desired ½ inch specimen thickness. These rough-cut specimens were then inspected and only those free of knots and other defects were selected for inclusion in the study. The

Table 4.1. Specimen and parameters for DEC study.

		Grain Angle		
		0	20	90
Weeks Decayed	0	2	1	2
	2	2	2	2
	4	2	2	2
	6	2	0	2
	8	2	2	2
	12	2	0	2
	18	2	1	2
	20	2	1	2
	23	2	1	2
	26	2	1	2

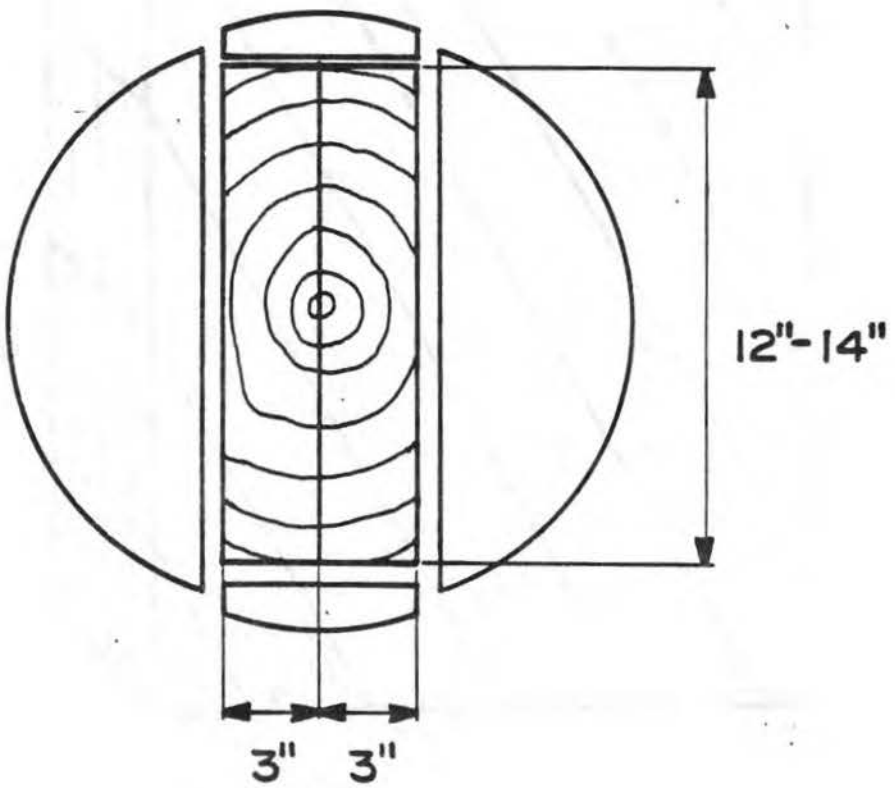

Figure 4.1. Material selection from log.

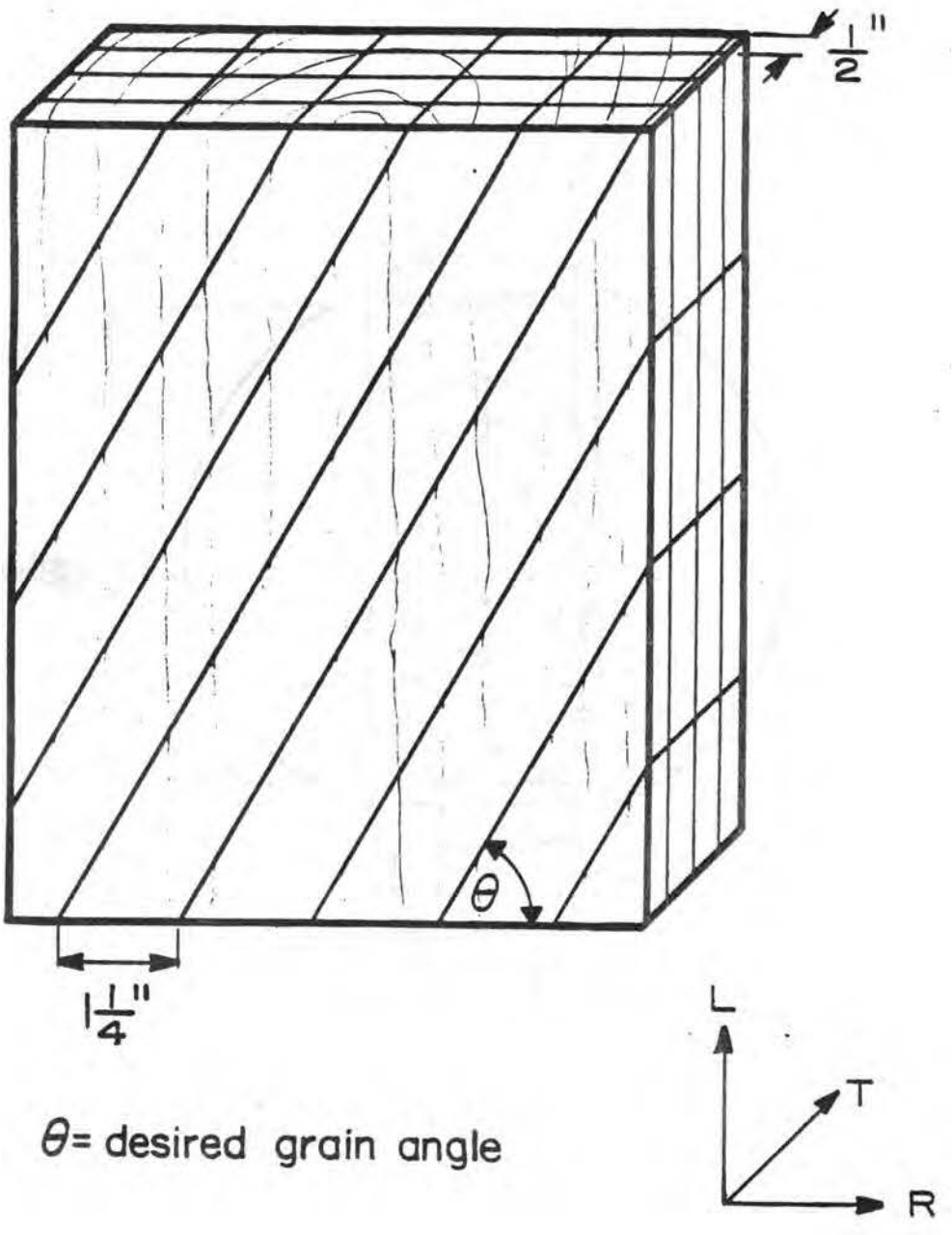

Figure 4.2. Specimen selection from wood slabs.

same procedure was followed for the DEC study with the exception that the 0 degree specimens were cut from the outside of the half-cylinders as shown in Figure 4.3. All decay study specimens were then machined to final test dimensions of 11" x1" x3/8" as shown in Figure 4.4. The GAMC specimens were left oversize to account for shrinkage due to drying and finished after they reached their designated moisture content.

4.3.1 Moisture Conditioning

Samples from the rejected specimens (after cutting out the knots) representing similar locations within the tree were used in each group to assist in reaching the desired moisture content. The saturated moisture content group was subjected to three alternating cycles of pressure (40 psi) and vacuum (10 psi) under water to overcome the refractive nature of Rocky Mountain variety Douglas-fir.

Dimensions were measured to determine the volume of each specimen. A density estimate provided by the matched specimens was used to determine the specimen weight required for the target moisture content. For example, consider the following information:

Specific Gravity (Sg) = 0.5*

Green Volume (Vg) = 100 cm^3

Desired Moisture Content = 12%

The required specimen weight, W, would then be;

$$W = Sg*Vg*(1 +U) \qquad (4.1)$$

where U = desired fractional moisture content

Substitution of data into the above equations produces W = 56 grams.

*Based on oven-dry weight and green volume.

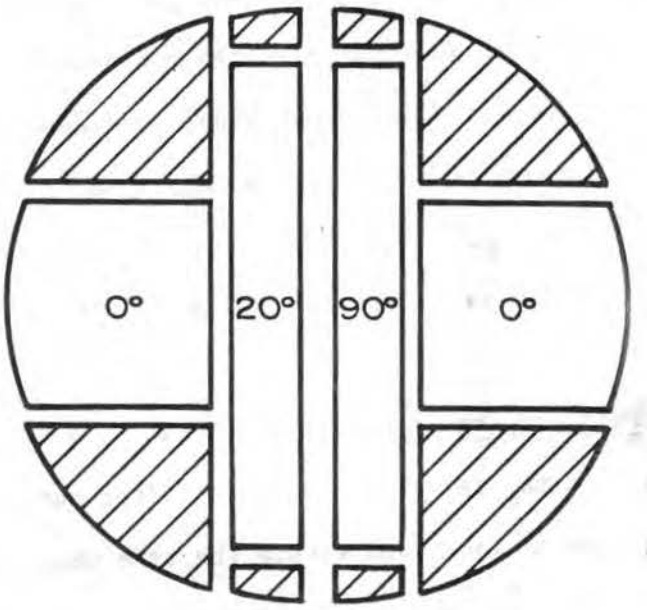

Figure 4.3. Specimen locations for DEC study.

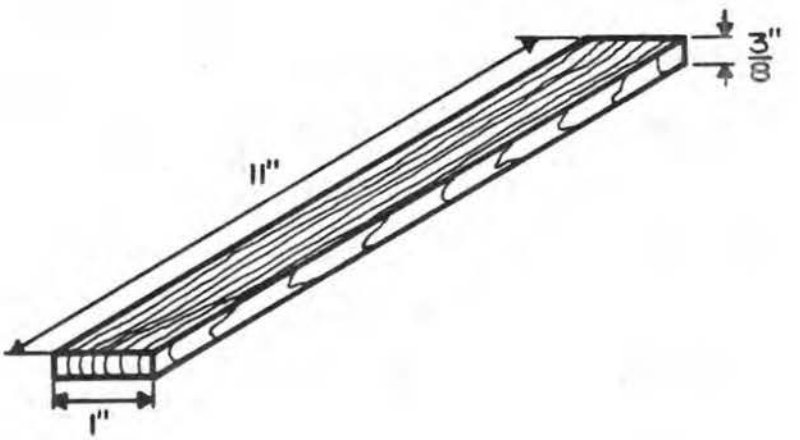

Figure 4.4. Final specimen dimensions.

Once a specimen reached the desired moisture content, it was wrapped in Saran wrap and kept for at least 7 days to reduce any moisture gradient present and to preserve the overall moisture content until testing.

The grain angle of all specimens was determined by use of a 40 power microscope equipped with a gradated cross-hair eyepiece. The grain angle on the four faces of the specimen length was measured at three equally spaced locations ($\ell/6$, $\ell/2$, $5\ell/6$). The grain angle of the specimen was computed by use of Eq. 4.2 at each location, and the three grain angle values were averaged.

$$\theta = \arctan \sqrt{(\tan\alpha)^2 + (\tan\beta)^2} \tag{4.2}$$

where:

α = measured fiber angle in the x_1x_2 plane

β = measured fiber angle in the x_2x_3 plane

Both α and β are the average of two measurements.

4.3.2 Decaying of Specimens

The decay specimens were segregated into the 10 groups listed in Table 4.1. The first group was tested without being decayed for control. All other specimens were placed in three inches of soil which had been inoculated with decay fungi two months previously. The inoculation procedure was as follows. Wood from the deitrus layer of the forest soil exhibiting advanced decay was hammer-milled and the resulting particles mixed with soil. Water was added to the soil at weekly intervals to allow for optimum growth conditions. The soil was covered with Saran wrap to keep the moisture content high and to increase the temperature of the soil. The decay bin (Figure 4.5) was

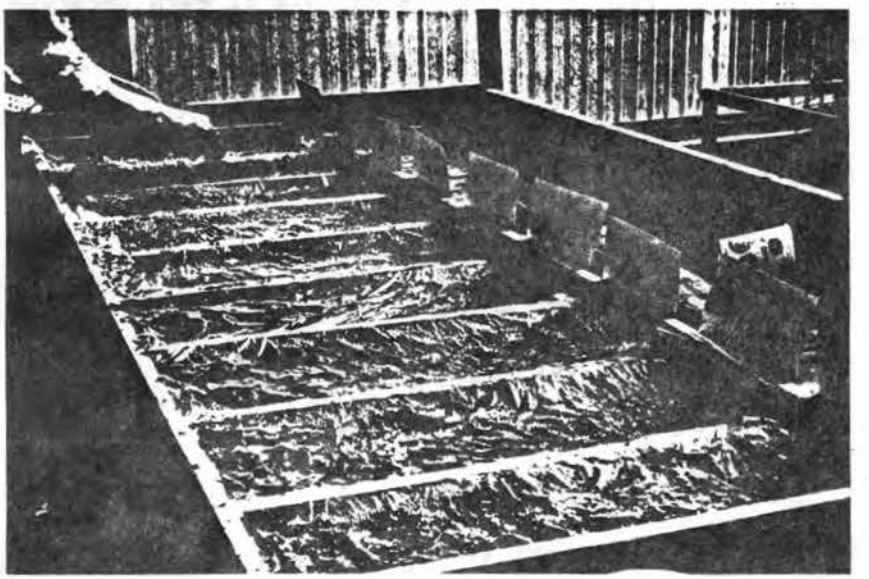

Figure 4.5. Decay bin for specimens.

located in the Department of Forest and Wood Science greenhouse on campus.

After specimens were placed in the inoculated soil and covered with plastic, the specimens were removed according to the time schedule listed in Table 4.1. Matched specimens were also included along with the actual test specimens. Each of these matched specimens were divided into two samples from which the density of the wood before decay was determined. The other matched sample was buried in the soil and used for density determination after removal to give an indication of the amount of weight loss experienced by the associated decay group.

4.4 NONDESTRUCTIVE EVALUATION (NDE) PROCEDURE

After the specimens were conditioned to the designated moisture contents and their grain angles measured, they were ready for NDE. Each specimen was weighed to the nearest 0.01 g and dimensions measured to the nearest 0.001 inch with calipers. Each dimension was computed on an average of three measurements.

4.4.1 Instrumenting the Specimen

Attachment of two accelerometers and a small pin were required for each specimen for testing. Each accelerometer was attached to the specimen by means of an accelerometer holder held by pins driven into the specimen. The accelerometers were inserted into the holders. The accelerometer holders (Figure 4.6) were made of aluminum, with all dimensions machined to a tolerance of ±0.002 inch. The holders were designed to meet three criteria:

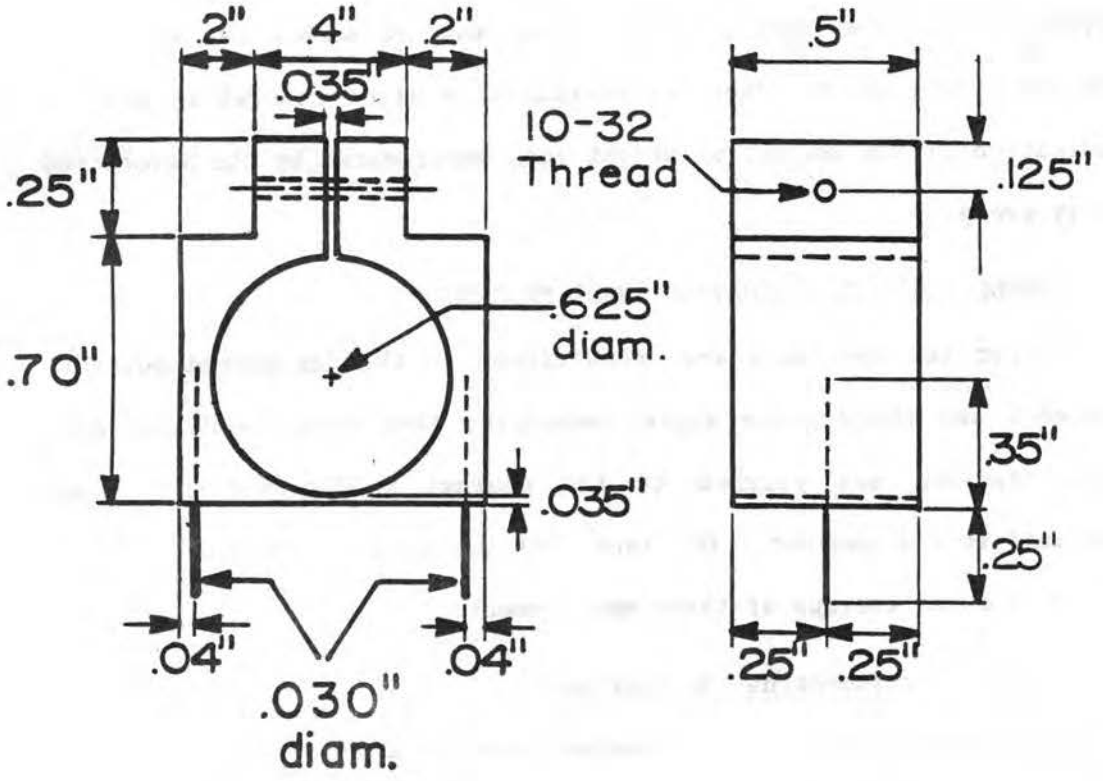

Figure 4.6. Accelerometer holder.

1. low mass,

2. secure attachment to the specimen,

3. location of accelerometer close to the specimen surface.

The weight of each holder was 8.33 gram. Low mass was considered desirable to minimize any alteration of the specimen response. Secure attachment between the accelerometer and specimen--via the holder--was essential to ensure accurate sensing of the stress wave in the material. Two 0.035 inch diameter hardened steel pins protruding from the holder ⅛ inch provided the attachment. The pins were fabricated from piano wire. The close proximity of the accelerometer to the specimen surface was desirable to minimize any phase shift resulting from vibration of the holder itself. The accelerometer holders were attached 3/4 inch from each end of the specimen by use of the specimen preparation apparatus (prep jig) shown in Figure 4.7 . A ½ inch long steel pin made of piano wire was inserted into the end of the specimen through a hole in the metal plate at one end of the prep jig. After the holders and pin were attached to each specimen, the specimen was removed (Figure 4.8) and the accelerometers were inserted. The screw on the holders were tightened to insure rigid attachment between the holder and accelerometer.

The accelerometers used were Model 3021, produced by Columbia Research Laboratories, Inc., Woodlyn, PA. The specifications of the accelerometers are summarized in Table 4.2. The accelerometers were capable of measuring up to a 2,000 g acceleration in impact.

4.4.2 Testing Frame

The NDE testing frame was designed to meet several objectives. The overall requirement was to provide isolation of the specimen from

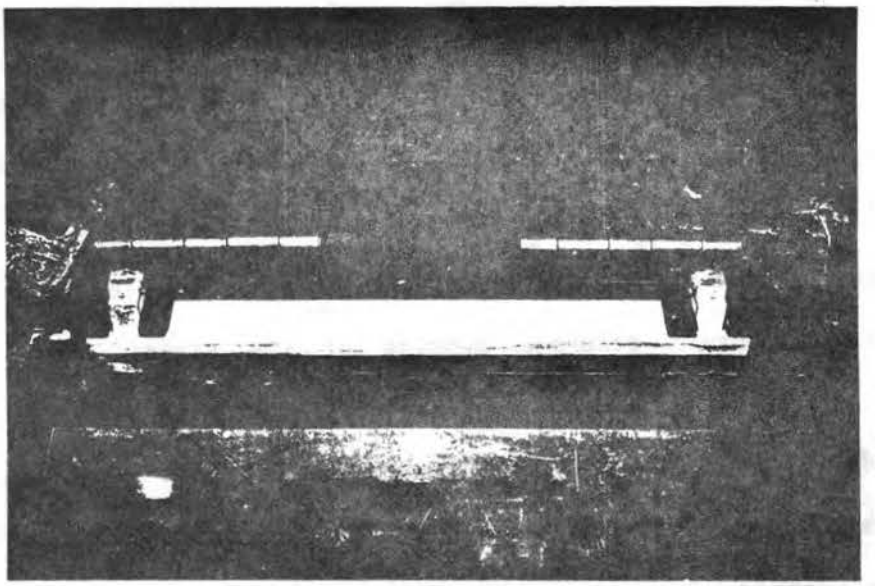

Figure 4.7. Specimen preparation frame.

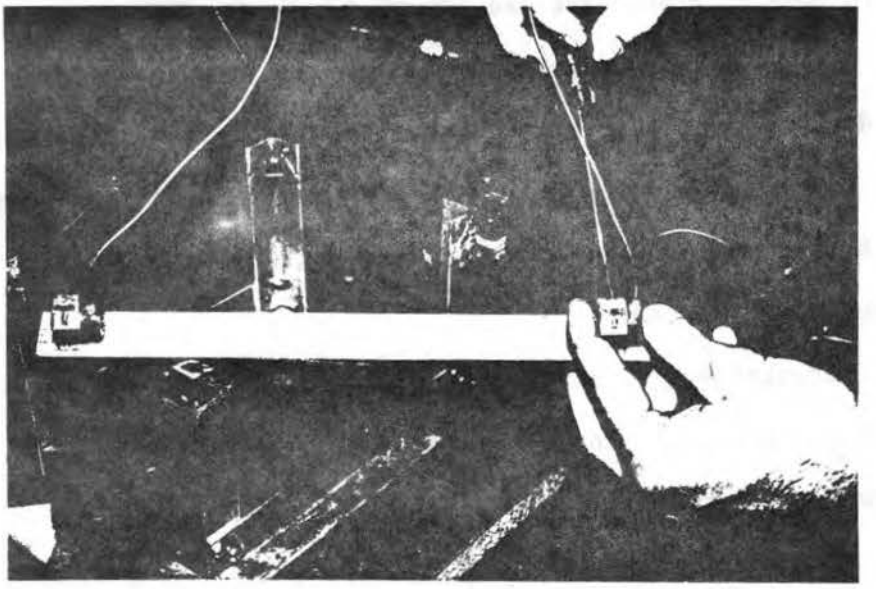

Figure 4.8. Fully instrumented specimen.

Table 4.2. Specifications of Columbia Model 3021 accelerometer.

Model:	3021 Low-G Vibration
Nominal Sensitivity:	70 pcmb/g*
	100 mv/g
Frequency Response:	2 Hz to 5 KHz, ±5 %
Resonant Frequency:	25 KHz
Maximum Acceleration in Vibration:	1000 g sinusoidal
in Shock :	2000 g
Linearity:	±1 % per 300 g
Output Resistance:	2×10^{10} ohms
Capacitance:	400 pf**
Size:	5/8" hex x 0.78" H
Weight:	35 gm
Material:	Stainless Steel
Altitude:	No effect
Temperature Range:	-100°F to + 350°F
Mounting:	#10-32 detachable stud
Connector:	Coaxial #10-32 thread

*pcmb = picocoulomb
**pf = picofarad

all outside influences (except accelerometer and holder masses) so that the measured response would be due to the material characteristics only. Repeatability of the tests was a primary consideration. Suspension of the specimens by wires resulted in better reproducibility than use of either foam supports or rigid clamping. No difference in any wave property was measurable when specimens were removed from the test frame, resupported, and tested again. The suspension wires used were high strength, small diameter (0.002 inch) stainless steel recording wire. The wires were attached to the aluminum frame mounted on a leveled wood base. The accelerometer cables connecting the accelerometers and the analyzing equipment were suspended from overhead. This arrangement allowed free translation of the specimen with a minimum of energy loss. The test frame is shown in Figure 4.9.

The impact delivery system consisted of an instrumented pendulum released from a set height with the use of an electromagnet powered by a 6 volt dry cell battery. The pendulum was mounted on a double ball bearing collar which gave a nearly perfect free swing. The optimum height from which the pendulum was released was determined by experiment to produce a sharp input signal resulting in sufficient accelerometer output voltages.

A Columbia Model 3021 accelerometer was attached to the end of the pendulum so that the input could be determined. The electromagnet was connected to a reversing field switch, designed by the author, allowing alternating fields of flux to be used for each energizing cycle. This device reduced any buildup of residual magnetism which would result in "sticking" of the pendulum to the magnet. The

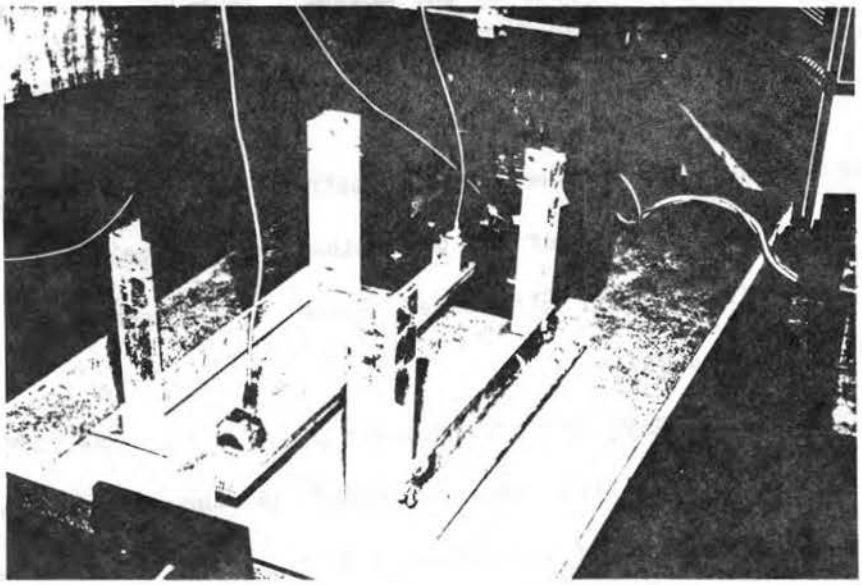

Figure 4.9. Nondestructive evaluation test frame.

pendulum impacted the steel pin inserted into the end of the specimen. Preliminary testing showed that a better defined input pulse resulted when a pin is used rather than impacting the specimen directly. A triangular foam end piece was butted against the specimen at the opposite end from the pendulum. This was used to insure accurate placement of the specimen in relation to the pendulum arc and to increase the repeatability of the impacts. This foam also damped the translation of the specimen after impact, speeding up testing. Studies showed no difference in the measured response of the system as a result of the foam end piece.

4.4.3 Data Collection Procedure

The cables from the accelerometers were attached to the Metriguard stress wave timer for determination of wave velocity and to the Hewlet-Packard 5423A Structural Dynamics Analyzer (SDA) for all other waveform analysis.

Output from only two accelerometers could be analyzed at one time. The accelerometers used depended on the parameters to be measured. Two transducer arrangements were used. The first arrangement consisted of the two accelerometers mounted on the specimen. The alternate arrangement involved analyzing the output from the pendulum and the specimen accelerometer mounted furthest from the pendulum.

Six replications were made of each test and the results averaged. Averaging increased the accuracy of the measurements. Preliminary testing showed averaging more than six signals did not alter any wave parameter by more than 0.5 percent.

Four sets of measurements, each entailing six replications, were carried out. Three of the four sets were obtained using the first

accelereometer arrangement, with the final analysis set using arrangement two. The actual measurements performed for these sets are explained fully in the next section. The transit time was determined independently from the wave analysis. Six transit time values were determined for accelerometer arrangement one and averaged.

4.4.4 Analyzing Equipment

Two analysis instruments were used for characterizing the wave propatation of the system. The first was the Metriguard Model 239 stress wave timer. This system gave a digital reading of the initial stress wave time delay in microseconds between the front and back accelerometers mounted on the specimen. The same timer was used previously by Mulheren (55) for his NDE study on wood transmission poles. The two accelerometers mounted on the specimen were ten inches apart.

The 5423A Structural Dynamics Analyzer (SDA) was a critical component of the testing procedure (Figure 4.10) consisting of a dedicated minicomputer capable of dual-channel time domain and frequency domain measurements. It is also capable of animated displays of mechanical systems in various modes of vibration. The measurement parameters are functions of the chosen input signals. The bandwidth is variable with 25KHz the maximum acceptable frequency. Other measurement parameters include a choice of AC/DC coupling; selection of four trigger modes; selection of bandwidth center frequency; time record length; pre- and post-trigger delay capabilities; and transducer calibration factors. The parameter settings are displayed in tabular form through the "Measurement State." Two measurement states were used, one for time domain and the other for frequency domain.

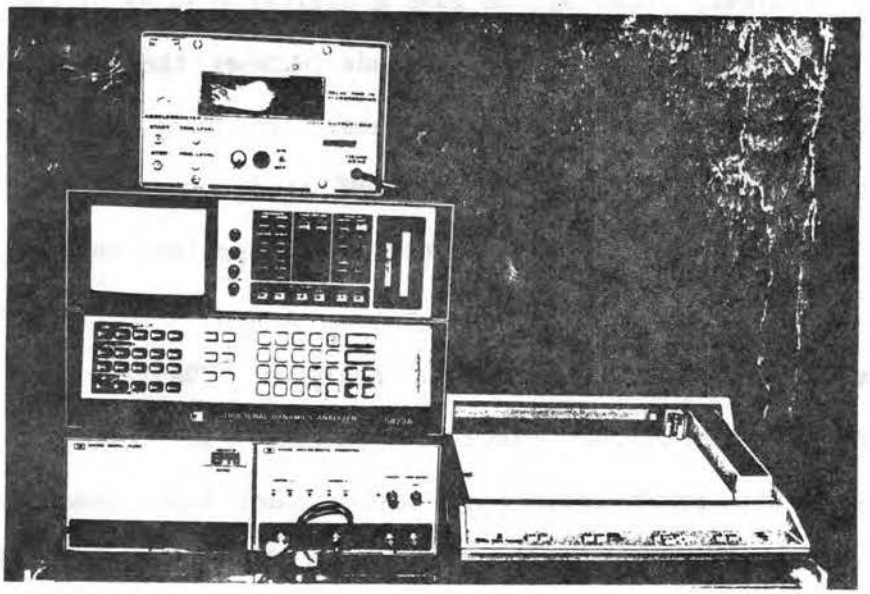

Figure 4.10. HP5423A structural dynamics analyzer, Metriguard stress wave timer, and HP7225A plotter.

Measurement State one, (Table 4.3), was used to obtain the time record and linear spectral content for accelerometer arrangement one. Six measurements were taken and the arithmetic mean obtained. This is designated as "stable" averaging in the meaurement state. The signals were analyzed as transients. An internal trigger level was set for channel one with a 507.812μs pretrigger delay programmed in for both channels. This delay enabled both time records to be viewed in their entirety. A 6.4KHz bandwidth extending from 0 to 6.4KHz was used with a frequency resolution of 50Hz. The associated time record length was 20 ms with the interval between sample data being 39.0625μs based on the sampling rate of the HP5423A.

Calibration factors were determined from assessing the response of each accelerometer in impact using 50 replications. The nominal sensitivity of each accelerometer was 10 g per volt output and the calibration factor corresponding to this was 1.0. Using one accelerometer as a reference, the remaining accelerometers exhibited lower response amplitudes to impact and were assigned calibration factors of 0.97 and 0.91. Cross-correlation was determined using parameters identical to those used in Measurement State one. Measurement State two, Table 4.4 was used for the determination of the frequency response function, coherance function, energy spectral density, and the cross-spectral energy density for both accelerometer arrangements one and two. Due to the HP54234 operating program the time length increased from 20 ms to 40 ms while the frequency resolution decreased from 50 Hz to 25 Hz as compared to that used for Measurement States one.

Table 4.3. Measurement state one for time domain analysis.

MEASUREMENT STATE

MEASUREMENT :	TIME RECORD		
AVERAGE :	6 , STABLE		
SIGNAL :	TRANSIENT		
TRIGGER :	INTERNAL , CHNL 1		

CENT FREQ :	0.0 HZ	ΔF :	50.0000 HZ
BANDWIDTH :	6.40000 KHZ		
TIME LENGTH :	20.0000 mS	ΔT :	39.0625 μS

CHAN #	RANGE	AC/DC	DELAY	CAL (EU/V)
1	10 V	AC	-507.812μS	970.000 m
* 2	10 V	AC	-507.812μS	910.000 m

Table 4.4. Measurement state two for frequency domain analysis.

MEASUREMENT STATE

MEASUREMENT :	TRANSFER FUNCTION
AVERAGE :	8 , STABLE
SIGNAL :	TRANSIENT
TRIGGER :	INTERNAL , CHNL 1

CENT FREQ :	0.0 HZ	ΔF :	25.0000 HZ
BANDWIDTH :	6.40000 KHZ		
TIME LENGTH :	40.0000 mS	ΔT :	39.0625 μS

CHAN #	RANGE	AC/DC	DELAY	CAL (EU/V)
* 1	10 V	AC	-507.812μS	970.000 m
* 2	10 V	AC	-507.812μS	910.000 m

The input signals to the SDA are converted from analog to digital form. Selectable digital filters, part of the SDA, adjusted the data for the desired bandwidth. The SDA is capable of averaging up to 13,120 input signals on each channel. A fast-Fourier transform (FFT) algorithm is used by the SDA to produce frequency component measurements of the input. After completion of the wave property calculations, the information may be stored on a digital cassette tape and/or plotted by the associated HP7225A plotter. The measurements taken are explained in greater detail in the following section.

4.4.5. Nondestructive Wave Parameters

The transit time was determined six times for each specimen using the Metriguard stress wave timer. Time domain measurements made were the time records of the stress waves using accelerometer set one. Cross-correlation between these accelerometers were also carried out. Frequency domain measurements included, linear spectrum of frequency components, frequency response function, coherance function, energy spectral density, and energy cross-spectral density for accelerometer arrangement one. In addition, the frequency response function, coherance function, energy spectral and cross-spectral density measurements were determined for accelerometer arrangement two. A total of fifteen time and frequency domain measurements were made on each specimen.

4.5 DESTRUCTIVE TESTING

After NDE the specimens were tested in flexure to failure. An Instron testing machine, Model TMS, equipped with a 100 lb load cell and load and deflection recording capability was used. The test

frame, shown in Figure 4.11, was double-hinged at each support to allow self-alignment of the specimen during testing.

The test span was 10 1/8 inch. The crosshead speed of 0.1 inch per minute produced a maximum strain rate of 2.19×10^{-3} in./in./min. The length to depth ratio of the specimens was approximately 27. After testing, the Modulus of Rupture (MOR), and Modulus of Elasticity (MOE) was determined. The MOE values were not corrected for shear deflection. Two samples near the failure location were then cut from each specimen. The dimensions and weights were recorded and the samples oven dried. Average moisture content and specific gravity were calculated from the two samples. All specific gravity values were converted to an oven dry weight-green volume basis using the following relationship (6);

$$D_g = D_a/(1 + 0.00983\ D_a(M_f - M_a)) \qquad (4.3)$$

where: D_g = specific gravity at green volume,

D_a = specific gravity at test moisture content,

M_f = moisture content at fiber saturation point (26%),

M_a = test moisture content

Criteria for selection of stress wave spectral analysis properties and their quantification is presented in the next chapter. Material properties, strength, and stiffness values for all specimens are also summarized.

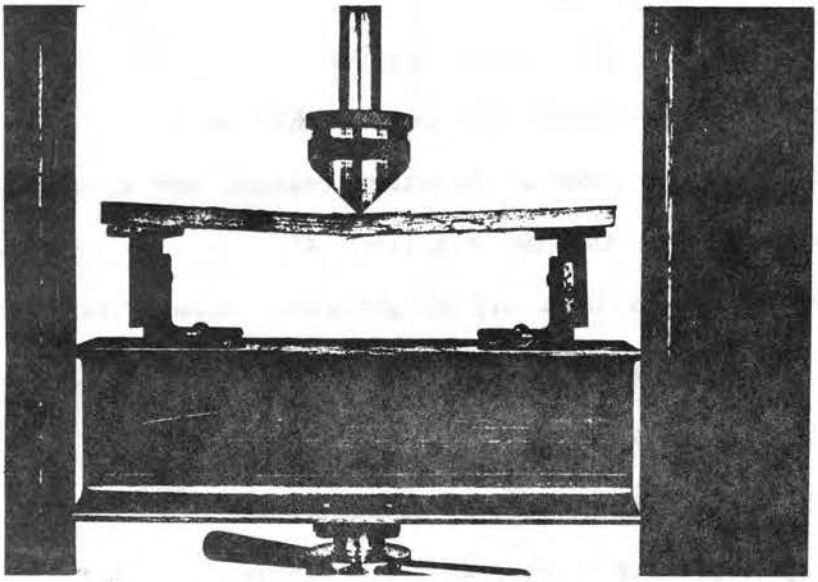

Figure 4.11. Test frame for specimens in flexure.

Chapter 5

DATA REDUCTION

5.1 MEASUREMENT OF WAVEFORM PARAMETERS

The spectral analysis procedure results in an almost endless number of parameters which could be studied. Thus, the NDE data collection was limited to three criteria which showed the greatest promise in preliminary studies and found useful by other investigators (5, 17, 67). One of the NDE variables, stress wave velocity, has been reported extensively and was included here. Measures of the energy content was judged to be important, especially for detection of incipient decay. This parameter was selected because toughness, a measure of energy absorbed at failure, is a highly sensitive destructive parameter for decay effects. Finally, the third NDE parameter chosen was the frequency response function, which by definition describes the dynamic characteristics of a system.

Representative waveform plots for the various experimental conditions were inspected visually to help define promising characteristics before using the plots in actual quantitative analyses. Initially the influence of experimental variables on the stress wave propagation was inspected for two extreme cases. The time records of a perpendicular to grain specimen at a 160 percent moisture content and an air-dry specimen (7 percent moisture content) with a parallel

to grain orientation are plotted in Figures 5.1 (a), (b), respectively. From visual examination it is apparent that the perpendicular specimen exhibits less high frequency content and more damping. The difference in frequency content is more visbile upon examination of the ESD of each waveform. The parallel to grain specimen exhibited energy peaks at frequencies of 300, 550, and 2750 Hz, Figure 5.2 (b). Frequency peaks ranging from 150 to 2400 Hz with a predominant peak at 1300 Hz were evident in the perpendicular to grain specimen, Figure 5.2 (a).

The frequency response function, H(f), shows more clearly the frequency characteristics than the ESD or time response curves. The amplitude response for the above two specimens are plotted in Figures 5.3 (a) and (b). Note that the largest gain factors for the parallel to grain specimens occur above 3000 Hz, Figure 5.3 (b), while the largest gain for the perpendicular to grain specimen occurs at about 800 Hz. Along with the transit time obtained from the stress wave timer, the information available in Figures 5.2 and 5.3 provided the NDE information used for correlation with other parameters and wood characteristics.

Values of parameters were obtained from each plot using the cursor capabilities of the HP 5423A. For example, the frequency at which the gain H(f) reached a maximum for the 90° specimen with 160 percent moisture content (Figure 5.3 (a)) is shown in Figure 5.4. The maximum gain was 2.2832 at a frequency of 775 Hz as seen at the top left of the figure. The parameters investigated from the frequency response function were, the maximum gain (FRAMP), the frequency at which the maximum gain occurred (FRFREQ), and the maximum

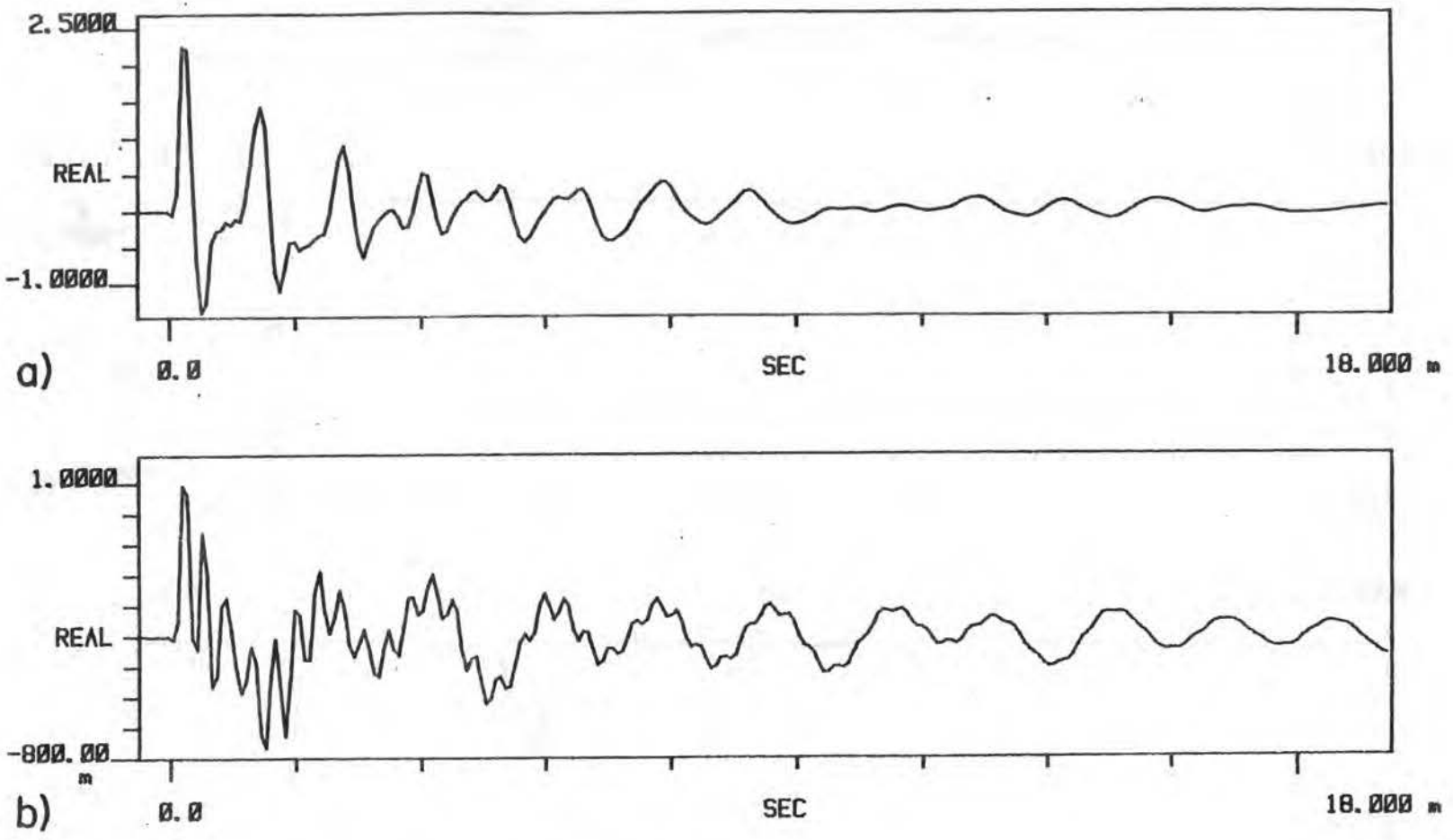

Figure 5.1. Time record of stress wave in
a) 90 degree specimen at 160% moisture content
b) 0 degree specimen at 7% moisture content.

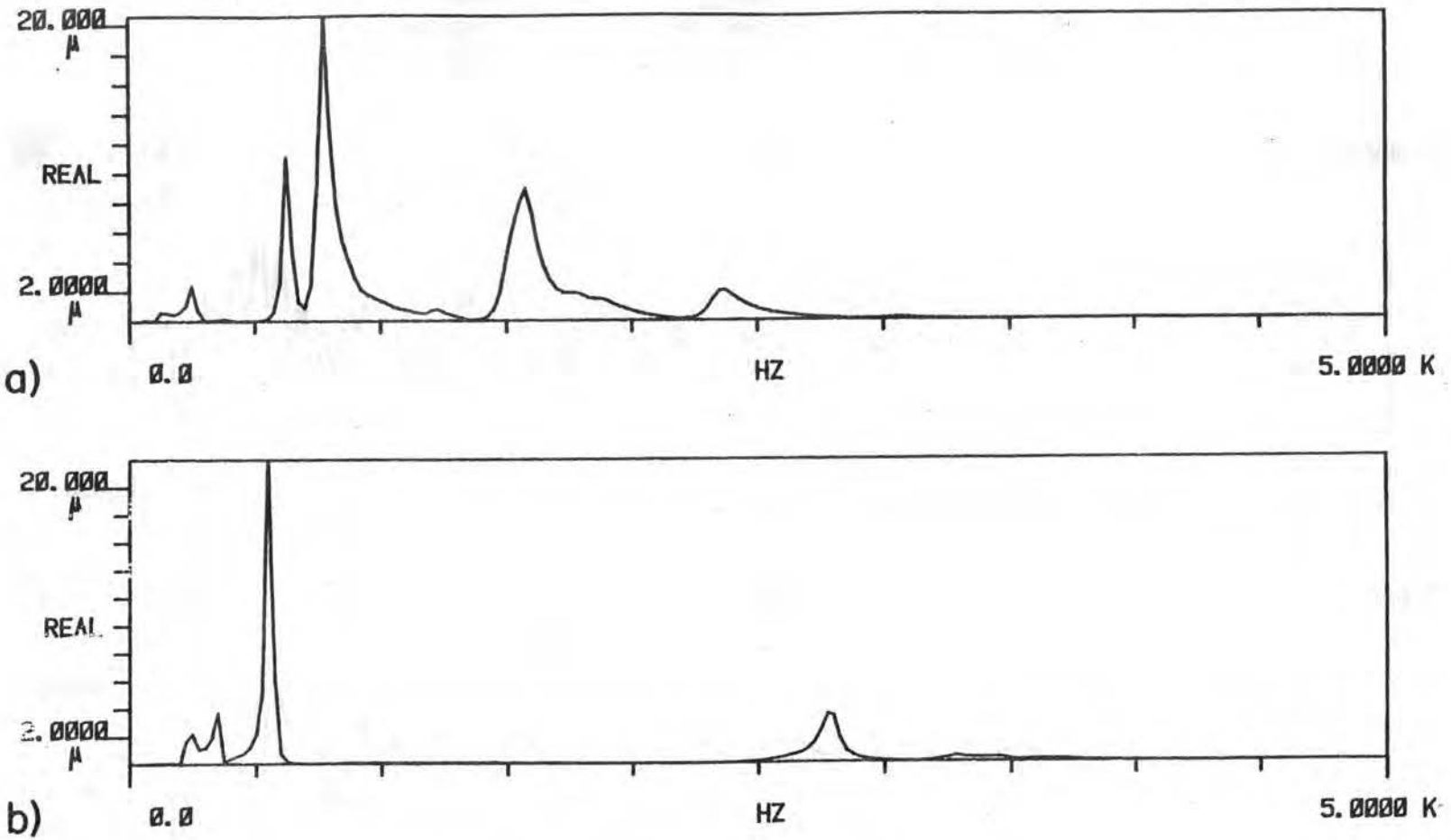

Figure 5.2. Energy spectral density of
a) 90 degree specimen at 160% moisture content and
b) 0 degree specimen at 7% moisture content.

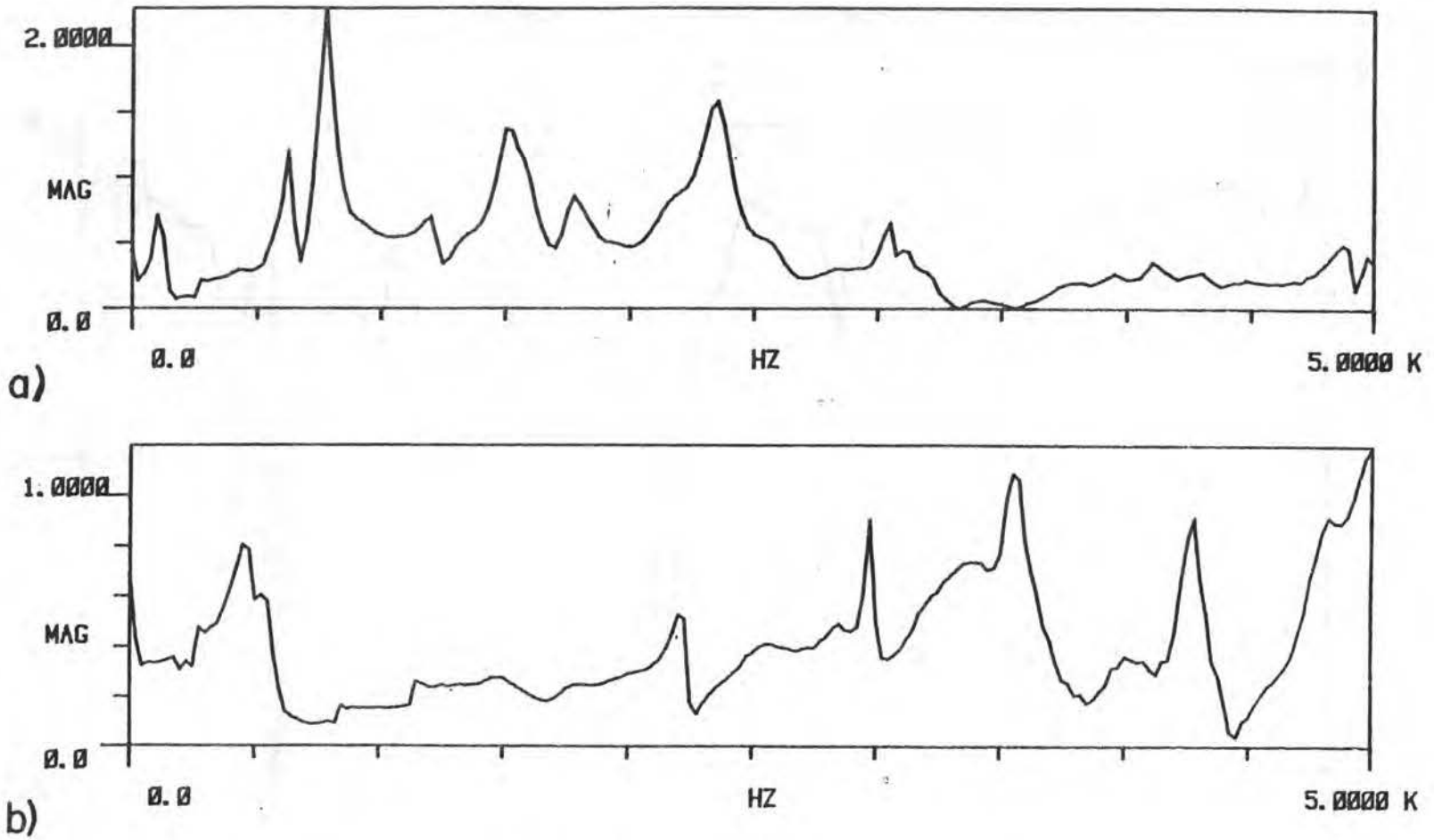

Figure 5.3. Frequency response function of
a) 90 degree specimen at 160% moisture content and
b) 0 degree specimen at 7% moisture content.

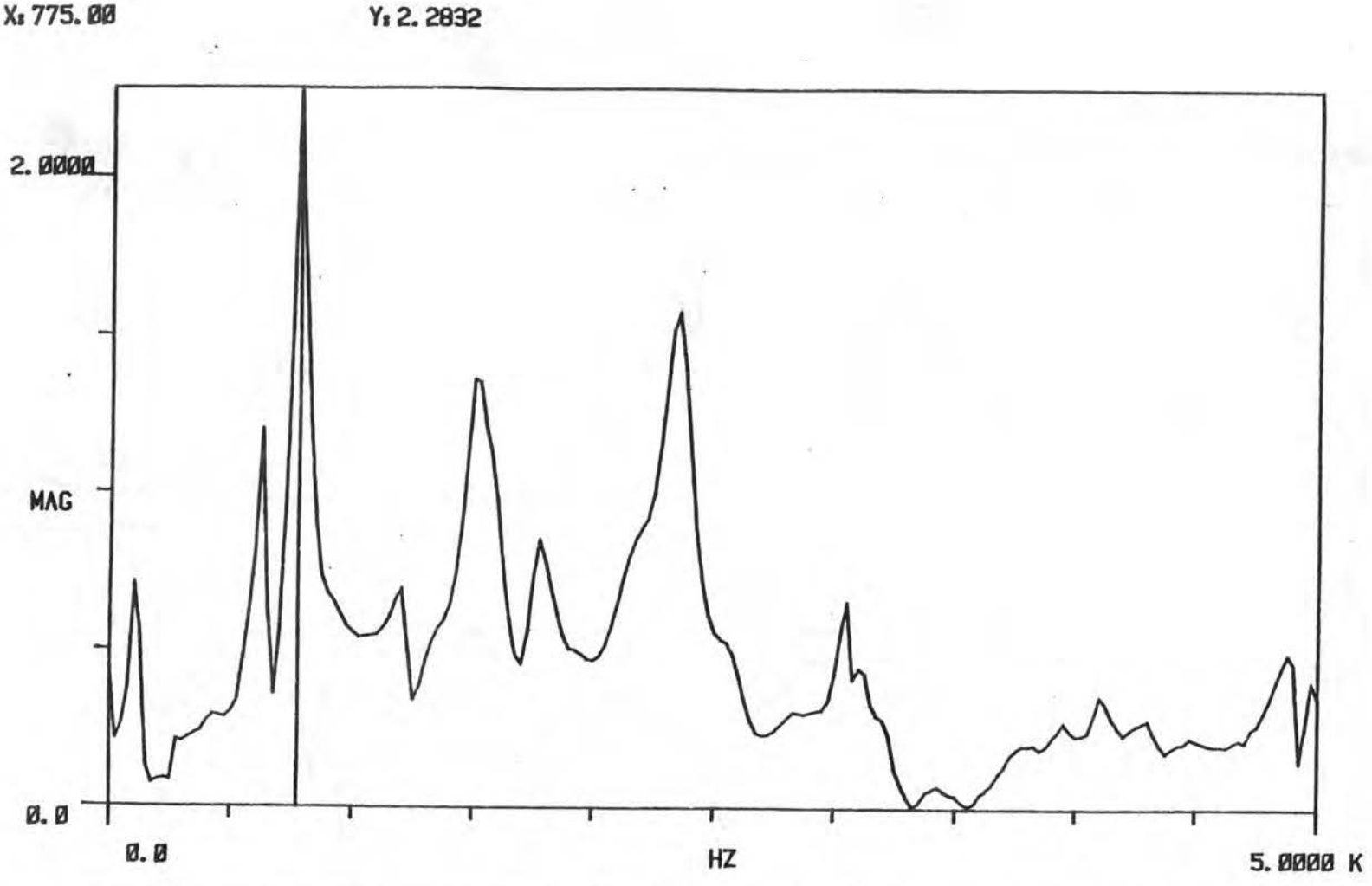

Figure 5.4. Use of cursor capability to identify maximum gain factor and attendant frequency.

value of the integrated amplitude response (FRINT). From the energy spectrum, the energy content from 0 to 5 KHz (ENGINT) were obtained for the input to the wood. The total energy content was determined by integrating the ESD with the aid of the HP 5423A. A plot of an ESD and the corresponding integration is shown in Figures 5.5 (a) and (b), respectively. The peak and total energy content values of the system response (ENGAMP, INTENG) were also determined.

For the grain angle-moisture content study, three sets of response energy spectrums were measured. The response of the front accelerometer were designated ENGFAMP and INTFENG. Back accelerometer energy spectrum values measured concurrently with the front accelerometer were designated ENG1AMP and INT1ENG while those measured with the system input were labeled ENG2AMP and INT2ENG. A summary of all acronyms used to identify the NDE variables is given in Appendix A. The specimen identification consisted of two sets of numbers. The first two specified the nominal grain angle while the second set indicated the moisture content group. Thus, specimen 90-1 had a nominal 90 degree grain angle and was in moisture content group 1, i.e., saturated condition. A summary of frequency response function values and the transit time (TTIME) for the GAMC specimens is given in Appendix B. Energy spectrum values are summarized in Appendices C and D.

For the decay study specimens, energy spectrum values were obtained before and after decay. The maximum energy input amplitude before and after decay (ENGINPD and ENGIND) and integrated energy content (ENGINTPD and ENGINTD) of the input are summarized in Appendix E. The maximum response energy amplitude (ENGAMPPD and ENGAMPD)

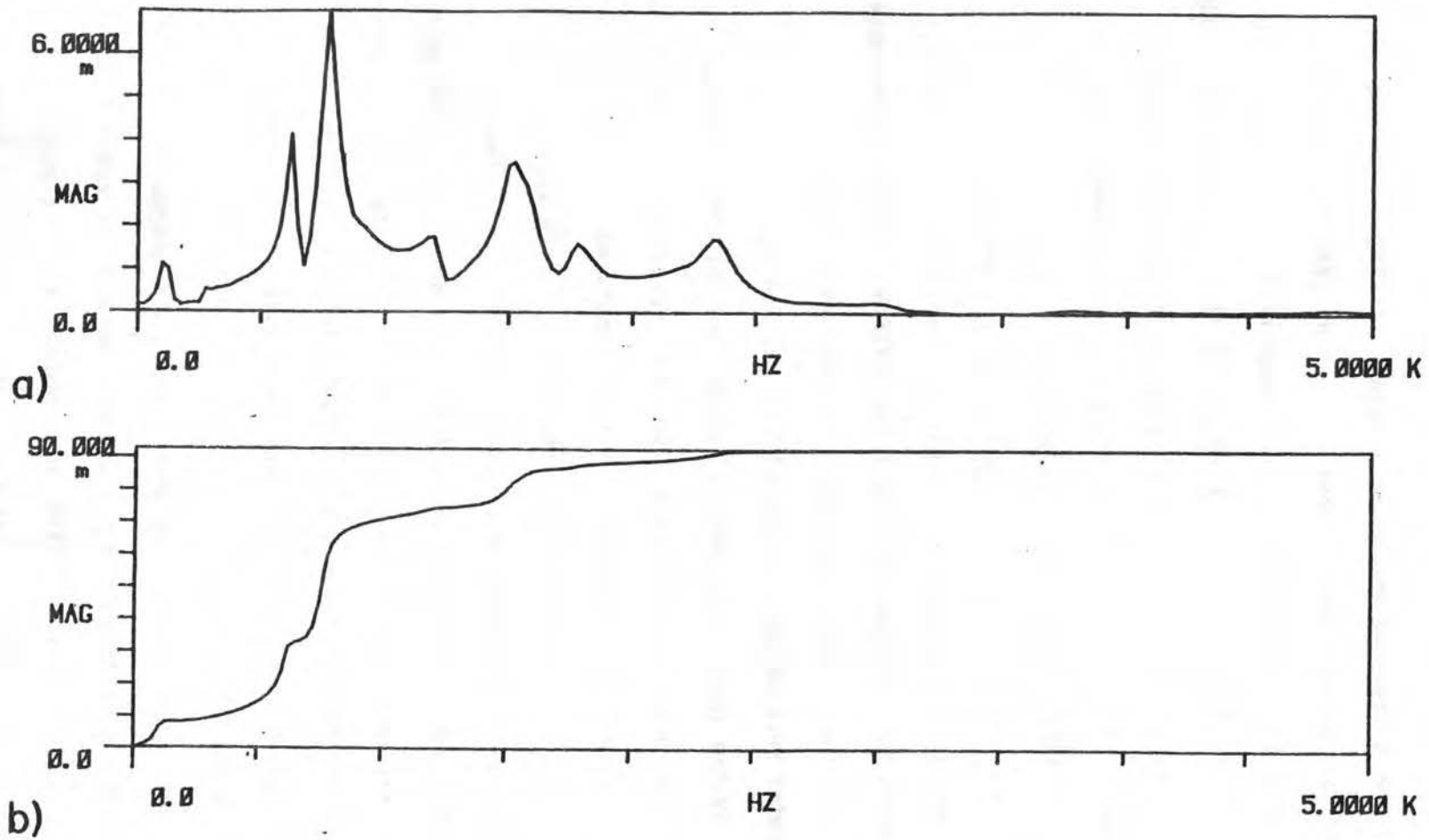

Figure 5.5. Plot of a) energy spectral density and b) integration of energy spectrum.

before and after decay as well as the total energy responses (INTENGPD and INTENGD) are presented in Appendix F. DEC specimens were assigned a three-digit identification number. The first digit indicating the nominal grain angle in tens of degrees, while the last two numbers were sequentially indexed for bookkeeping purposes. The frequency response parameters for the DEC specimens are summarized in Appendix G.

Several tests were invalid due to incomplete attachment of the accelerometer holders to the specimen. This could be ascertained by observation of the time record of the response. The nonrigid fixture resulted in the accelerometer responding to vibration of the holder in addition to the passage of the stress wave. A typical time record indicative of faulty contact is shown in Figure 5.6. Specimens with invalid NDE results are indicated in Appendices H and I.

5.2 DESTRUCTIVE PARAMETERS

The characteristics determined for each specimen were specific gravity (oven dry wt/green vol), moisture content, grain angle (degrees), MOE, MOR, as well as percentage weight loss for the decayed specimens. For the 63 study specimens, specific gravity ranged from 0.34 to 0.46 with a mean value of 0.41 and standard deviation of 0.02. Grain angle ranged from one to 90 degrees and moisture content from 7 to 160 percent. MOE values ranged from 30,000 psi to 1,730,000 psi while MOR varied from 310 psi to 12,590 psi. No correction for shear deflection was made in calculating the modulus of elasticity. A listing of all material parameters for the GAMC study is given in Appendix H.

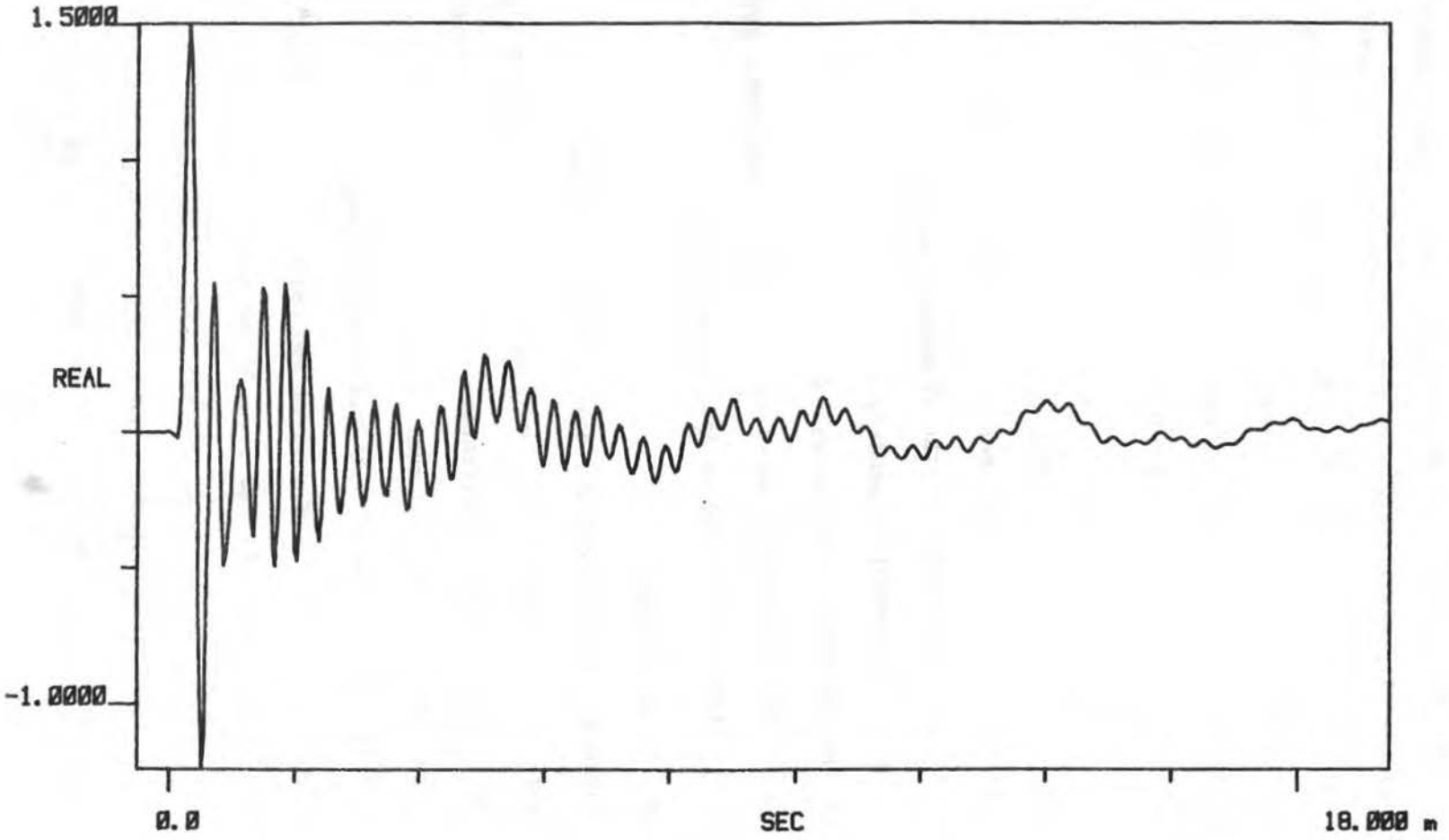

Figure 5.6. Example of invalid test due to poor attachment of accelerometer holder.

The physical parameters measured on each decay specimen included all parameters determined for the GAMC specimens. In addition, the weight loss of each specimen was calculated. Accuracy in the weight loss estimates was less than desired. Fifteen out of forty-four specimens experiencing decay showed a weight gain. This anomaly may result from two factors. The specimens were infiltrated by soil which could not be completely removed. This artificially decreased the weight loss measurements. Additional error possibly resulted from variation in density between the actual specimens tested and the matched specimens used to calculate the weight loss. Weight loss values ranged from 1 to 5 percent with the exception of specimen 919 which has a 9 percent weight loss. All specimens were tested in green condition with a moisture content range of 62 to 114 percent. Specific gravity of the specimens averaged 0.53 with a standard deviation of 0.02. Values of moisture content, specific gravity, grain angle, MOE, MOR, and weight loss for each DEC study specimen are given in Appendix I. Four of the twenty 90 degree specimens were broken during handling, as indicated in Appendix I.

Chapter 6

PREDICTION OF SELECTED WOOD PROPERTIES

6.1 OVERVIEW

The influence of grain angle, moisture content, and weight loss on wave propagation characteristics as measured in the NDE tests constituted the major thrust of the investigation. Regression analysis involving the NDE parameters given in the previous chapter were performed to obtain predictive models of chosen wood characteristics. Specimens from the GAMC group were used to study the relationships between grain angle and moisture content with the NDE parameters. The DEC specimen group was used to study the effect of weight loss on the wave propagation parameters. Additionally, the NDE variables were correlated with strength and stiffness values of all specimens.

The selection of regression models for predictive purposes was based on the smallest residual scatter about the regression equation, as measured by the standard error of the estimate (SEE). Polynomial and multivariate regression models were used when appropriate and tested for significance of the inclusion of higher order terms. Regression analyses were performed using the MINITAB statistics package available on the CSU computer sytem.

6.2. PREDICTION OF GRAIN ANGLE

For investigation of the relationship between grain angle and the NDE parameters, the 58 GAMC specimens were segregated into six groups

of moisture content values. This choice was to minimize variability other than that due to grain angle. The specimens included in each moisture content group (designated CMC) and the associated material properties are listed in Table 6.1. Grain angle values for each group ranged from 0 to 90 degrees. In the experimental design, seven moisture content groups were desired. However, due to variances from the target moisture content values, the specimens were regrouped into six categories. Mean moisture content values ranged from 109.6 percent for group CMC1 to 7.1 percent for group CMC6. Specific gravity of the groups varied from 0.39 to 0.41. The average moisture content values between all groups were significantly different at the 5 percent level using the appropriate t-statistic. Mean specific gravity between groups was not significantly different at the 5 percent level with the exception of groups CMC2 and CMC4. The difference in specific gravity between these groups was ignored as a factor in this analysis.

The NDE parameters used as predictor variables included integrated amplitude response (FRINT), frequency of maximum amplitude response (FRFREQ), maximum amplitude response (FRAMP), and transit time of the stress wave (TTIME). Henceforth, these will be designated as NDE Set I. These terms were defined in the previous chapter and additionally are given in a list of NDE acronyms located in Appendix A. Initially, a straight-line regression analysis was performed between grain angle and the NDE Set I parameters for each group. The r^2 values ranged from 0.0 percent (for FRAMP) to 98.8 percent (for TTIME). The SEE values varied from 35.9 degrees to 4.0 degress grain angle. Based on its nonsignificance, FRAMP was deleted from further statistical analysis.

Table 6.1. Specimen groupings of constant moisture content for grain angle study.

Group Designation	Group Member	Specimens	Material Parameters: Moisture Content Mean	Moisture Content Std. Dev.	Grain Angle Mean	Grain Angle Std Dev.	Specific Gravity Mean	Specific Gravity Std. Dev.
CMC1	00-1*	03-1						
	15-1	20-1	109.6	29.5	27.0	32.1	0.41	0.016
	30-1	90-1						
CMC2	00-2	03-2						
	06-2	10-2						
	15-2	30-2	47.8	7.7	27.3	31.6	0.39	0.015
	60-2	90-2						
CMC3	00-3	10-3						
	15-3	30-3						
	60-3	90-3	29.0	3.0	23.6	27.7	0.40	0.025
	20-2	03-4						
	00-5	03-5						
	30-5							
CMC4	00-4	06-4						
	10-4	15-4						
	20-4	30-4						
	60-4	90-4	20.1	2.4	27.5	29.6	0.42	0.019
	03-3	06-3						
	20-3	15-5						
	20-5	90-5						
CMC5	00-6	03-6						
	06-6	10-6						
	15-6	20-6						
	30-6	60-6	15.5	0.3	27.9	28.4	0.41	0.027
	90-6	10-5						
	60-5							
CMC6	00-7	06-7						
	10-7	15-7	7.1	0.15	29.7	33.3	0.42	0.027
	20-7	60-7						
	90-7							

*First two numbers indicate nominal grain angle. The final number indicates the target moisture content group.

Plots of grain angle versus each of the three remaining NDE parameters showed the curvilinear trends illustrated in Figure 6.1. Based on this curvilinear trend, a parabolic model was fit to the data for all groups. The parabolic model is of the form:

$$y = a + bx + cx^2 \tag{6.1}$$

Tests of significance for inclusion of the squared NDE terms were performed for each regression. Based on these tests, the polynomial model was rejected for the variable TTIME, but justified for the FRFREQ and FRINT regressions. Based on the SEE values, the models involving TTIME and FRINT were selected as best predicting grain angle when moisture content was constant. The parameters for the TTIME and FRINT regresssion equations for each group are summarized in Table 6.2.

A plot of the regression equations involving TTIME for all six groups is shown in Figure 6.2. There is a fairly consistent trend of increasing slope as moisture content decreases. The slopes range from 0.21894 to 0.34145 degrees per μsec as moisture content decreases from a mean value of 109.6 to 7.1 percent. The parabolic equations involving FRINT are plotted in Figure 6.3 for all groups. With the exception of group CMC5 with a mean moisture content of 15.5 percent, there is a shift to the right of the equations as moisture content increases. The integrated amplitude gain at a specified grain angle increases as the moisture content decreases, again with the exception of CMC5. No consistent relationship between moisture content and the parabolic equations involving FRFREQ was found.

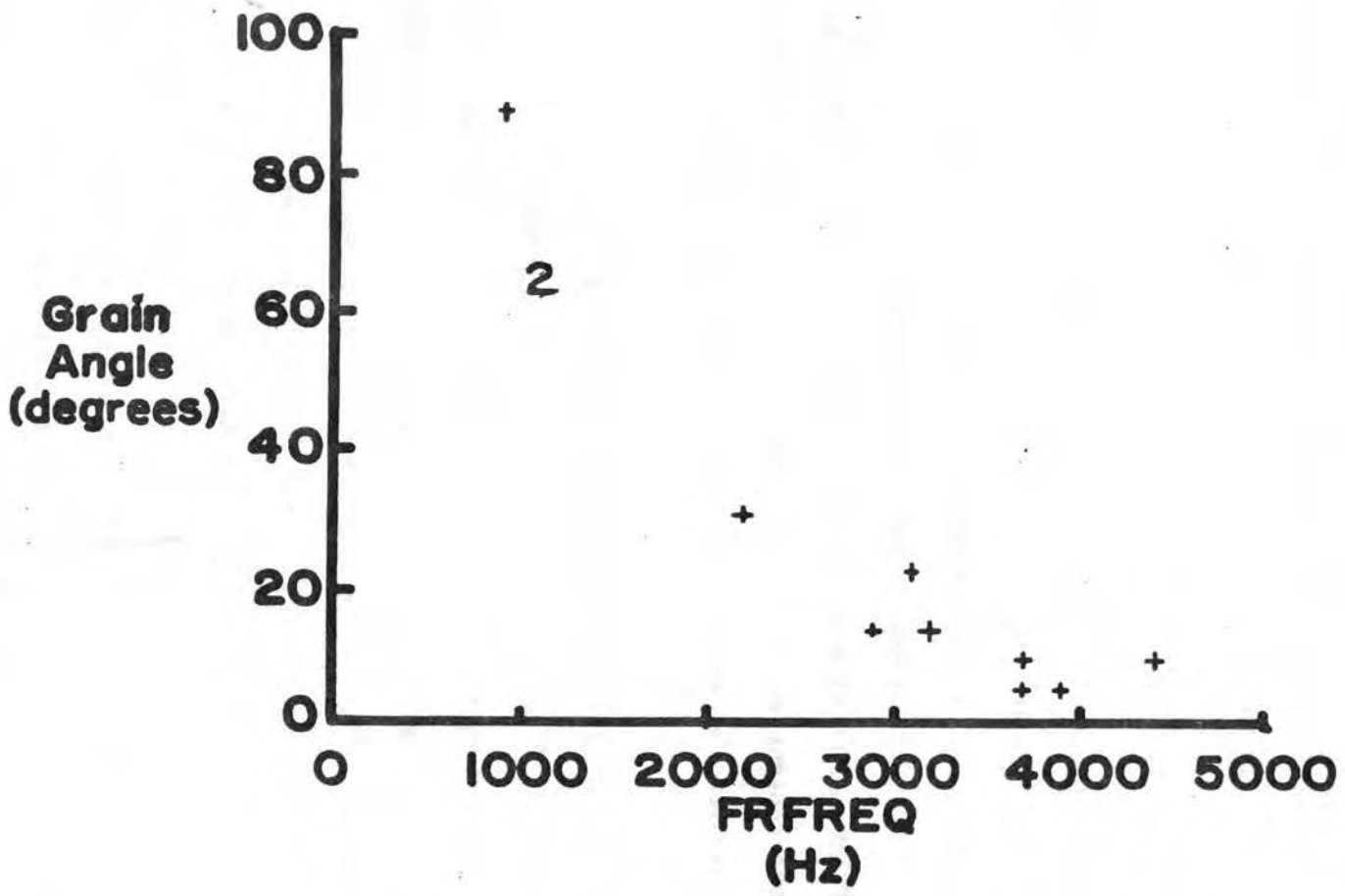

Figure 6.1. Scatter diagram of grain angle (degrees) versus FRFREQ (Hz) for group CMC3 exhibiting curvilinear behavior.

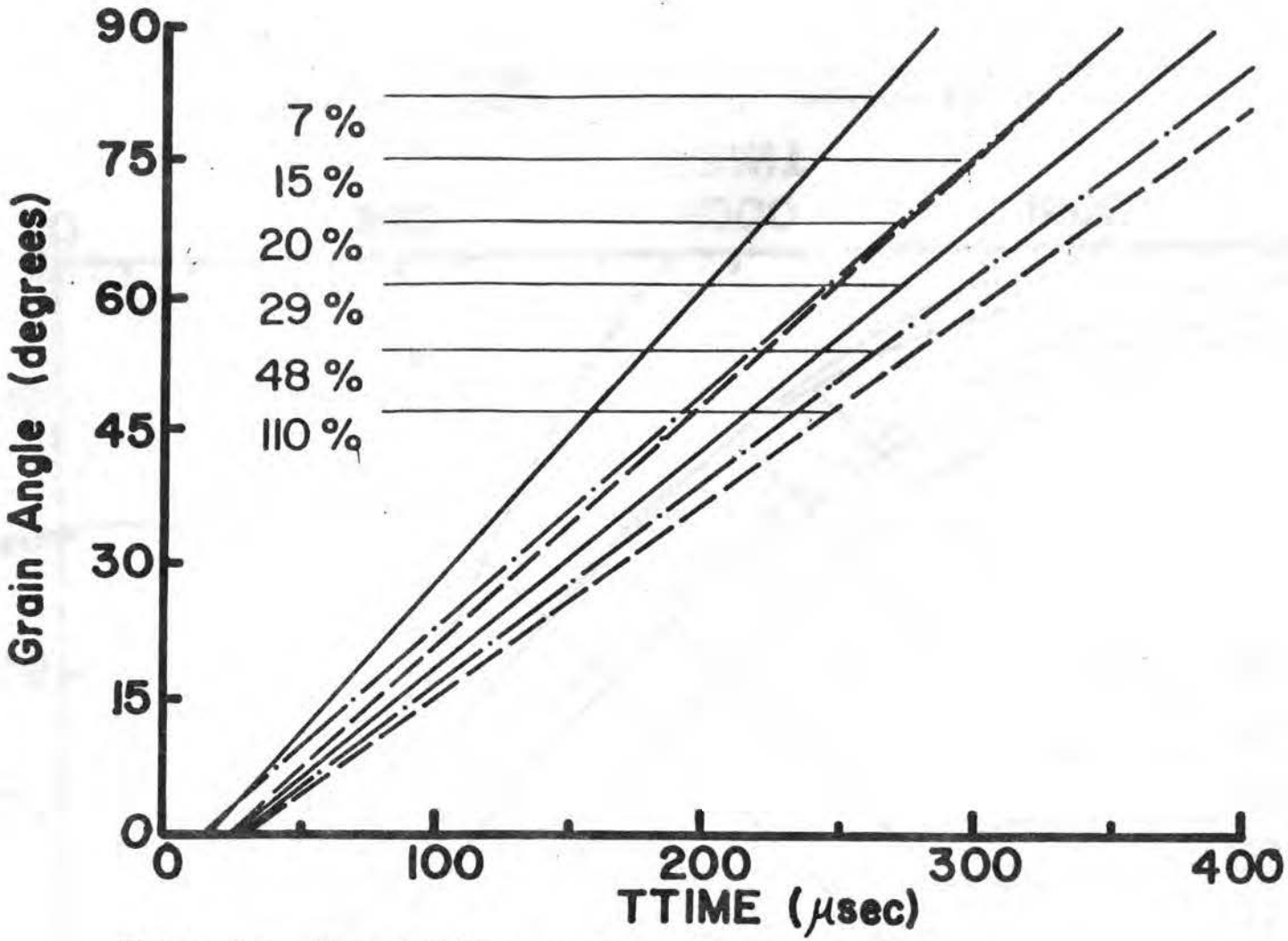

Figure 6.2. Plot of TTIME regression equations for grain angle prediction at various moisture contents.

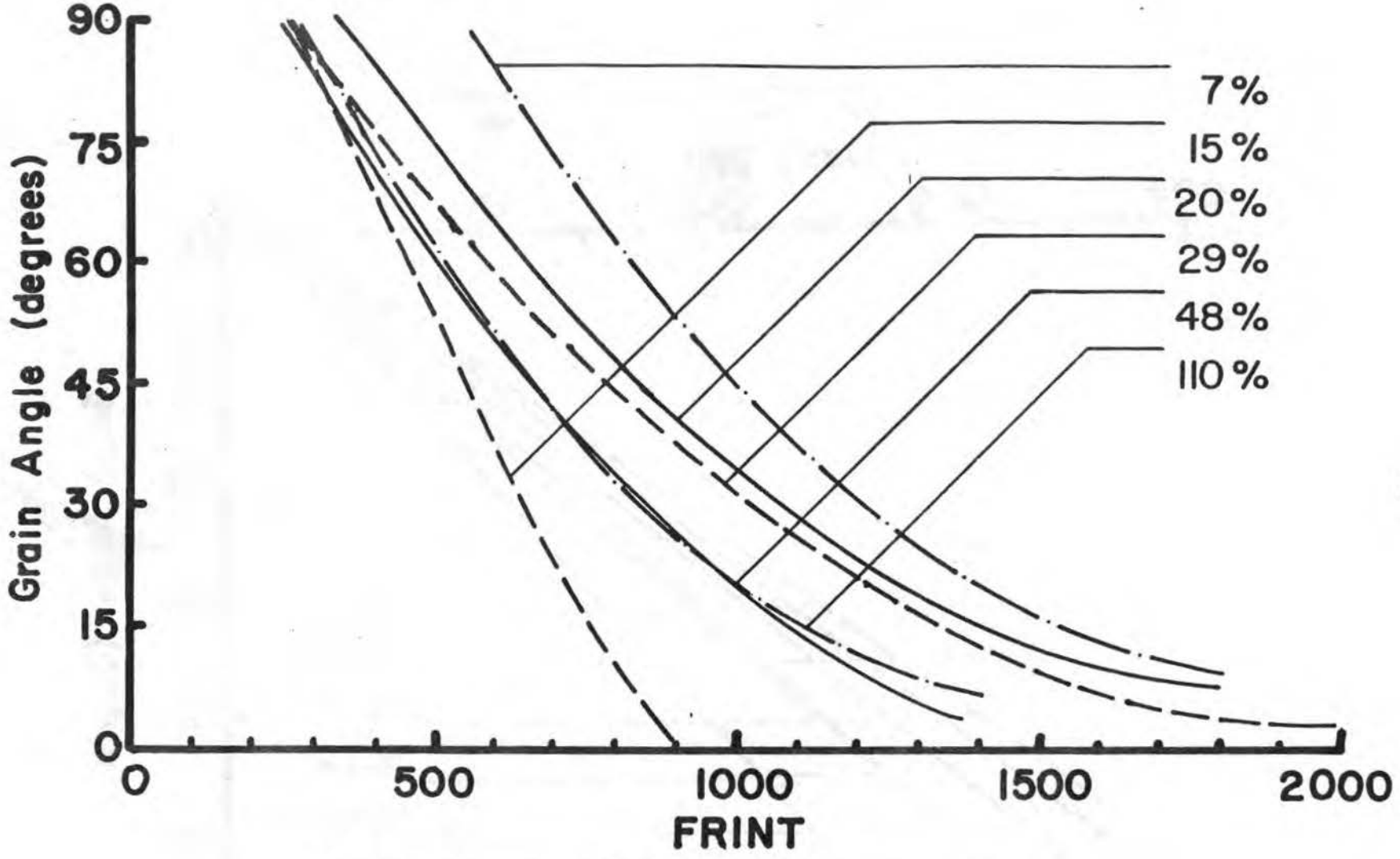

Figure 6.3. Plot of FRINT parabolic regression equations for grain angle prediction at various moisture contents.

All GAMC specimens were regressed with FRFREQ since moisture content did not consistantly influence the regression equations. A third degree polynomial of the form:

$$y = a + bx + cx^2 + dx^3 \tag{6.2}$$

was found to describe this relationship significantly better than a parabolic model. A parabolic model involving TTIME was regressed with all GAMC specimens and was significantly better than a straight-line model, although a parabolic model was rejected for the individual groups. The regression equations involving TTIME and FRFREQ to predict grain angle irrespective of moisture content are;

$$\text{Grain Angle} = -15.499 + 0.41752(\text{TTIME}) - 4.076 \times 10^{-4}(\text{TTIME})^2 \tag{6.3}$$

$$\text{Grain Angle} = 156.33 - 0.11151(\text{FRFREQ}) + 2.85 \times 10^{-5}(\text{FRFREQ})^2 - (2.478 \times 10^{-9})(\text{FRFREQ})^3 \tag{6.4}$$

The r^2 and SEE values for Eqs. (6.3 and 6.4) were 93.5 percent, 7.5 degrees and 93.0 percent and 7.8 degrees respectively. Both regressions had an overall significance at the 0.1 percent level. If moisture content is unknown, either Eq. (6.3 or 6.4) may be used to predict the grain angle of the specimens in this study. If moisture content is known, the appropriate models involving TTIME or FRINT (given in Table 6.2) may be used with an expected increase in predictive accuracy, based on their smaller associated SEE values.

Table 6.2. Summary of best predictive equations for grain angle at various moisture contents.

Group Designation	Mean Moisture Content	GA = a + b(TTIME)		Model	Used	GA = a + b(FRINT) + C(FRINT)^2				
		a	b	r^2	SEE	a	b	$C*10^{-6}$	r^2	SEE
	(%)	(degrees)	(degrees/μsec)	(%)	(degrees)	(degrees)	(degrees)	(degrees)	(%)	(degrees)
CMC1	109.6	-6.613	0.2189	98.8	4.0	119.5	-0.1368	37.5	86.4	15.3
CMC2	47.8	-7.404	0.2309	96.6	6.3	135.2	-0.1732	58.1	96.1	7.4
CMC3	29.0	-7.571	0.2520	92.8	7.9	119.3	-0.1190	30.5	95.8	6.4
CMC4	20.1	-6.965	0.2748	97.1	5.2	134.7	-0.1366	36.6	95.1	7.2
CMC5	15.5	-4.815	0.2649	96.4	5.6	134.3	-0.1746	29.7	96.7	5.8
CMC6	7.1	-7.484	0.3415	90.8	11.1	164.9	-0.1598	40.3	95.3	8.9

6.3 PREDICTION OF MOISTURE CONTENT

To investigate the influence of moisture content on the measured NDE parameters, it was necessary to segregate the 58 GAMC specimens into nine groups, each with relatively constant grain angles while allowing the moisture content to vary. The specimens in each of the nine groups, designated CGA (for constant grain angle), are listed in Table 6.3 along with the mean grain angle and specific gravity of each group. Values of the average grain angle for the groups ranged from 2.6 degrees for group CGA1 to 88.3 degrees for CGA9. A t-test was performed between each group and the grain angles of all groups found to be significantly different at the 5 percent level. Mean specific gravity values of the groups ranged from 0.39 to 0.43.

Two sets of NDE parameters were investigated. The NDE Set I also used for prediction of grain angle was used in a straight-line regression analysis for each group. Coefficient of determination values ranged from 0.3 percent to 95.7 percent, while SEE values varied from 38.3 percent moisture content to a low of 4.8 percent moisture content.

Basing acceptance of a model on the 5 percent level, none of the predictor variables were significant for all nine groups. The groups had relatively small sample sizes, ranging from 5 to 8 specimens. This small sample size could cause any predictive equation to be of limited value. However, certain trends were apparent in some groups. In general, as moisture content increased, the associated TTIME increased. The remaining NDE parameters in set I decreased as moisture content increased.

Table 6.3. Specimen groupings of constant grain angle for moisture content study.

Group Designation	Group Member	Specimens	Material Parameters: Moisture Content Mean	Moisture Content Std. Dev.	Grain Angle Mean	Grain Angle Std Dev.	Specific Gravity Mean	Specific Gravity Std. Dev.
CGA1	00-1	00-2*						
	00-3	00-4	40.3	26.6	2.6	0.51	0.39	0.028
	03-2	03-4						
	00-5	03-7						
CGA2	00-6	03-1						
	03-3	03-1	31.2	28.6	4.1	0.27	0.43	0.025
	03-6							
CGA3	06-1	6-2						
	06-3	5-4	43.9	60.6	7.2	0.73	0.43	0.019
	06-6	6-7						
CGA4	10-2	10-3						
	10-4	10-5						
	10-6	10-7	22.5	10.3	11.2	1.21	0.41	0.015
	15-3	15-5						
CGA5	15-1	15-2						
	15-4	15-6	35.4	33.2	14.1	0.64	0.43	0.018
	15-7							
CGA6	20-1	20-2						
	20-3	20-4						
	20-5	20-6	32.4	36.3	19.5	1.37	0.41	0.008
	20-7							
CGA7	30-1	30-2						
	30-3	30-4	45.2	40.3	28.9	1.17	0.39	0.010
	30-5	30-6						

Table 6.3. Specimen groupings of constant grain angle for moisture content study (continued).

Group Designation	Group Member	Specimens	Material Parameters: Moisture Content Mean	Moisture Content Std. Dev.	Grain Angle Mean	Grain Angle Std Dev.	Specific Gravity Mean	Specific Gravity Std. Dev.
CGA8	60-2	60-3						
	60-4	60-5	23.3	15.1	61.9	1.51	0.40	0.016
	60-6	60-7						
CGA9	90-1	90-2						
	90-3	90-4						
	90-5	90-6	41.4	53.7	88.3	0.81	0.40	0.028
	90-7							

* First two numbers indicate nominal grain angle. The final number indicates the target moisture content group.

The scatter diagrams of most groups showed a curvilinear relationship (Figure 6.4). Thus, a parabolic model was fitted to each data group using the NDE parameters of Set I. Each model was tested for overall significance and the significance of the added variable. Results from the parabolic regressions, including r^2, SEE, overall significance, and significance level of the additional square term, is given in Appendix J-1. The SEE values ranged from a low of 3.1 percent moisture content for the parabolic model involving FRFREQ for group CGA7 to 39.1 percent moisture content for CGA6 with the FRFREQ model. Based on a 5 percent acceptance level, most polynomial models were rejected. Even the TTIME polynomial model for group CGA2, with an r^2 of 99.4 percent was rejected. This is due in part to the small sample sizes. Additionally, the distribution of the moisture content values was concentrated below the fiber saturation point (fsp), with usually one or two points above the fsp. The NDE parameters appeared to be influenced only slightly by moisture content below the fsp.

The Set I NDE variables were then normalized by four methods. Normalization involved division or multiplication by the peak amplitude of the energy spectrum (ENGINP) and total energy content (ENGINT) of the impact. This normalization was employed to decrease any influences on the measured NDE parameters due to differences in impact levels rather than moisture content. No consistant effect from normalization on the SEE was obtained when compared to nonnormalized data. A multivariate regression between the Set I NDE variables and the two input variables used for normalizing was also performed, but was not found to be significant for predictive purposes.

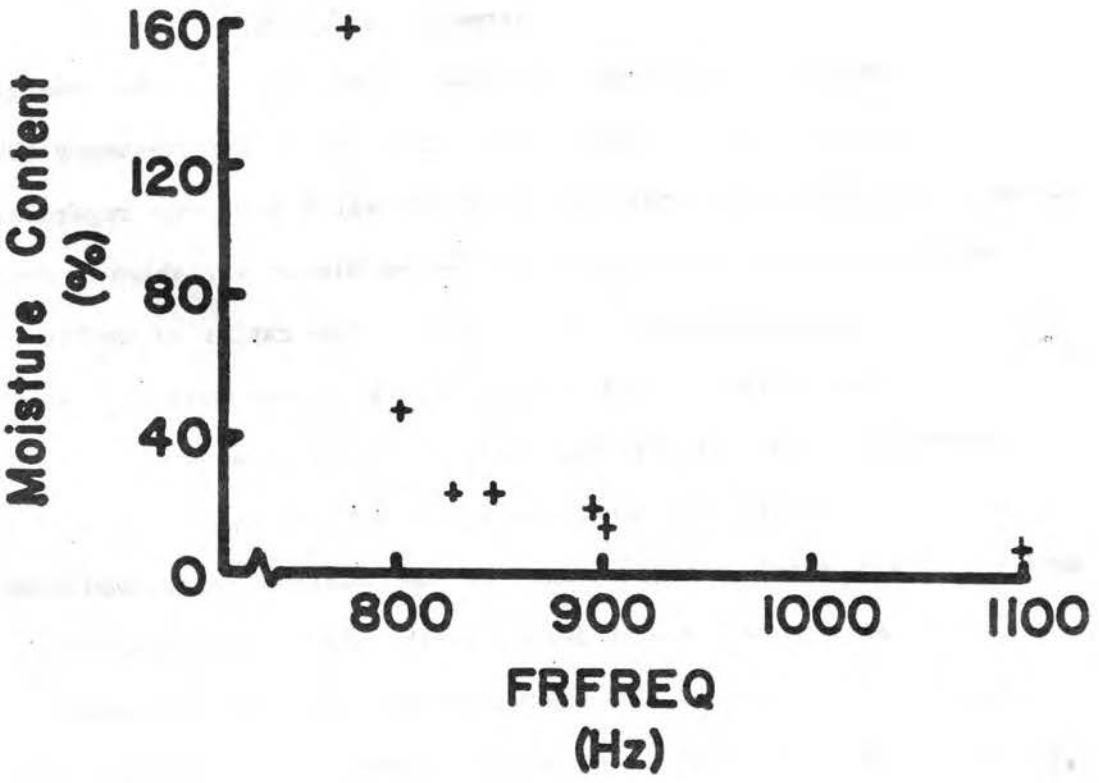

Figure 6.4. Scatter diagram of moisture content (percent) versus FRFREQ (Hz) for group CGA7 exhibiting curvilinear behavior.

A collection of 14 NDE parameters involving measures of energy spectral density was also investigated in relation to the moisture content of each group. An explanation of the variables, designated as NDE Set II, was given in Chapter 5. A listing of the variables and their acronyms is presented in Appendix A. The r^2 values ranged from 0.0 percent to 83.2 percent. Based on the SEE, none of the equations involving the Set II variables were better than those employing set I variables for the corresponding group.

Some comments regarding relative strengths of the energy predictor variables are in order. As in the case of the frequency NDE variables, there was no consistant trend for all 9 groupings regarding the relative strength or ranking of the predictor variables. Some general trends may be noted. In all groups, the ratios of amplitude and total energy content of the front and back accelerometers (RENGAMP and RINTENG) as predictor variables were poorly correlated with specimen moisture content. In most cases, normalization of the energy amplitudes and total energy values by the maximum input amplitude increased the r^2 values and decreased the SEE of the regressions. However, the amplitude of the input (ENGINP) was a better predictor than the response amplitudes. As moisture content increased above the fiber saturation point a general pattern of decreasing peak energy and total energy was usually apparent.

None of the regression analyses proved significant for the prediction of moisture content at all grain angles. The smallest SEE values were obtained with the parabolic models employing the Set I NDE variables. However, due inpart to the small sample sizes these equations were not significant in most cases.

6.4 PREDICTION OF WEIGHT LOSS

The weight loss of 48 specimens in the DEC study was defined in Chapter 5 and listed in Appendix I. For analysis of weight loss and the relationship with the energy NDE parameters, all weight gains were treated as 0 percent weight loss. Initially, all DEC specimens were analyzed together. The NDE parameters were measures of energy response of the specimen, both peak amplitudes (ENGAMP) and total energy content (INTENG). Energy parameters were measured before and after the specimens were decayed. Input peak energy (ENGIN) and total input energy (ENGINT), before and after decay, were measured and used to normalize the response amplitudes. These NDE variables were designated as Set III and their acronyms are listed in Appendix A.

The standard deviation of weight loss for all specimens was 1.944 percent. Based on the SEE of the regression, the best predictor variable was NENGAMPPD, i.e., the ratio of response to input energy spectrum amplitude before exposure to decay. This regression had an r^2 of 14.6 percent and a SEE of 1.797 percent weight loss. However, NENGAMPPD represents a measure of energy content before specimen exposure to decay. Since it has no physical relationship with the decay process, it was discarded. None of the regression analyses were significant for predictive purposes of specimen weight loss due to decay.

Specimens were then divided into three groups based on their nominal grain angle, i.e., 0, 20, and 90 degrees. The same NDE parameters were used as defined previously, these being designated as Set III. None of the regression analyses were significant for the 0 and 20 degree groups. For the 90 degree specimens, seven regressions

representing different NDE parameters were significant at least at the five percent level. The regression parameters for these relationships are given in Table 6.4. The best predictor variable was NNINTENGD, which has an r^2 of 56.7 percent, a SEE of 1.6 percent weight loss versus the 2.45 percent standard deviation of the gross data, and was significant at the 0.1 percent level. A plot of the regression equation and scatter diagram is presented in Figure 6.5.

The variable NNINTENGD is a measure of the total response energy in the specimen normalized through division by the total energy input to the system. Thus a value of 0.40 represents a response with 40 percent of the input energy. This response energy decreased as the weight loss of the system increased, as indicated by the negative slope of the regression equation. It should be noted that none of the NDE parameters which involved ratios of energy before and after decay were significant at the 5 percent level in predicting weight loss in

Table 6.4. Summary of regression statistics for prediction of weight loss (percent) in 90 degree specimens.

Predictor Variable	r^2 (%)	SEE (% weight loss)	Significance* Level	a	b
ENGIND	27.7	2.08	5	4.45	-0.518
NENGAMPD	31.3	2.03	2.5	4.67	-0.743
NENGAMPD	29.9	2.05	5	5.56	-0.465
RENGAMPD	28.9	2.06	5	3.86	-0.877
RRENGAMPD	26.2	2.10	5	4.19	-1.03
NINTENG	49.7	1.74	0.5	6.23	-9.14
NNINTENGD	56.7	1.61	0.1	9.13	-14.8

*5 Significant at the 5 percent level.
2.5 Significant at the 2.5 percent level.
0.5 Significant at the 0.5 percent level.
0.1 Significant at the 0.1 percent level.

wood, for this study. This nonsignificance, however, has to be viewed in light of the small range and suspect nature of the weight loss values obtained from the decay procedure.

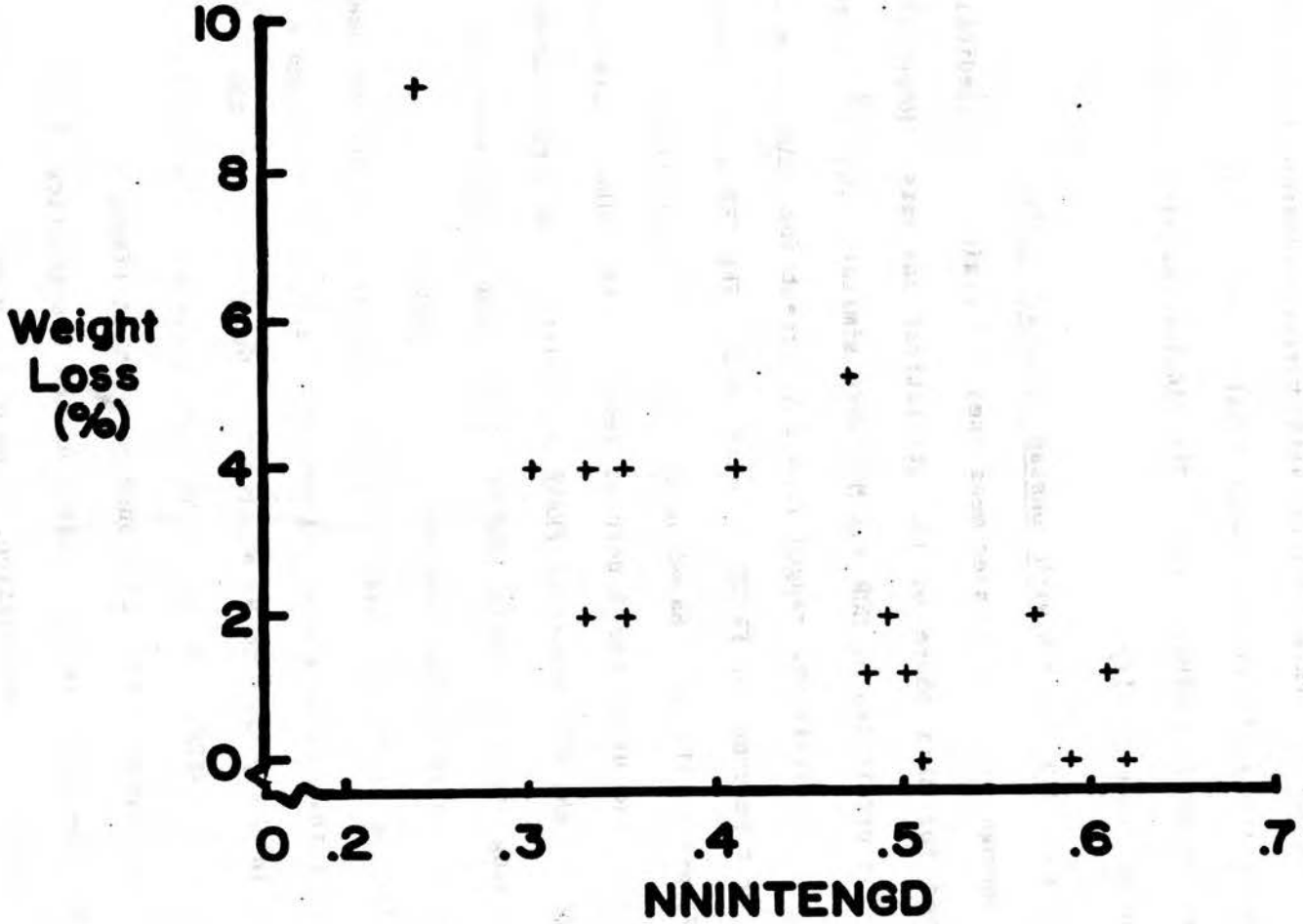

Figure 6.5. Scatter diagram of weight loss (percent) versus NNINTENGD for 90 degree DEC specimens.

6.5 PREDICTION OF MOR AND MOE

The relationship of all NDE parameters previously listed with MOR and MOE were investigated for the GAMC specimens. Analyses were performed on the GAMC specimens with three segregation plans, which were: constant moisture content with variable grain angle (CMC), constant grain angle with variable moisture content (CGA), and all specimens grouped together (GAMC). The results for each grouping will be presented sequentially.

6.5.1 MOR and MOE with Constant Moisture Content

Groupings of the GAMC specimens used for grain angle prediction were used for this phase of the statistical analysis. Regression results for prediction of MOR and MOE were similar. The r^2 of the straight-line regressions ranged from 2.5 percent for FRAMP in group CMC4 to 98.6 percent for FRINT in group CMC2. The SEE values ranged from 3071 psi to 315 psi. Based on the F-test for significance of the regressions, and using the 5 percent level as the cutoff point for significance, the NDE parameter FRAMP was deleted from further study. The remaining three variables (FRFREQ, FRINT, and TTIME) were significant in all cases at the 5 percent level or better.

Prediction of MOE was made with the same variables and specimen groupings as that given above. Values of r^2 ranged from 4.2 percent for FRAMP in Group CMC3 to 92.6 percent in Group CMC6 with the predictor variable FRFREQ. Ranges in the SEE value are from 162 ksi to 604 ksi. In general, the relationships with stiffness were not as strong as those for strength. Based on the F-statistics, FRAMP was deleted from further consideration. None of the variables were significant at the 5 percent level for group CMC1.

Plots of FRFREQ, FRINT, and TTIME against MOR and MOE exhibited curvilinear trends and to each a parabolic model was fitted. The parabolic regressions involving FRFREQ and FRINT were rejected at the 5 percent significance level and therefore the straight-line regressions models were used. All TTIME second-order polynomial models were significant at least at the 5 percent level.

The FRFREQ regressions were superior to the FRINT regressions based on the SEE values. A summary of the r^2, SEE, significance levels, and regressions coefficients for the straight-line FRFREQ and parabolic TTIME regressions are given in Tables 6.5 and 6.6, respectively. These regressions are for both MOR and MOE prediction.

A plot of the six straight-line FRFREQ regressions is given in Figure 6.6. The increase in slope as moisture content decreases is clearly discernable. This trend was not as consistent for MOE as for MOR, but in general the same trend of increasing slope applied. The NDE, FRFREQ and FRINT values were directly related to MOR and MOE, while TTIME was inversly proportional to both.

6.5.2 MOR and MOE with Constant Grain Angle

Segregation of the 58 GAMC specimens into the 9 groups used for moisture content prediction was performed to investigate the influence of moisture content on MOR and MOE as related to the NDE set I variables. A summary of the r^2, SEE, and significance level of the straight-line regression equations for prediction of MOR and MOE is presented in Appendices J-2 and J-3, respectively. Most regressions were nonsignificant at the 5 percent level, though r^2 values up to 95.7 percent were obtained. As indicated by the slopes of the regression analysis, trends were consistent for TTIME, FRFREQ, and

Table 6.5. Summary of best predictive equations for MOR at various moisture content values.

Group Designation	Mean Moisture Content (%)	MOR = a + b(FRFREQ) r^2 (%)	SEE (psi)	Significance Level	Model Used a (psi)	b (psi/hz)	MOR = a + b(TTIME) + c(TTIME^2) r^2 (%)	SEE (psi)	Significance Level	a (psi)	b (psi/μsec)	c (psi/μsec^2)
CMC1	109.6	46.2	1923	N.S.*	619	1.16	89.9	321	0.5	9937	-64.8	0.0985
CMC2	47.8	89.2	894	0.1**	-241	1.55	98.7	335	0.1	8743	-51.7	0.0801
CMC3	29.0	98.2	371	0.1	-1495	2.12	97.4	468	0.1	11511	-98.3	0.1950
CMC4	20.1	79.3	1555	0.1	-1603	2.29	90.2	1118	0.1	15305	-153	0.3330
CMC5	15.5	89.5	1269	0.1	-2162	2.83	90.3	1297	0.1	15387	-150	0.3430
CMC6	7.1	85.3	1991	0.5***	-2590	2.99	84.8	2261	2.5****	21445	-276	0.7790

*N.S. - Not significant at the 5 percent level.

**0.1 - Significant at the 0.1 percent level.

***0.5 - Significant at the 0.5 percent level.

****2.5 - Significant at the 2.5 percent level.

Table 6.6. Summary of best predictive equations for MOE at various moisture content values.

Group Designation	Mean Moisture Content (%)	MOR = a + b(FRFREQ) r^2 (%)	SEE (ksi)	Significance Level	Model Used a (ksi)	b (ksi/hz)	MOR = a + b(TTIME) + c(TTIME^2) r^2 (%)	SEE (ksi)	Significance Level	a (ksi)	b (ksi/μsec)	c (ksi/μsec^2)
CMC1	109.6	39.4	436	N.S.*	-16.6	0.229	94.0	158	2.5***	2056	-16.1	0.0261
CMC2	47.8	89.8	189	0.1**	-285	0.345	95.2	142	0.1	2087	-18.4	0.0351
CMC3	29.0	91.9	162	0.1	-46.7	0.427	96.0	121	0.1	2461	-25.4	0.0544
CMC4	20.1	69.6	345	0.1	-386	0.393	86.6	239	0.1	2768	-30.9	0.0696
CMC5	15.5	89.1	206	0.1	-459	0.450	89.3	217	0.1	2417	-25.8	0.0606
CMC6	7.1	92.6	193	0.1	-408	0.424	92.9	211	0.5**	2976	-38.4	0.108

*N.S. - Nonsignificant at the 5 percent level.

**0.1 - Significant at the 0.1 percent level.

***2.5 - Significant at the 2.5 percent level.

****0.5 - Significant at the 0.5 percent level.

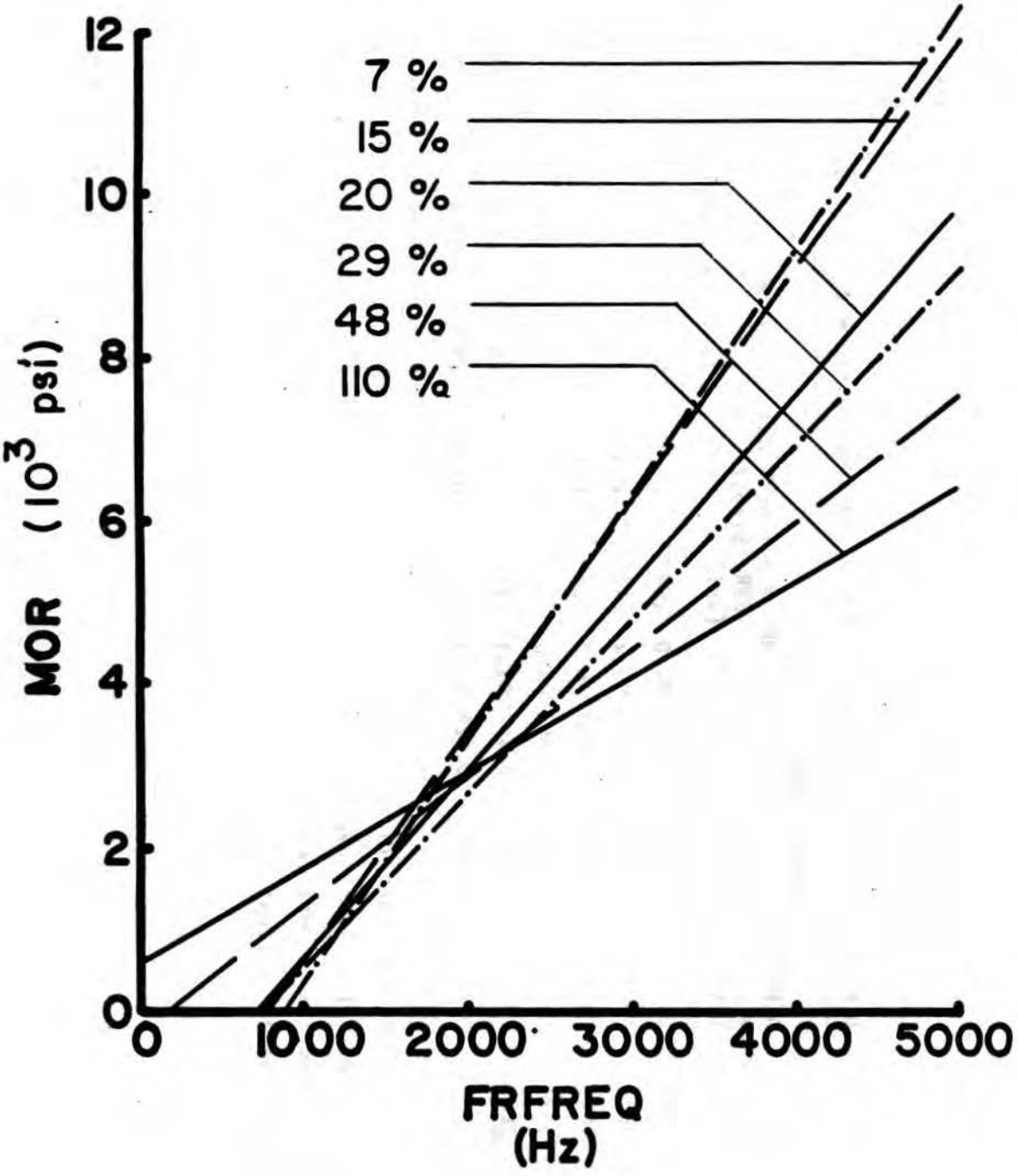

Figure 6.6. Plot of FRFREQ straight-line regressions for MOR prediction at various moisture content values.

FRINT. As MOR and MOE decreased in each group, due to increasing moisture content, TTIME values increased while FRFREQ and FRINT values generally decreased. A graph of MOR versus TTIME for the 9 groupings is presented in Figure 6.7. The slopes decrease substantially as the grain angle increases above 10 degrees.

6.5.3 MOR and MOE with Varying Grain Angle and Moisture Content

Based on the significance of regressions involving the NDE variables FRFREQ, FRINT, and TTIME for grain angle prediction, these variables were selected to regress with all 58 GAMC specimens grouped together.

Plots of MOR and MOE versus FRFREQ are given in Figures 6.8 and 6.9 respectively. Polynomial regressions up to third-degree were nonsignificant at the 5 percent level and were rejected. The significant straight-line regression equations are as follows;

$$MOR = -1293 + 2.20(FRFREQ) \tag{6.5}$$

$$MOE = -341 + 0.384(FRFREQ). \tag{6.6}$$

The r^2 and SEE values for Eq. (6.5) were 74.4 percent and 1642 psi. For the regression for prediction of MOE the r^2 value was 76.1 percent with an SEE of 273 ksi.

MOR and MOE are plotted as a function of FRINT in Figures 6.10 and 6.11 respectively. In both cases the third-degree polynomial was significantly better at least at the 5 percent level. For MOR prediction, the SEE value of 1669 psi was larger than that for the straight-line model involving FRFREQ. Similarly, the SEE of 306 ksi for the MOE polynomial regression involving FRINT was larger than that for Eq. (6.6).

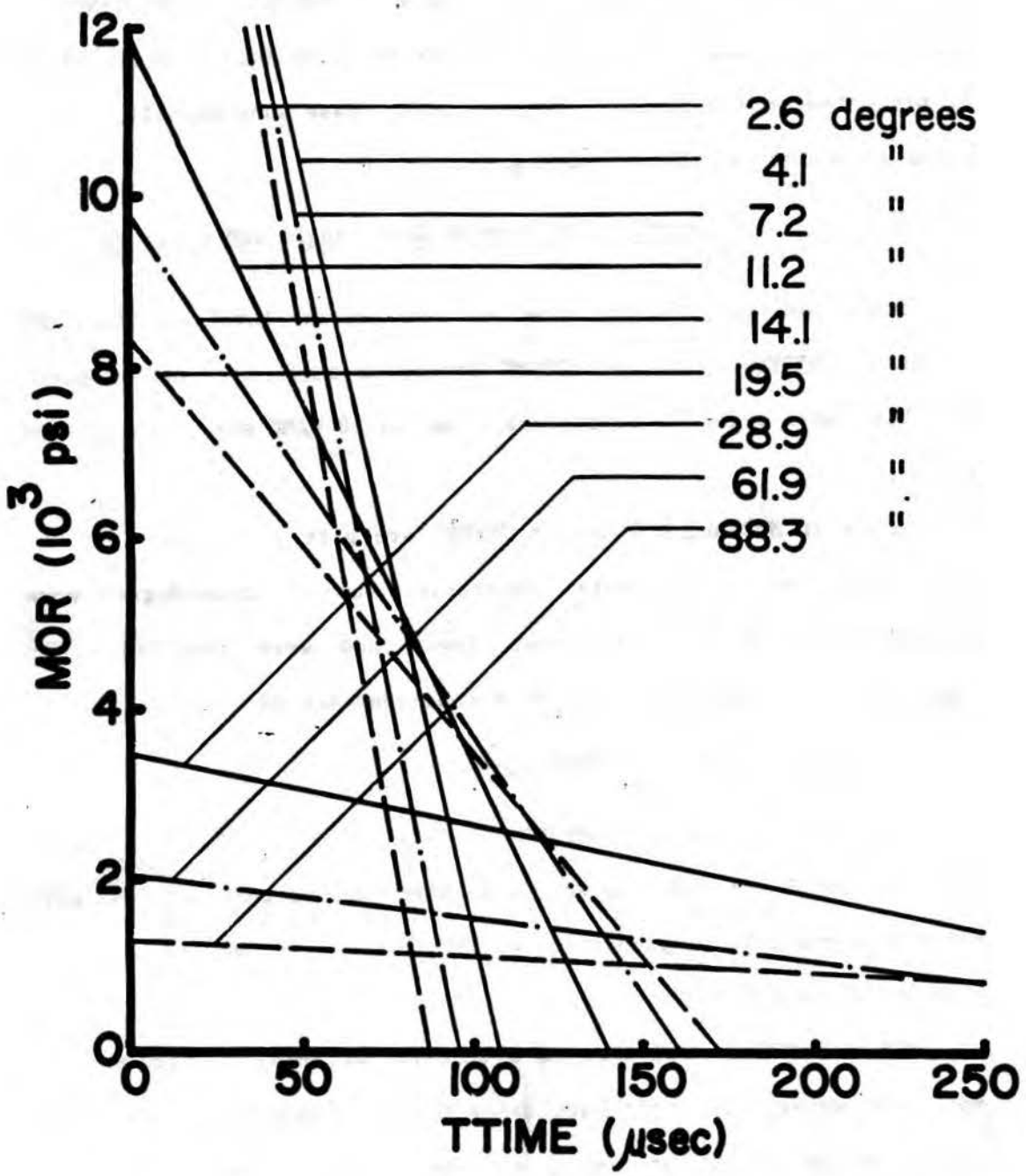

Figure 6.7. Plot of TTIME straight-line regression equations for MOR prediction at various grain angles.

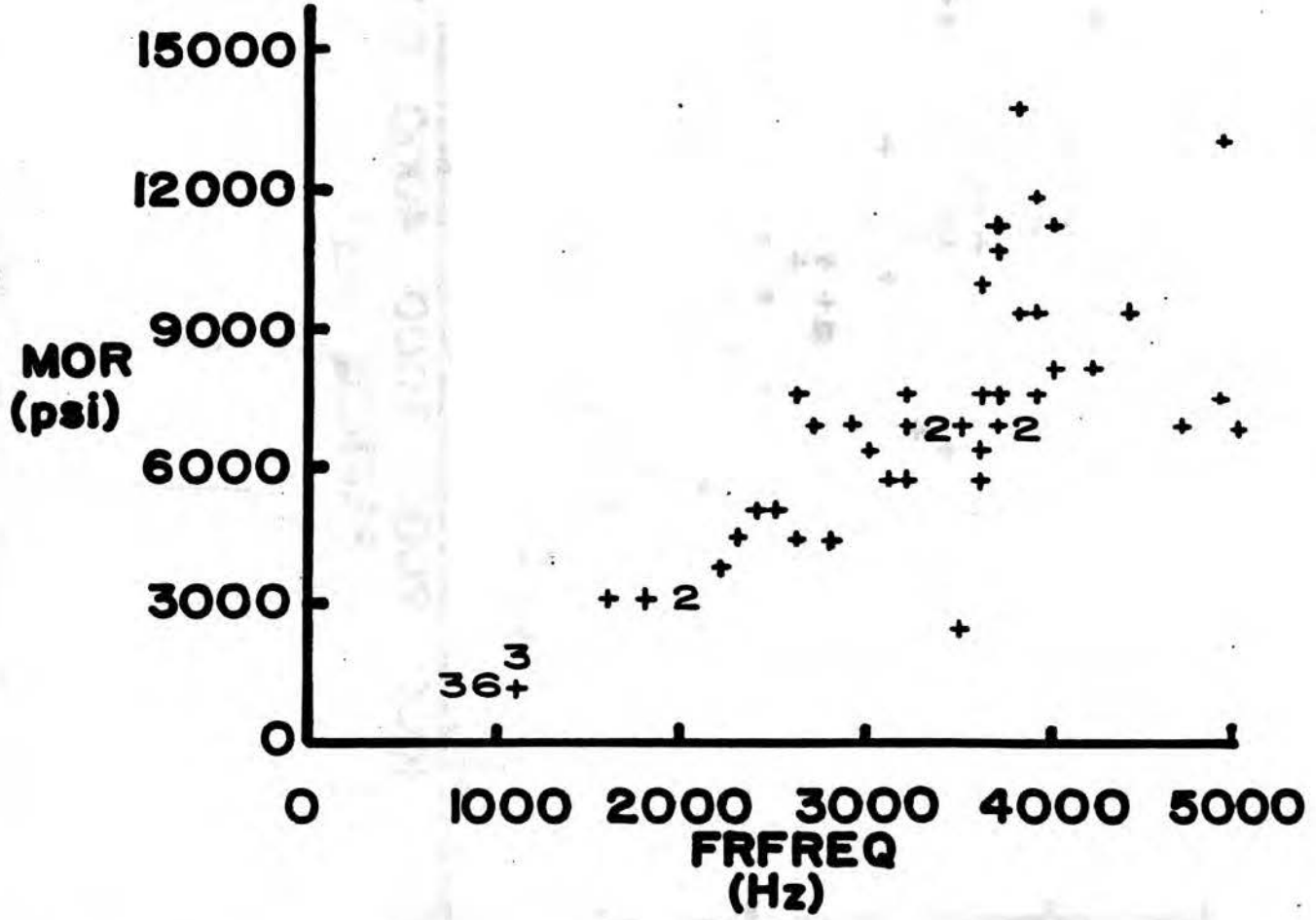

Figure 6.8. Scatter diagram of MOR versus FRFREQ (Hz) for all specimens.

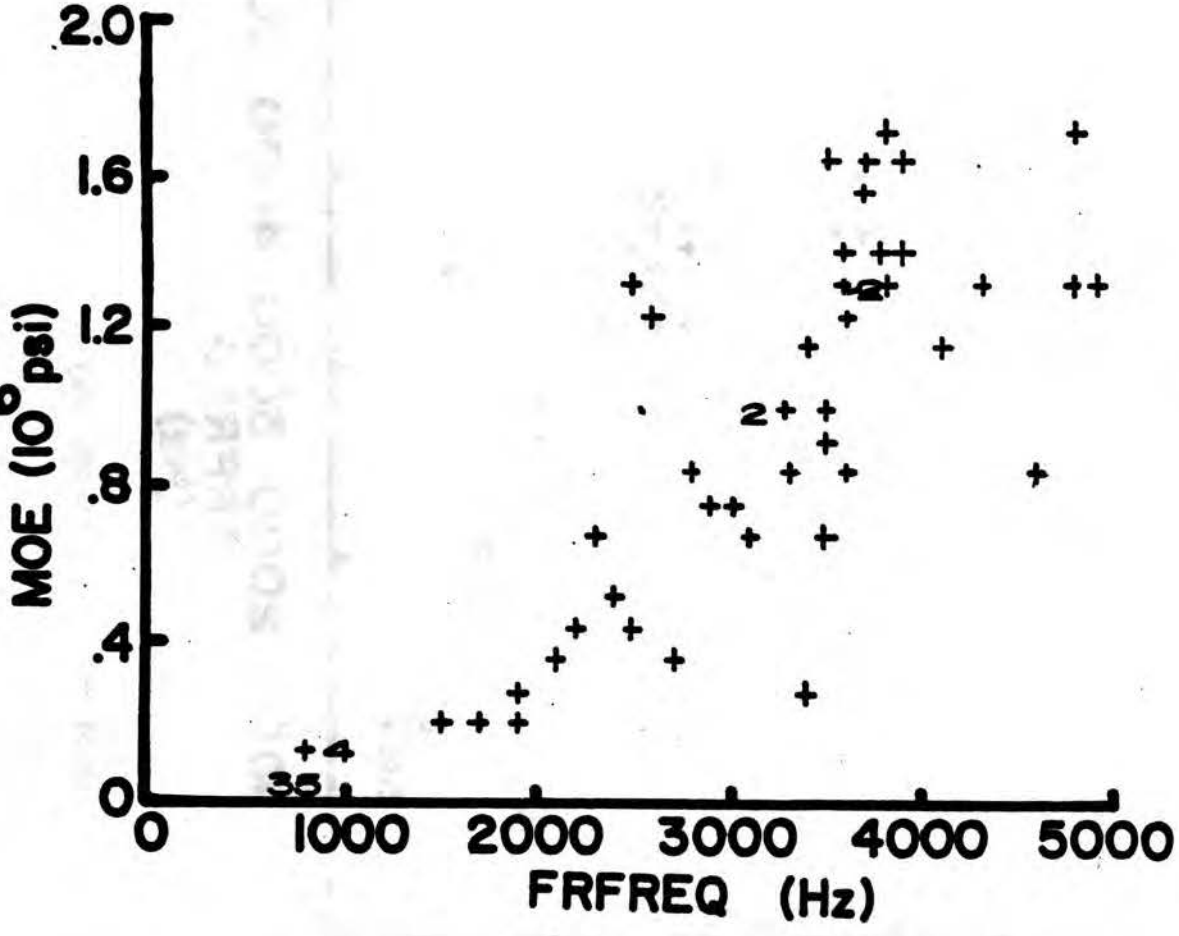

Figure 6.9. Scatter diagram of MOE versus FRFREQ (Hz) for all specimens.

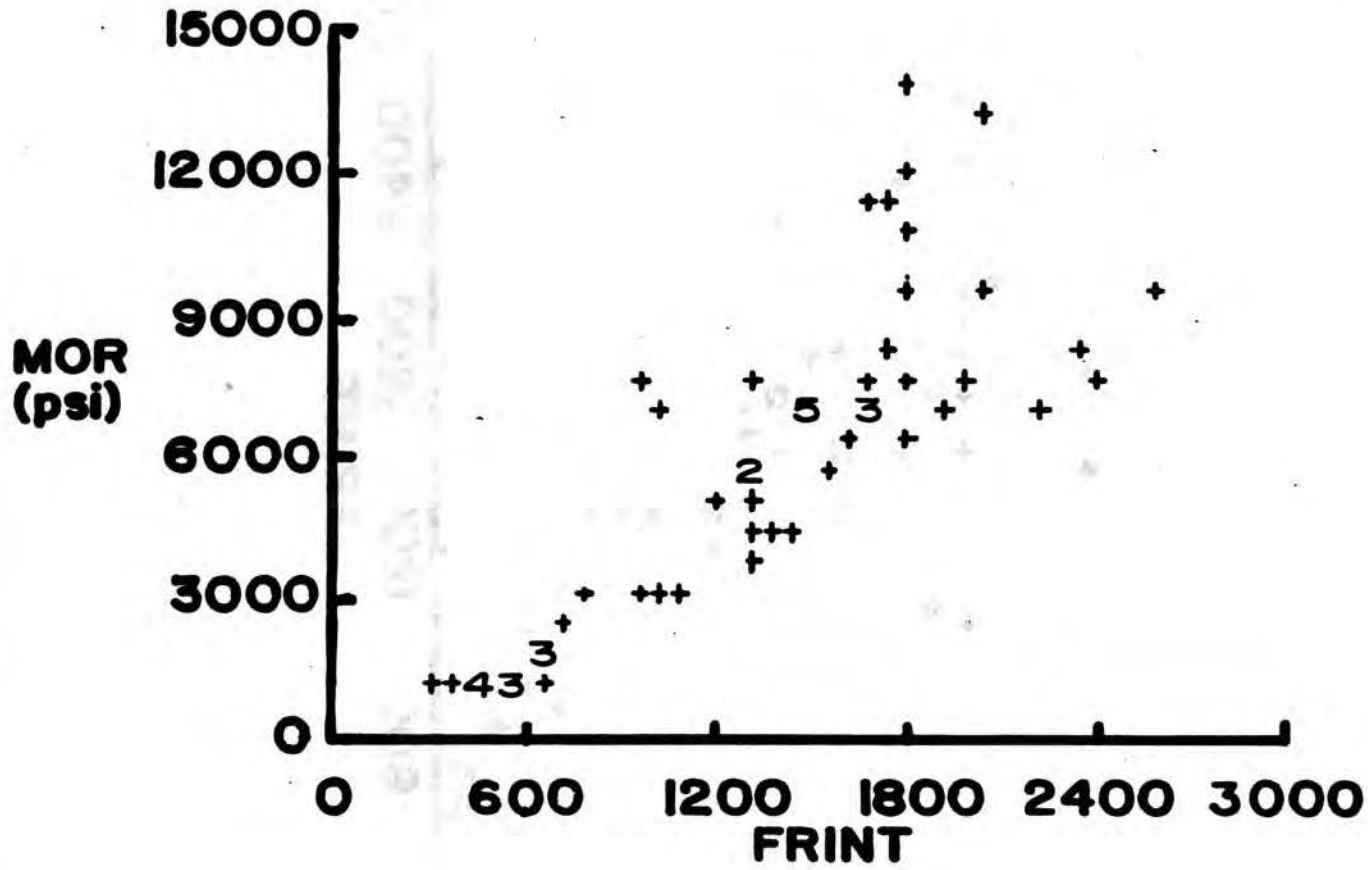

Figure 6.10. Scater diagram of MOR versus FRINT for all specimens.

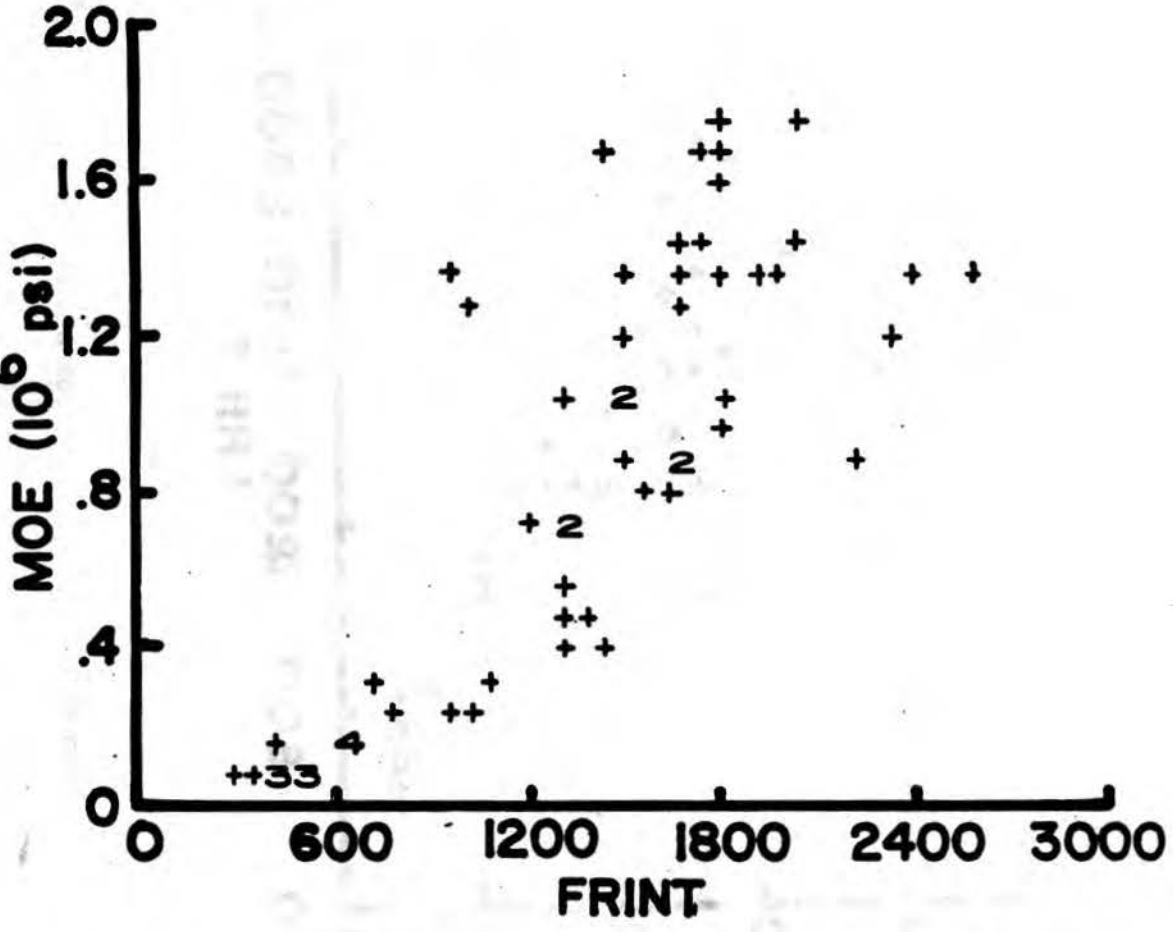

Figure 6.11. Scatter diagram of MOE versus FRINT for all specimens.

Scatter diagrams involving the NDE variable TTIME plotted against MOR and MOE are given in Figures 6.12 and 6.13, respectively. Based on the curvilinear trend, polynomial models up to the third degree were tried to fit the data. The third-order polynomial model was selected for prediction of both MOR and MOE. The regression equations are given below;

$$MOR = 15653 - 177(TTIME) + 0.649(TTIME)^2 - 0.0007(TTIME)^3 \quad (6.7)$$

$$MOE = 2780 - 34.6(TTIME) + 0.130(TTIME)^2 - 0.0002(TTIME)^3 \quad (6.8)$$

The r^2 of the MOR regression was 87.2 percent with an SEE value of 1180 psi. The associated statistics for prediction of MOE were an r^2 of 90.3 percent and an SEE of 177 ksi. Multiple regression equations involving FRFREQ, FRINT, and TTIME were not found to be significantly better than the polynomial models already reported.

The best prediction of MOR and MOE for all material combinations from direct correlation with the NDE variables was obtained using a third-order polynomial model with TTIME. These relationships are given in Eqs. (6.7 and 6.8), respectively.

The TTIME value and specific gravity of each specimen was used to determine the dynamic stiffness E_d by use of Eq. (2.4). A listing of the E_d and MOE values for each specimen is given in Appendix J-4. The values are plotted in Figure 6.14. A straight-line regression analysis was significant at the 0.1 percent level. The r^2 and SEE values were 88.9 percent and 191 ksi. The regression equation is as follows:

$$MOE = 75.4 + 0.898\ E_d \quad (6.9)$$

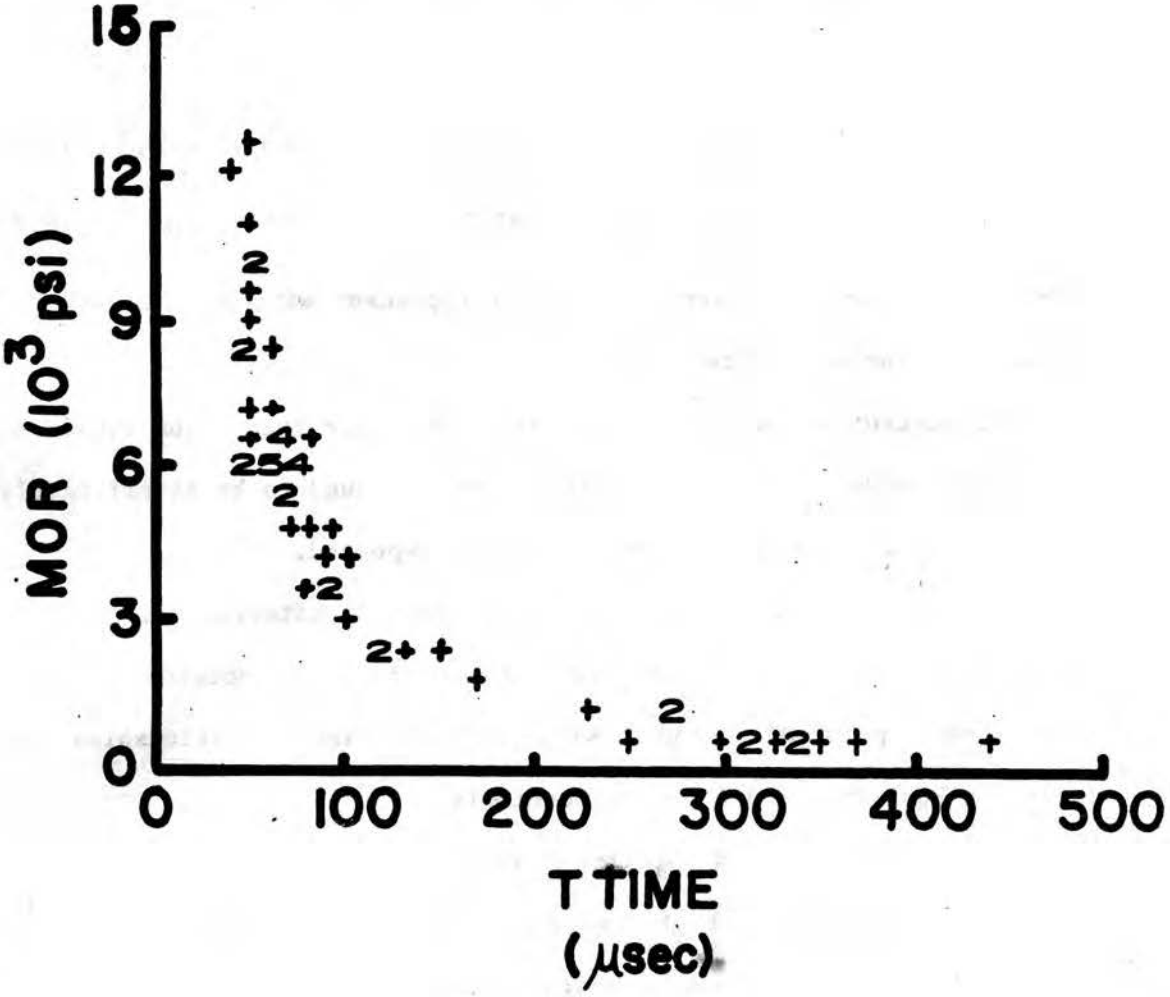

Figure 6.12. Scatter diagram of MOR versus TTIME for all specimens.

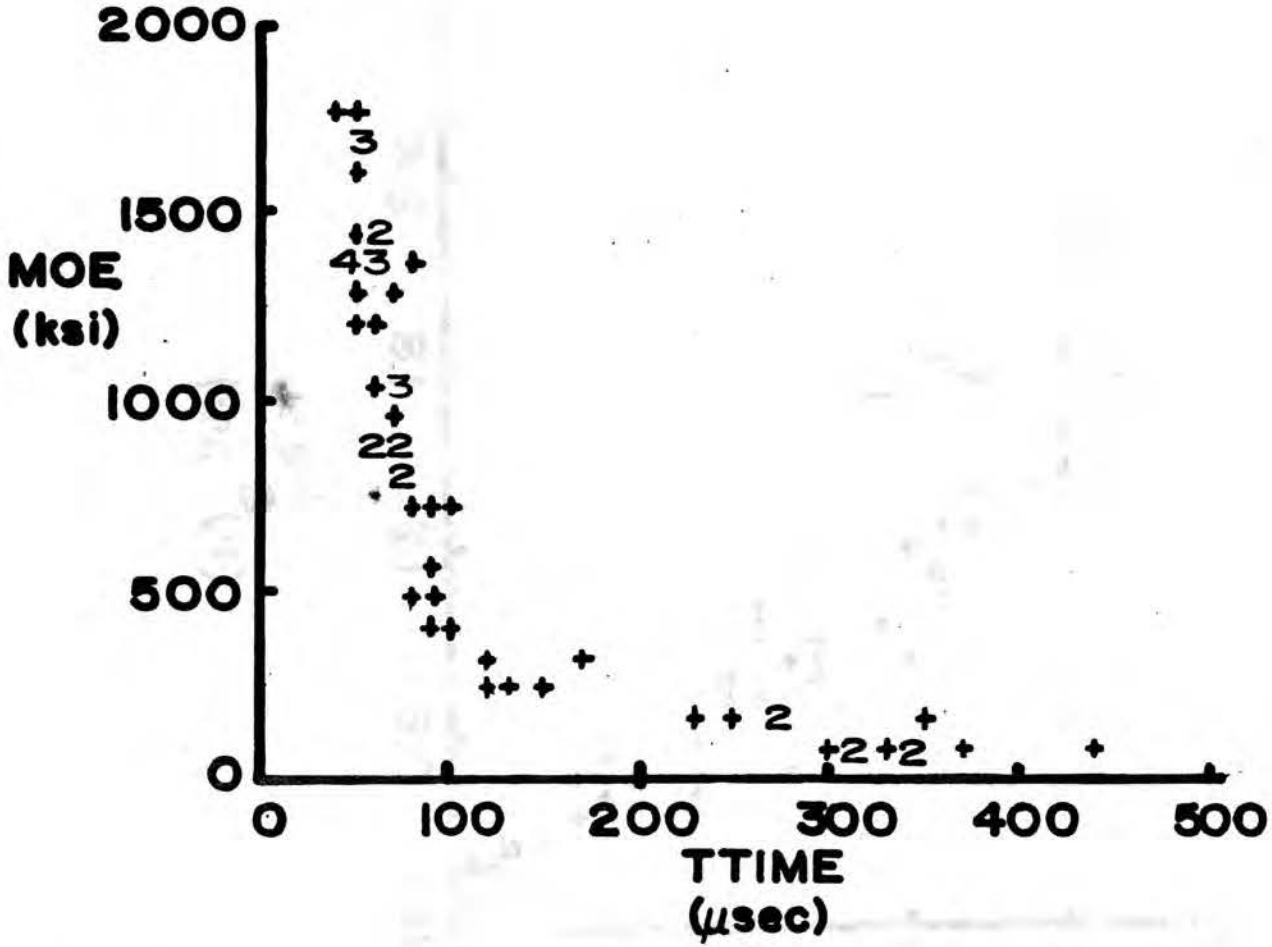

Figure 6.13. Scatter diagram of MOE versus TTIME for all specimens.

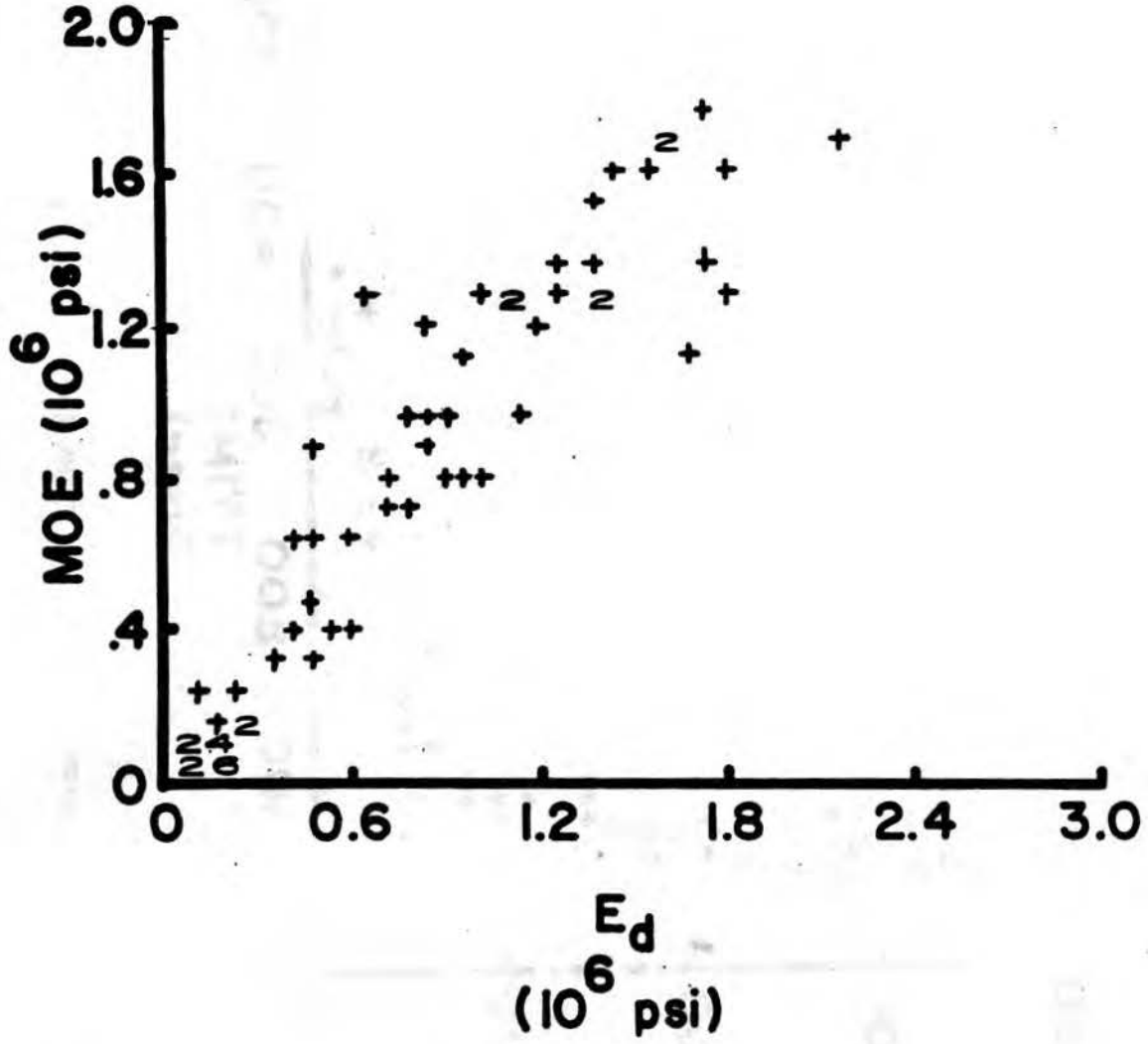

Figure 6.14. Scatter diagream of MOE versus E_d for all specimens.

From Eq. (6.9) we see that E_d averaged approximately 10 percent larger than the corresponding MOE value which is usually the case for wood due to its time dependent behavior. The SEE of 191 ksi was only surpassed by Eq. (6.8) involving TTIME, with an SEE value of 177 ksi.

Chapter 7

WAVE PROPAGATION ANALYSIS AS AN NDE TECHNIQUE

7.1 INTRODUCTION

The purpose of this investigation was to ascertain the suitability of wave propagation characteristics as an NDE technique for predicting the strength of an individual piece of wood. To accomplish this, a better understanding of the relationship between wave propagation patterns and wood properties is necessary. The analysis of waves in conjunction with regression evaluation was carried out to reach the goal of strength prediction. The investigation of the relationship of wave properties with material characteristics is closely linked with that of strength prediction. However, these two classes of relationships are treated separately in this chapter.

7.2 INFLUENCE OF WOOD PROPERTIES ON WAVE PROPAGATION

The anatomy and condition of wood have a marked influence on wave propagation. As shown in Chapter 6, grain angle is highly correlated with the time of travel through the material (TTIME), frequency at which the amplitude response spectrum reaches a maximum (FRFREQ), and total gain of the response (FRINT). In working with transverse impacts on anisotropic plates, Moon (54) found that wave velocity was influenced by the orientation of the material. In wood, as the grain angle increases, the velocity decreases in a curvilinear fashion.

Dunlop (16) has speculated that the wave front primarily follows the S2 layer of the cell wall. While this is open to debate, the author feels that the cellular structure of the wood does necessitate that the wave must travel in the cell walls, at least below the fiber saturation point. When the wave energy is transmitted from cell to cell it must pass through the middle lamella material, which is less dense than the cell wall itself. This density change results in an impedance difference which will cause some energy to be reflected back into the cell wall.

When waves are propagating in the longitudinal direction, there are less lamella "connections" to pass through per unit length than in the perpendicular direction. This is due to fiber axis alignment in the longitudinal direction. The ratio of length to diameter of a typical fiber in Douglas-fir is on the order of 120. Thus, this many times larger number of connections must be crossed per unit length in the perpendicular to grain direction than in the longitudinal direction, which is likely to cause increased attenuation in the transmitted energy. Oved et al. (58) found that layered media gave larger shock attenuation values than a solid material. In wood, there is a variation in the gross density of the cells between early and late wood. This is prominant in such abrupt transition woods as Douglas-fir. It is felt that this produces a layering effect in the perpenducular to grain direction similar to that studied by Oved. Variation in cell density may also be present within a growth increment (60). At either level of material organization, the variation in density is most pronounced in the perpendicular to grain direction. This would cause larger wave attenuation than that occurring in the parallel to grain direction.

Results from this research indicates that wood behaves as a visco-elastic material during wave propagation. In visco-elastic materials, high frequency waves are damped more readily than are lower frequency waves (49). This characteristic, coupled with the higher attenuation inherent in the perpendicular direction leads us to expect a propagated wave to possess less higher frequency content at higher grain angles. The amplitude gain function, which measures the gain of frequencies, may be interpreted as indicating the amount of transmitted energy. FRFREQ values indicating the frequency of most gain is in the order of 800 Hz for perpendicular to grain specimens regardless of moisture content. For 0 degree specimens, values range from 4000 Hz to 5000 Hz. Additionally, the total gain experienced, as indicated by the FRINT value, decreased from 1500 at parallel to grain orientations to 400 for 90 degree specimens. The magnitude of the above differences could be expected to be species dependent. This is partly due to the differences in specific gravity between early and late wood as well as overall cell density of each species.

The influence of moisture content on wave propagation parameters may be dependent of the orientation of the material and whether free and/or bound water is present. Bound water, situated in the cell walls may not interfere with propagation as much in the parallel to grain direction as at higher grain angles. This contention is based on the absence of significant relationships between moisture content below fsp for the NDE variables studied.

Free water is present in the cell voids. It is assumed that propagation through the free water should cause an increase in energy loss because water's density is low in relation to the cell wall, and

reflection and refraction are caused by this impedance mismatching. In the parallel to grain direction, it is assumed the the wave propagation occurs primarily in the cell wall. At higher grain angles, free water in the cell cavities present a substantial mass through which the wave may pass. Additionally, this free water causes an increase in the overall mass of the material. At low grain angles (0 and 3 degress), where free water may not interfere significantly with propagation, little difference in the average FRAMP value was present, regardless of moisture content. At 0 degrees the average FRAMP values were 3.61 above and 3.52 below the fsp, respectively. Similar results for the 3 degree nominal grain angle specimens were obtained, as shown in Table 7.1. The FRAMP values above fsp for large grain angles (30, 60, and 90 degrees) were significantly lower than that below fsp, indicating increased attenuation. For those three orientations, FRAMP above fsp was 2.84, 2.84, and 2.48 while below fsp they were 4.24, 5.13, and 4.11. Thus, the influence of free water appears to be more predominate at higher grain angles.

While the influences of grain angle and moisture content on wave propagation energy as measured by the frequency response function and velocity values appears significant, the energy spectrum values themselves were not significantly affected. This difference may be partially explained in light of works conducted on other materials and the cellular structure of wood. From wave propagation theory it is known that if a void in a material is obliquely struck by a propagating stress wave, a scattering of the wave occurs (73). If the material is homogeneous, isotropic, linearly elastic, and if the crack is flat with a smoothly curved edge, the location and size of

Table 7.1. Average FRAMP values above and below the fiber saturation point at five grain angles.

Nominal Grain Angle (degrees)	Average FRAMP Value	
	<26% Moisture Content	≧26% Moisture Content
0	3.68	3.52
3	2.48	2.08
30	4.24	2.84
60	5.13	2.84
90	4.11	2.48

the void may be approximated (1). For comparison with wood, an assumption that the intrinsic cell cavities in wood may be modeled as voids in an otherwise solid material may be made. The cell cavity, however, is of complex shape. Additionally, modifications in structure such as decay pockets and ring shakes due to environmental influences create even more complex geometries of voids. Studies by Tittmann et al. (73) found that the frequency patterns in titanium which had a nonspherical defect were modulated in comparison to that obtained for a spherical defect. No quantitative relationships were obtained, however, in that study. Alder and Lewis (2) observed similar effects on the power spectra as the orientation of an elliptical crack was changed in bonded titanium alloy.

The anisotropic character of wood and predominanace of irregular shaped voids is sure to cause scattering of any propagated wave and thus significantly alter the energy spectrum. Further, the orientation of the flaw itself influences the scattering pattern and hence the power and energy spectra. It seems reasonable to assume that wood displays a response similar to that obtained with manmade composite materials. This is not surprizing since wood has been modeled as a composite of cellulose fiber embedded in a lignin matrix, a layup scheme which is analagous to many manmade composites.

7.3 PREDICTION OF WOOD STRENGTH THROUGH NDE PROCEDURES

Statistical analyses between various wood properties and NDE parameters were presented in Chapter 6. The resulting relationships are utilized in this section for the prediction of the MOR of individual pieces of wood. Several approaches are presented with comparisons. Each approach was conducted on the 58 grain angle-

moisture content (GAMC) specimens to examine their applicability to a wide range of material conditions. To assess their accuracy, the predicted MOR values from each method were compared with the MOR values obtained through destructive testing.

7.3.1 Prediction of Strength from Measured Material Properties

The prediction methods investigated were selected to provide for a wide range of possibilities and may not be practical for direct extension to NDE of poles. The methods may be divided into two general classes. The first approach toward prediction of strength values utilized the accepted relationship between strength and grain angle given by Hankinson's formula (Eq. 2.7) and the log MOR-moisture content relationship (6):

$$\log MOR = a - b(MC) \tag{7.1}$$

The procedure used to predict MOR from the material properties is as follows;

(1) Determine the grain angle,

(2) Use Hankinson's formula to determine green strength and strength at 7 percent moisture content,

(3) Determine by a straight-line relationship log MOR for the chosen moisture content in the selected grain angle,

(4) Convert log MOR to MOR.

This procedure was followed both when the material properties were known and when the material properties were predicted from NDE relationships determined in Chapter 6. The second approach was to correlate measured NDE properties directly with measured specimen MOR values. This approach is explained fully in section 7.3.3.

The use of Hankinson's formula for MOR adjustment requires the knowledge of the strength values at 0 and 90 degrees. If this knowledge was available for poles, the problem would already be solved. Actual test data, given in Appendix G, were used to determine these end points for the specimens in this study. For the green condition, a strength of 520 psi at 90 degree grain angle was used. There were no test specimen data with zero degree grain angle, so the values of four specimens with near zero degree grain angle were averaged. At the average grain angle of 2.5 degrees an MOR value of 6300 psi was obtained. Through Hankinson's formula a MOR value of 6450 psi was computed for the parallel to grain value for green wood. Following the same procedures, MOR values of 13,000 psi and 1000 psi were selected as the parallel and perpendicular to grain values at 7 percent moisture content. A computer program was written to obtain the strength at any grain angle and any moisture content value between 7 percent and green condition.

The predicted MOR (MOR_{pred1}) values for all specimens using measured grain angle and moisture content values are summarized in Appendix K. If the prediction was perfect, a linear regression between actual MOR (MOR_{act}) and predicted MOR would be a line passing through the origin with a slope of 45 degrees. The actual linear relationship between predicted MOR and actual MOR was evaluated. The resulting scatter diagram and regression equation is presented in Figure 7.1. The regression equation resulted in;

$$MOR_{act} = 256 + 1.05\ MOR_{pred1} \qquad (7.2)$$

The r^2 value is 93.9 percent with an associated SEE of 796 psi.

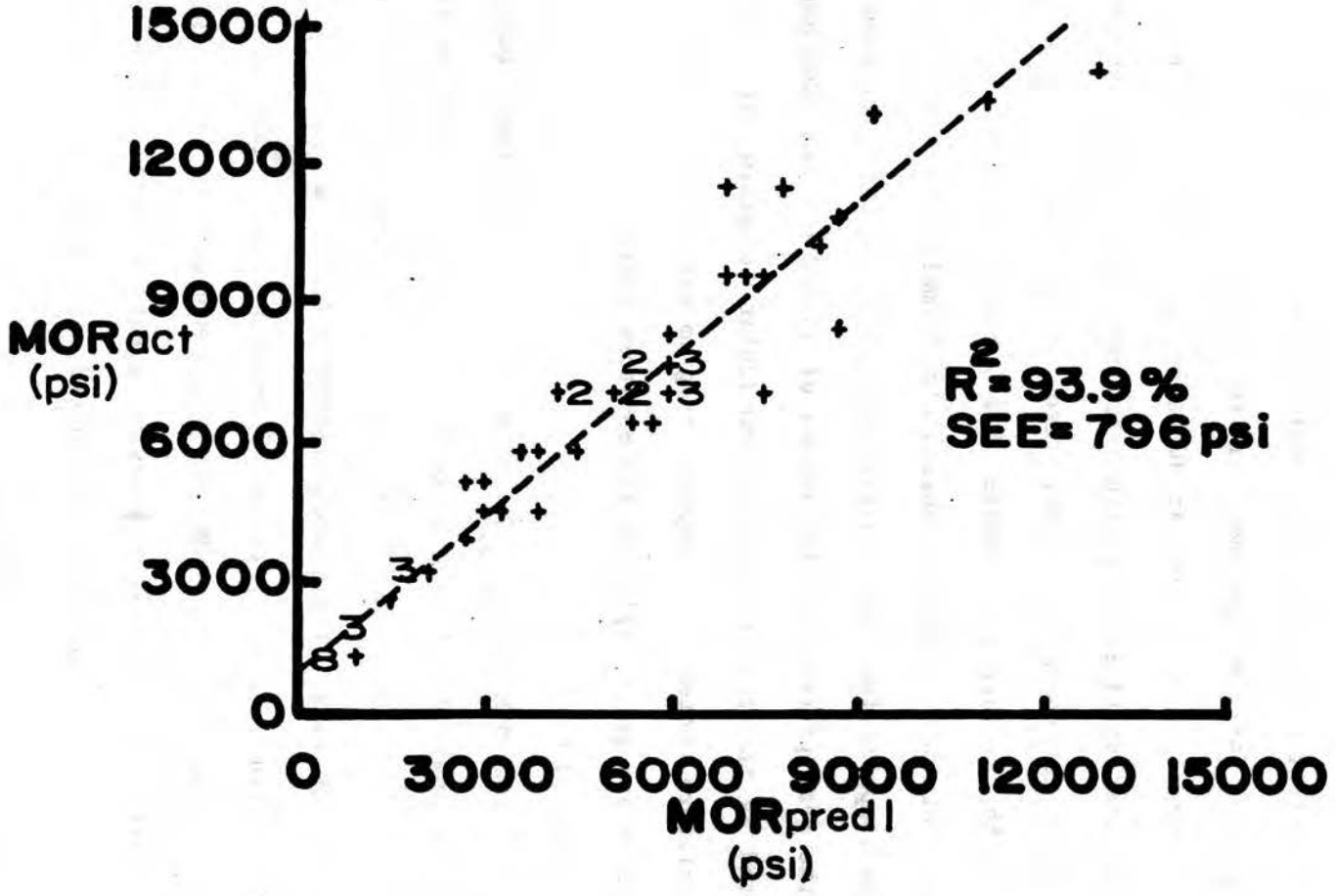

Figure 7.1. Scatter diagram of MOR_{act} versus MOR_{predl} as predicted from measured material properties.

Additionally, predicted and actual MOR values were compared and a percentage error was determined using the equation;

$$\% \text{ error} = \frac{(MOR_{pred} - MOR_{act}) * 100}{MOR_{act}} \tag{7.3}$$

Using Eq. (7.3), the average error between MOR_{pred1} predicted from the known material properties and the actual MOR was 16.0 percent.

The value of this predictive method is that of giving an estimate for the accuracy that can be expected if only grain angle and moisture content are used for strength prediction. If the NDE procedures could estimate grain angle and moisture content of wood exactly, the same accuracy in prediction of actual MOR would result. Inexactitude in estimation of the material properties would result in a poorer correlation with MOR_{act}. The influence of material property estimation on MOR prediction are investigated in the next section.

7.3.2 Prediction of Strength through Measured Moisture Content and Predicted Grain Angle

Moisture content values of the specimens used in the previous section were utilized in conjunction with predicted grain angles. Four methods were used to determine grain angle from NDE parameters. Once the predicted grain angle values were obtained, MOR was predicted in the same fashion as that used in the previous section. The four grain angle estimates resulted in four estimates of MOR, designated as MOR_{pred2}, MOR_{pred3}, MOR_{pred4}, and MOR_{pred5}.

The first two methods of grain angle prediction assumed no knowledge a priori of moisture content. Equations (6.3 and 6.4) involving the NDE variables TTIME and FRFREQ respectively were used. The MOR values predicted using these estimates of grain angle and

actual moisture content were designated MOR_{pred2} and MOR_{pred3}. Alternatively, moisture content was assumed known. Based on the moisture content the specimens were placed into one of six groups. These groups and the equations used are given in Table 7.2. The MOR values predicted from the two equations involving TTIME and FRINT for each grouping are designated MOR_{pred4} and MOR_{pred5}.

Regression analysis between actual MOR and the predicted MOR from the four methods explained is summarized in Table 7.3. A listing of the predicted MOR values is given in Appendix K. Scatter diagrams with associated equations are shown in Figures 7.2 to 7.5. The r^2 values ranged from a low of 78.4 percent for MOR predicted with grain angle estimated from Eq. (6.3) (MOR_{pred2}) to 90.2 percent for MOR_{pred4} (grain angle estimated for TTIME equations in Table 7.2). SEE values from 1007 psi to 1496 psi. If no a priori knowledge of moisture content exists, the model involving FRFREQ (MOR_{pred3}) to predict grain angle is better than that using TTIME(MOR_{pred2}), the former having an SEE of 1325 psi and an average error of 21.5 percent. When moisture content is known, use of the TTIME value to predict grain angle (MOR_{pred4}) was better than using FRINT, resulting in an SEE of 1007 psi and an average percentage error of 15.9 percent, as determined by Eq. 7.3.

7.3.3 Prediction of Strength by Direct Correlation with NDE Parameters

Regression analysis in Chapter 6 outlined two equations involving TTIME and FRFREQ and their relationship with MOR. These equations, Eq. (6.5 and 6.7), are repeated here.

Table 7.2. Summary of equations for prediction of grain angle when moisture content is known.

Moisture Content Range (%)	Prediction Equation Coefficients				
	TTIME		FRINT		
	a (degrees)	b (degrees/μsec)	a (degrees)	b (degrees)	c ($*10^{-6}$ degrees)
0≦MC≦8	-7.48	0.341	165.0	-0.160	40.3
9≦MC≦17	-4.82	0.265	134.	-0.125	29.7
18≦MC≦25	-6.97	0.275	135.	-0.137	36.6
26≦MC≦40	-7.57	0.252	119	-0.119	30.5
41≦MC≦55	-7.40	0.231	135.	-0.173	58.1
56≦MC	-6.61	0.219	119.	-0.137	37.5

Table 7.3. Summary of regression statistics for prediction of MOR.

Predictor* Variable	r^2 (%)	SEE (psi)	Regression Coefficients a (psi)	b (psi/psi)	Average Error (%)
MOR_{pred1}	93.9	796	256	1.05	16.0
MOR_{pred2}	78.4	1496	563	0.95	23.4
MOR_{pred3}	83.1	1325	881	0.88	21.5
MOR_{pred4}	90.2	1007	55.1	1.13	15.9
MOR_{pred5}	81.2	1396	438	1.01	20.5
MOR_{pred6}	74.4	1642	0.176	1.00	25.2
MOR_{pred7}	87.2	1159	-0.054	1.00	32.0

*Pred1 - Grain angle and moisture content of specimens known. Use of Hankinson's formula by logMOR-MC equations for adjustment.

Pred2 - Moisture content of specimens known. Grian angle predicted from Eq. 6.3 involving NDE parameter TTIME. Use of Hankinson's formula and logMOR-MC equations for adjustment.

Pred3 - Moisture content of specimens known. Grain angle predicted from Eq. 5.4 involving NDE parameter FRFREQ. Use of Hankinson's formula and logMOR-MC equations for adjustment.

Pred4 - Moisture content of specimens known. Grain angle predicted from equations in Table 7.2 involving NDE parameter TTIME. Use of Hankinson's formula and logMOR-MC eauations for adjustment.

Pred5 - Moisture content of specimens known. Grain angle predicted from equations in Table 7.2 involving NDE parameter FRINT. Use of Hankinson's formula and logMOR-MC equations for adjustment.

Pred6 - Direct prediction of MOR using Eq. 6.5 and NDE parameter FRFREQ.

Pred7 - Direct prediction of MOR using Eq. 6.7 and NDE Parameter TTIME.

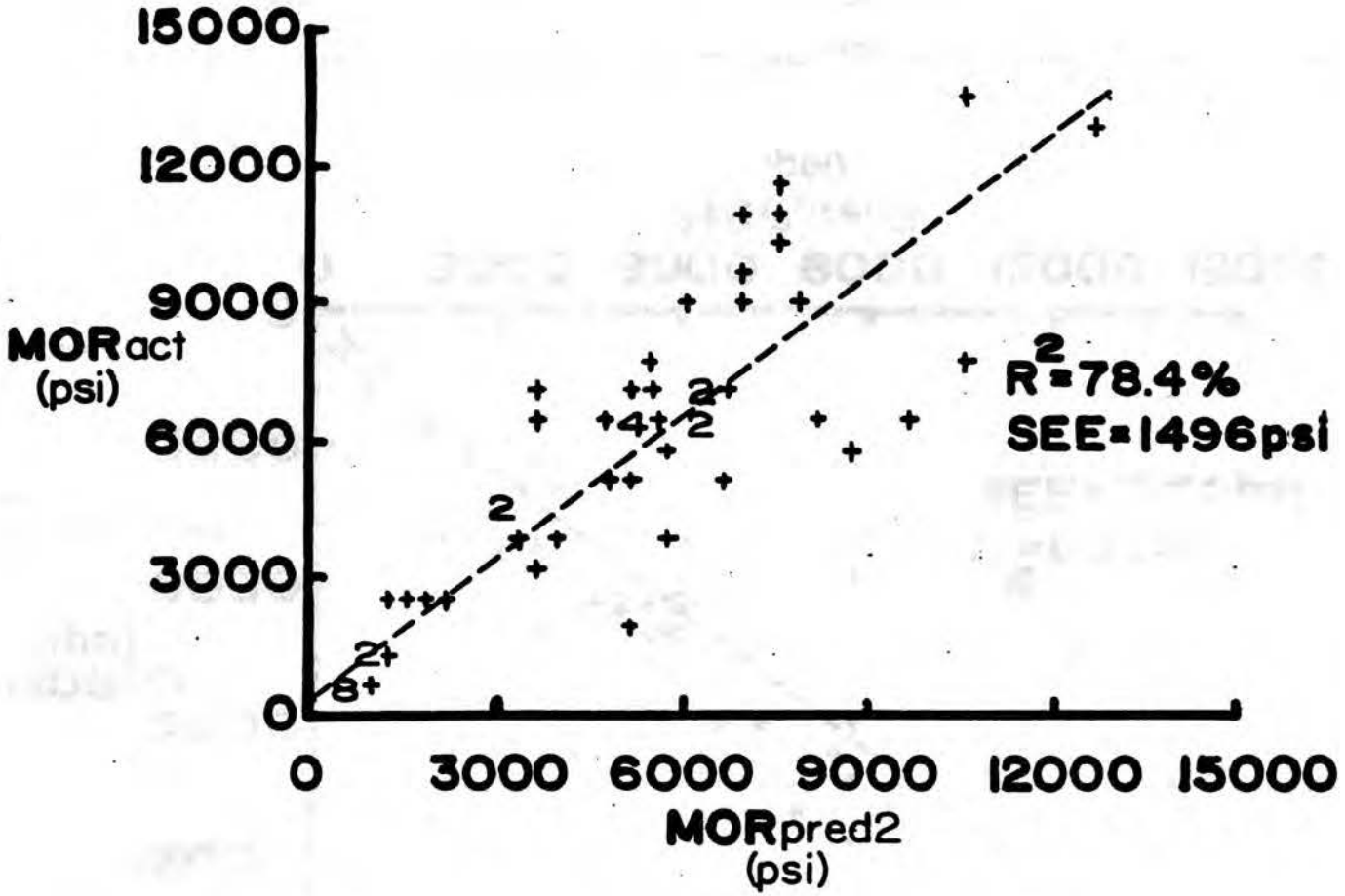

Figure 7.2. Scatter diagram of MOR_{act} versus MOR_{pred2} as predicted from measured moisture content and grain angle predicted from Eq. 6.3.

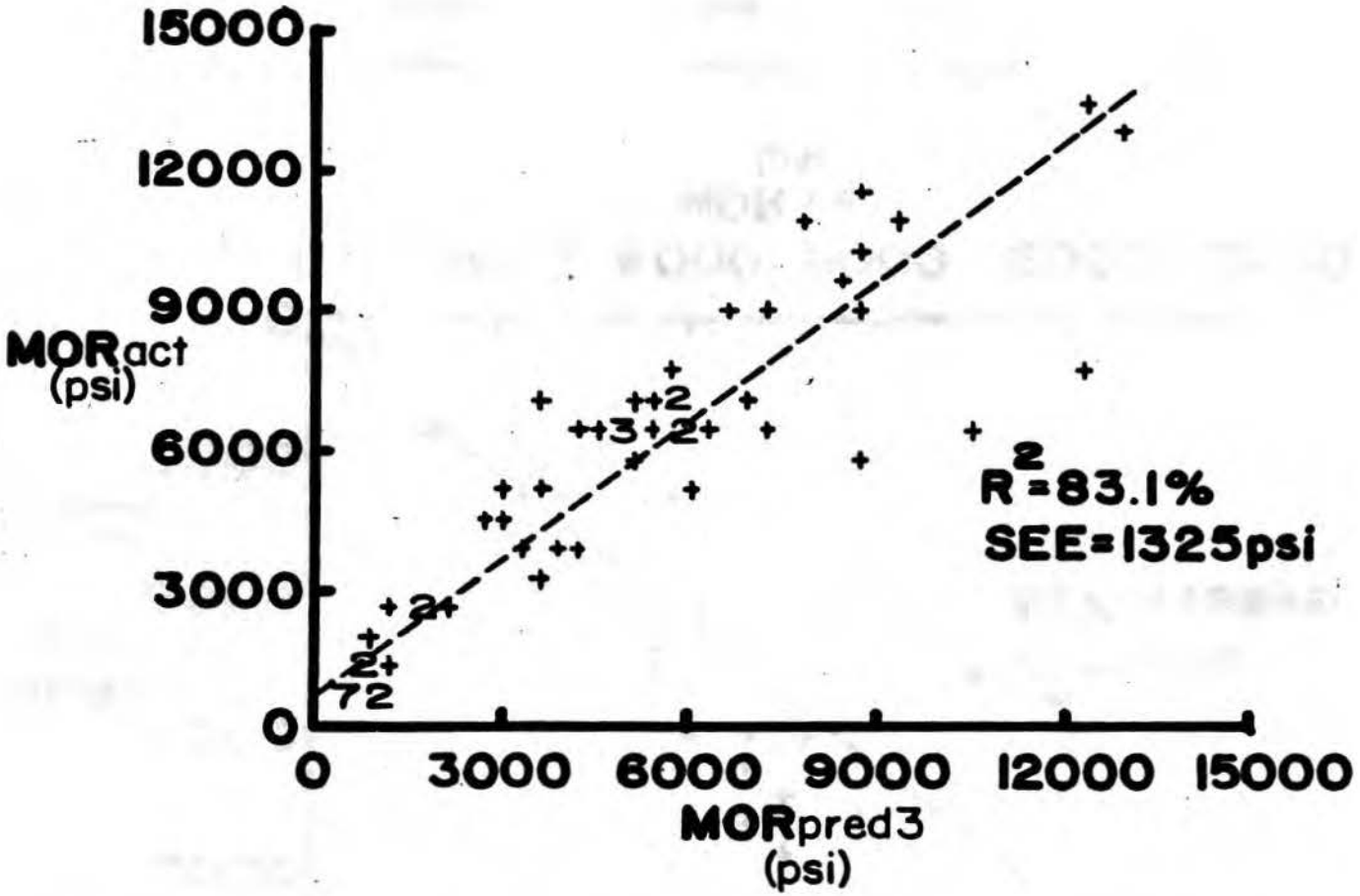

Figure 7.3. Scatter diagram of MOR_{act} versus MOR_{pred3} as predicted from measured moisture content and grain angle predicted from Eq. 6.4.

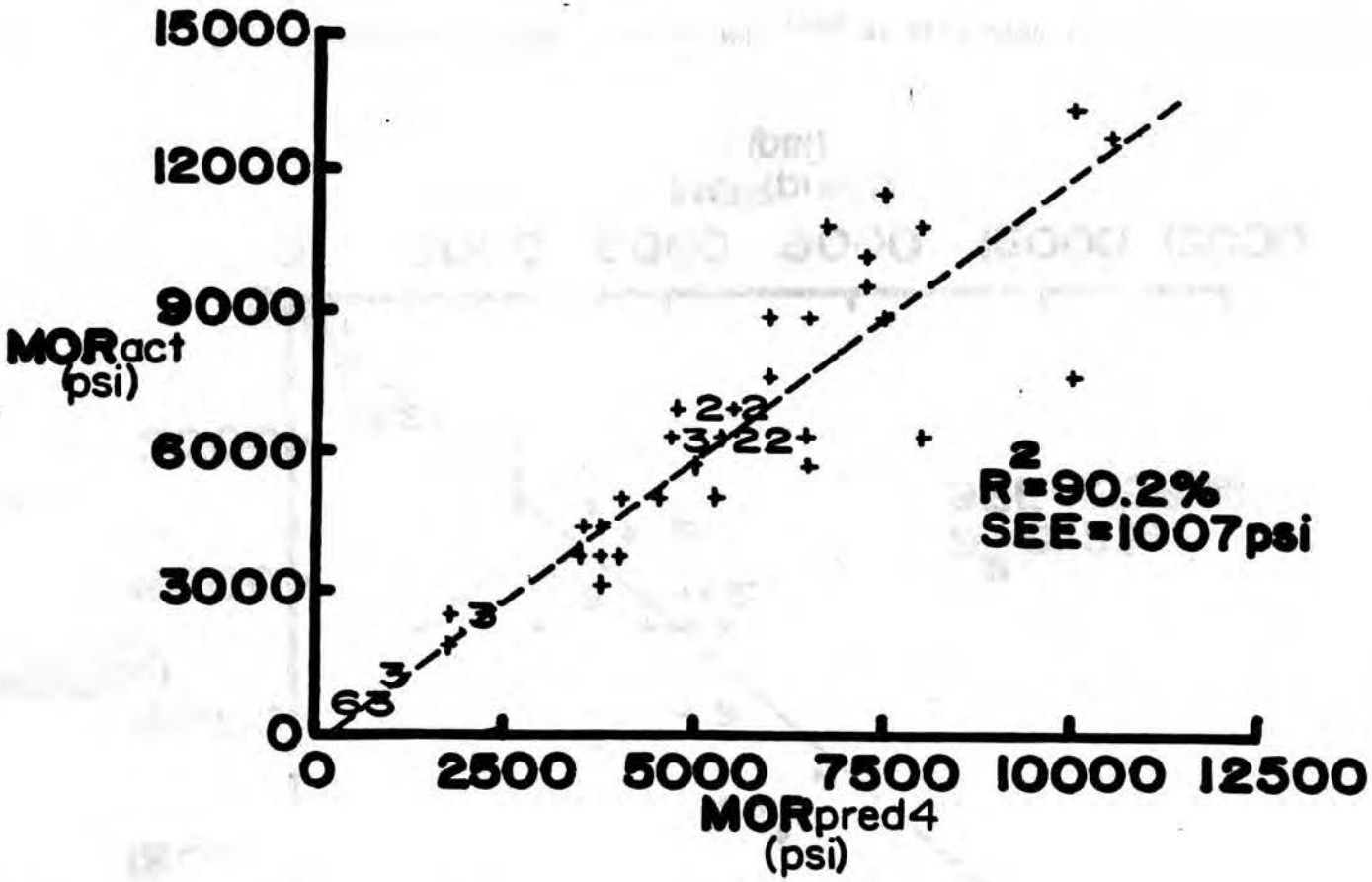

Figure 7.4. Scatter diagram of MOR_{act} versus MOR_{pred4} as predicted from measured moisture content and grain angle predicted from TTIME equations in Table 7.2.

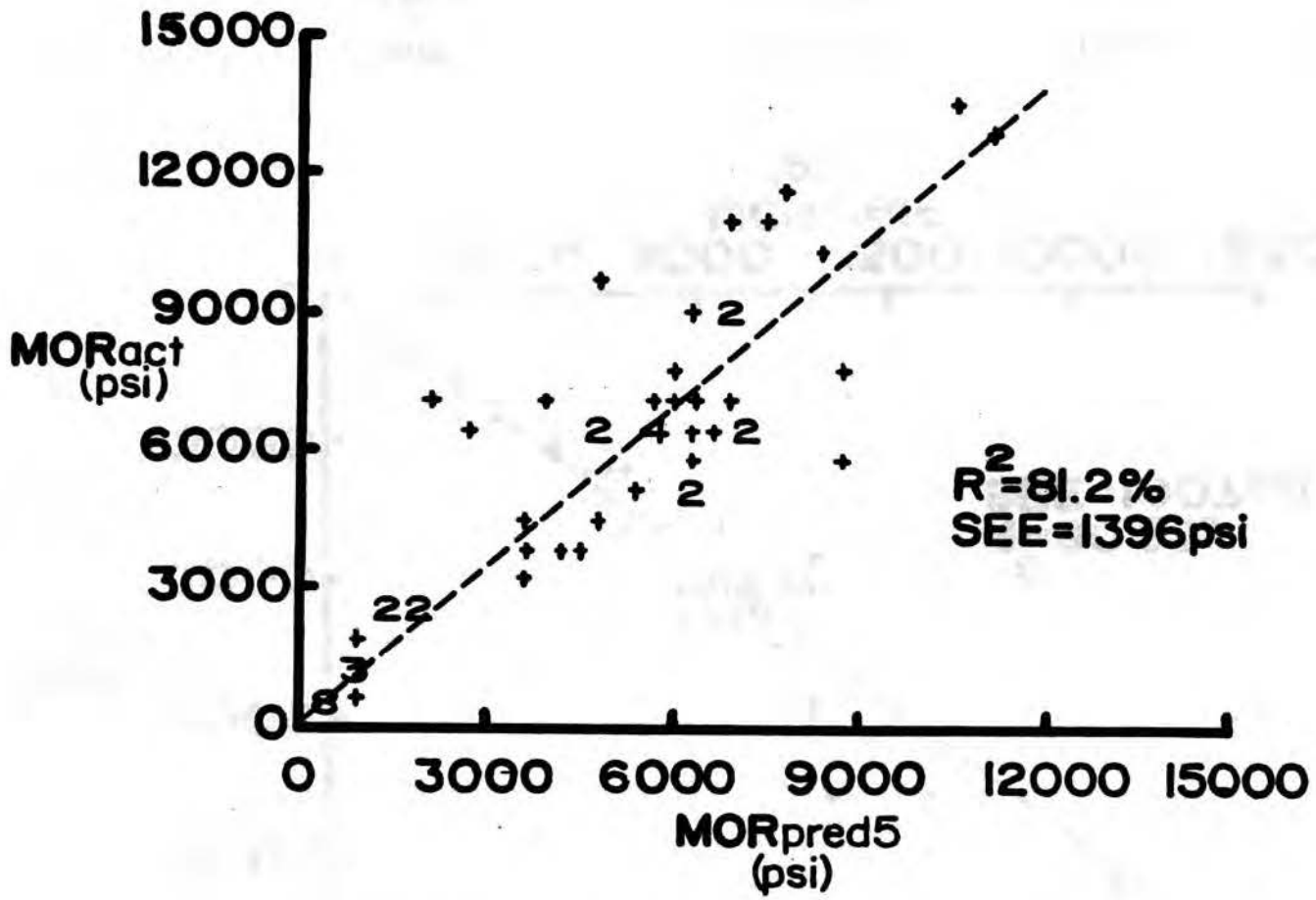

Figure 7.5. Scatter diagram of MOR_{act} versus MOR_{pred5} as predicted from measured moisture content and grain angle predicted from FRINT equations in Table 7.2.

$$MOR = -1293 + 2.20(FRFREQ) \quad (6.5)$$

$$MOR = 15653 - 177(TTIME) + 0.649(TTIME)^2 - 0.0007(TTIME)^3 \quad (6.7)$$

The FRFREQ and TTIME values of each specimen were then substituted into the above equations and predicted MOR values, designated MOR_{pred6} and MOR_{Pred7}, were obtained. The results are summarized in Appendix K. Regressions between predicted and actual MOR values for cases 6 and 7 were perfomred with the scatter diagrams and equations plotted in Figures 7.6 and 7.7, respectively.

The r^2 and SEE values for regressions involving MOR_{pred6} (use of FRFREQ as the predictor variable) and MOR_{pred7} were 74.9 percent, 1642 psi, and 87.2 percent 1180 psi respectively. These values are also shown in Table 7.3. Average errors were 25.2 percent and 32 percent for Cases 6 and 7, respectively.

7.4 COMPARISON OF NDE PREDICTION TECHNIQUES

The seven methods used to predict MOR involved different levels of sophistication and gave varying levels of results. Based on the SEE values, knowledge of exact grain angle and moisture content resulted in the best prediction of MOR with a SEE value of 796 psi. The second lowest SEE value of 1007 psi was obtained from Method 4, with grain angle being predicted from TTIME once the moisture content is known. However, both of these methods required knowledge of the MOR at 0 and 90 degrees. The third best model, using the SEE value as the selection criteria, involved direct correlation of the TTIME value with MOR, Method 7. The regression had an r^2 of 87.2 percent and an SEE of 1159 psi. The remaining four prediction methods has SEE values

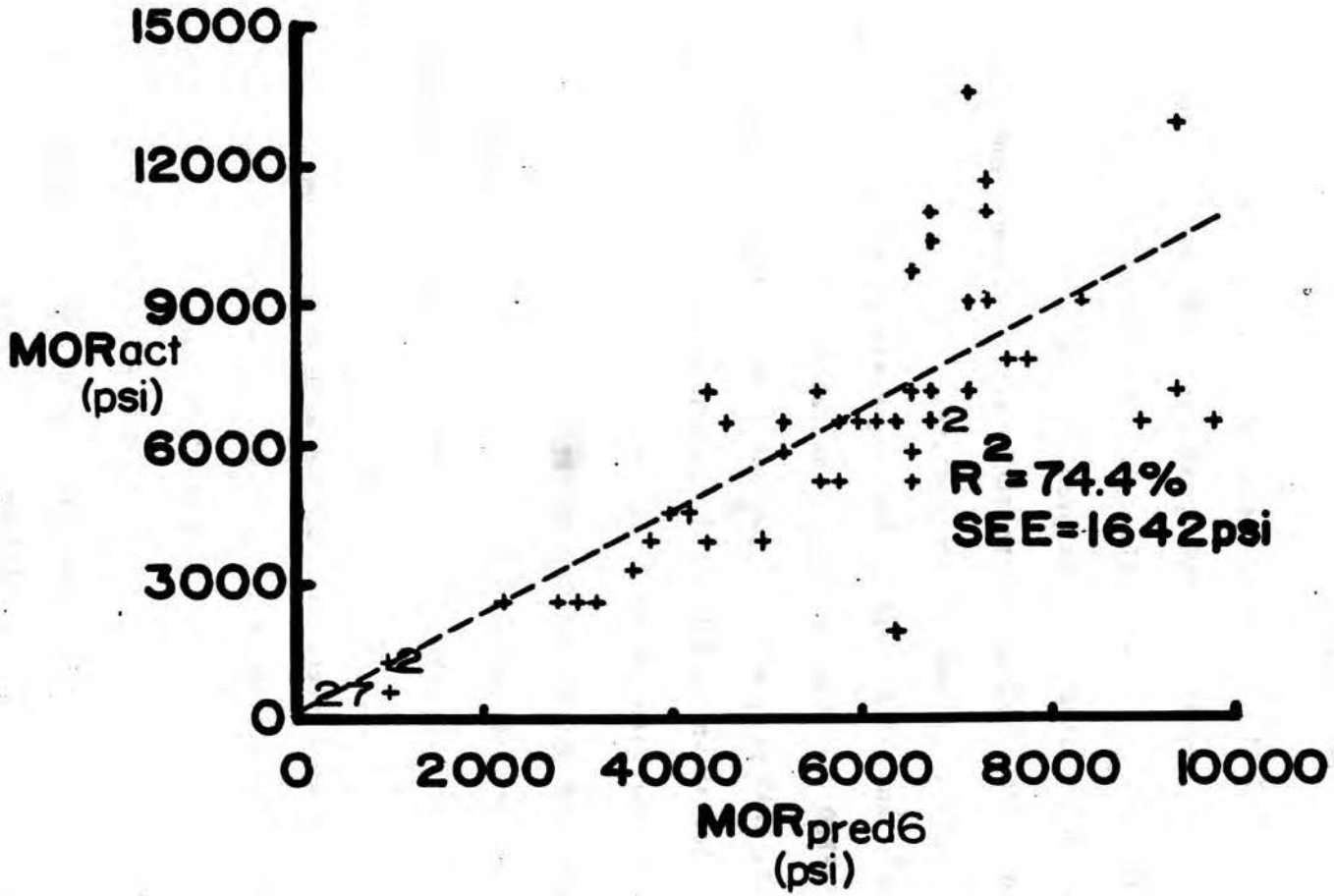

Figure 7.6. Scatter diagram of MOR_{act} versus MOR_{pred6} as predicted from measured NDE variable FRFREQ and Eq. 6.5.

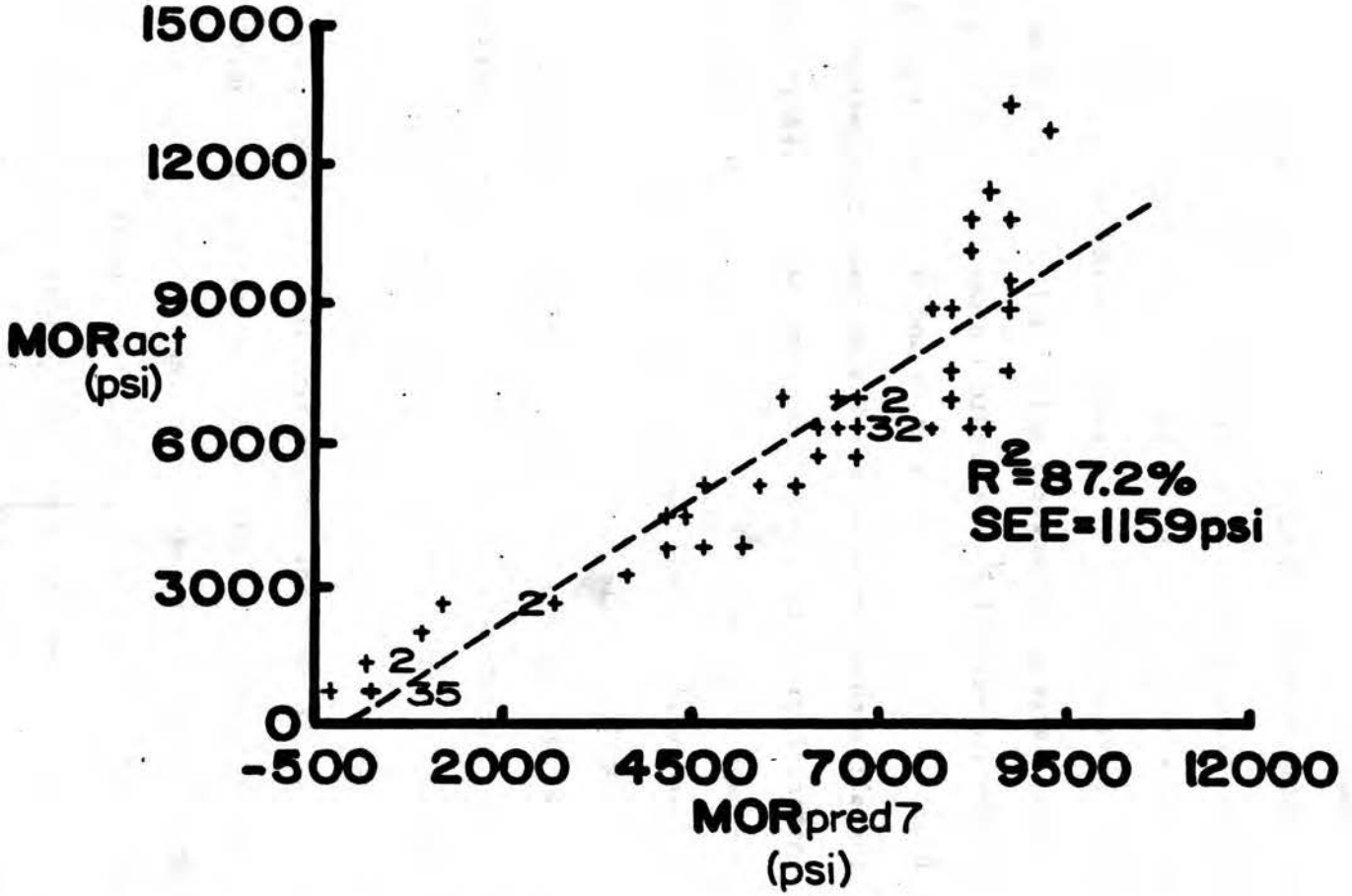

Figure 7.7. Scatter diagram of MOR_{act} versus MOR_{pred7} as predicted from measured NDE variable TTIME and Eq. 6.7.

ranging form 1325 to 1642 psi. The least accurate method, based on SEE values, was obtained by direct correlation of MOR with the NDE parameter FRFREQ.

Significantly different ranking of the regression methods results if the average error statistic is used instead of the SEE values. However, average error, as defined by Eq. (7.3) is highly dependent on the actual MOR value since relatively small absolute psi errors at low strength values (large grain angles) will result in large percentage errors. The average error for each prediction method at nominal grain angles of 0 and 3 degrees as well as at 60 and 90 degrees is given in Table 7.4 for all predictive schemes. Though prediction Method 1, in which the material properties were measured, has a slightly higher overall percentage error than Method 4, the error is much smaller at the high strength values. Thus, method 1 predicts strength better at smaller grain angles, while Method 4 in which grain angle is predicted, works better for large grain angles. Method 6, which involved direct correlation of TTIME with MOR had the third lowest SEE value but exhibited the largest percentage error of any of the predictive schemes.

Analysis of the spectral characteristics of stress waves in small, clear specimens of Douglas-fir resulted in significant relationships between grain angle and the NDE parameters FRFREQ, FRINT, and TTIME. Although no consistent relationship between moisture content and the NDE parameters studied was obtained, it appears that moisture above the fiber saturation point creates significant damping of the stress waves at grain angles larger then 30 degrees. The mode of wave propagation through the wood is speculated to change with grain angle and moisture content.

Table 7.4. Average errors of predicted MOR values as a function of grain angle.

Predictor* Variable	Grain Angle Range			
	Grain Angle ≤6	10 ≤ Grain Angle ≤30	Grain Angle >30	All Grain Angles
MOR_{pred1}	6.3	17.3	22.8	16.0
MOR_{pred2}	20.0	26.2	19.6	23.4
MOR_{pred3}	12.2	25.1	22.3	21.5
MOR_{pred4}	15.7	14.8	19.2	15.9
MOR_{pred5}	18.5	22.0	18.7	20.5
MOR_{pred6}	16.7	15.6	89.9	32.0
MOR_{pred7}	24.2	24.0	29.3	25.2

*Pred1 - Grain angle and moisture content of specimens known. Use of Hankinson's formula by logMOR-MC equations for adjustment.

Pred2 - Moisture content of specimens known. Grian angle predicted from Eq. 6.3 involving NDE parameter TTIME. Use of Hankinson's formula and logMOR-MC equations for adjustment.

Pred3 - Moisture content of specimens known. Grain angle predicted from Eq. 5.4 involving NDE parameter FRFREQ. Use of Hankinson's formula and logMOR-MC equations for adjustment.

Pred4 - Moisture content of specimens known. Grain angle predicted from equations in Table 7.2 involving NDE parameter TTIME. Use of Hankinson's formula and logMOR-MC eauations for adjustment.

Pred5 - Moisture content of specimens known. Grain angle predicted from equations in Table 7.2 involving NDE parameter FRINT. Use of Hankinson's formula and logMOR-MC equations for adjustment.

Pred6 - Direct prediction of MOR using Eq. 6.5 and NDE parameter FRFREQ.

Pred7 - Direct prediction of MOR using Eq. 6.7 and NDE Parameter TTIME.

Predictive of strength of an individual piece of wood by direct correlation with the NDE parameters studied was in general not as accurate as when basic relationships between grain angle and moisture content with MOR were used. However, these latter predictive schemes required knowledge of the strength at parallel and perpendicular to grain orientations. This may be impractical for direct application to poles. Best estimates of MOR by direct correlation was obtained with the NDE parameters TTIME and FRFREQ.

Chapter 8

SUMMARY AND CONCLUSIONS

8.1 RELATIONSHIPS OF WOOD PROPERTIES WITH STRESS WAVE SPECTRAL CHARACTERISTICS

The purpose of the investigation was to measure and quantify the spectral properties of stress wave propagation in wood with the goal of facilitating improved NDE methods for individual wood poles. Several physical properties of wood were varied to investigate their influence on the spectral properties. Four NDE Parameters were found to be significantly related to the wood properties studied. The velocity of wave propagation in the material, as measured by the transit time (TTIME), was significantly related to the grain angle of the wood. Two other significant NDE variables were the measures of the frequency response function of wood, i.e.; the frequency at which the amplitude gain reaches a maximum (FRFREQ) and the total gain of the specimen over the frequency range studied (FRINT). Additionally, the ratio of total energy content of the wave in the wood over the total energy input (NNINTENGD) was significant for certain cases.

Two methods were found to be best for grain angle prediction. When the moisture content of the wood was unknown, grain angle was best predicted by a third-order polynomial regression equation (Eq. 6.4) involving the variable FRFREQ. The regression equation produced an r^2 of 93.0 percent and an SEE value of 7.8 degrees. This parameter was not influenced much by the moisture content of the

specimens. When moisture content of the specimens was known, the NDE variable TTIME was found more accurate in the prediction of grain angle. Six regression equations, covering the range from 7 to 160 percent moisture content, were used to predict grain angle as presented in Table 7.2. The r^2 values varied from a low of 90.8 percent for a mean moisture content of 7.1 percent to a high of 98.8 percent at a mean moisture content value of 109.6 percent. Variation about the regression equation, as measured by the SEE, ranged from 4 percent to 11.1 percent moisture content.

None of the NDE parameters studied were consistently significant for the prediction of moisture content. However, at the higher grain angles, i.e., above 30 degrees, the influence of moisture content above the fiber saturation point resulted in significant decrease in the amplitude peak of the frequency response function (FRAMP), indicating increased attenuation of the stress wave.

Weight loss investigation proved significant only when the grain angle of the specimens was 90 degrees. The best predictor of weight loss was obtained with the NDE variable NNINTENGD. The regression resulted in an r^2 value of 56.7 percent and an SEE value of 1.6 percent weight loss. The variable NNINTENGD is a measure of the ratio of total spectral energy content in the wave before and after decay, each variable normalized to that of their respective inputs. The specimens experienced only limited values of weight loss. With the exception of one specimen, all weight loss values were less than 4 percent. The decay was confined to small, irregularly spaced pockets on the surface of the specimens. Additionally, several specimens produced a weight gain after exposure to decay. Though none of the 90 degree specimens

exhibited a weight gain, the presence of weight gain in other specimens renders all conclusions regarding the influence of decay on stress wave characteristics tentative.

8.2 PREDICTION OF STRENGTH FROM NDE STRESS WAVE CHARACTERISTICS

Due to the exploratory nature of this research, it was felt that such properties as knots and inhomogeneities in the specimens, which significantly influence the strength properties of poles, could not be included. This simplification must be recognized before extending the results of this research to the prediction of the strength of wood poles. With these simplifications in mind, two basic approaches toward strength prediction were attempted.

The first approach assumed that for the specimens studied, the two major wood properties influencing strength were grain angle and moisture content. Two proven relationships between strength and these properties were then employed. The influence of grain angle was accounted for by use of Hankinson's formula (EQ. 2.7). This relationship requires knowledge of the strength of wood both parallel and perpendicular to grain. The second relationship was used to adjust MOR for moisture content (MC) below fiber saturation point. The equation used was of the form;

$$\log MOR = a + b\ MC \qquad [8.1]$$

Using this approach and the wood properties measured from each specimen, the regression between predicted and actual MOR yielded an f^2 value of 93.9 percent and an SEE value of 796 psi. If grain angle and moisture content could be predicted exactly from the NDE parameters, the same accuracy in prediction of MOR would occur. Since moisture content could not be predicted any degree of precision over

the entire range covered by the specimens, the actual moisture content values were used. Grain angle was predicted using four relationships and the NDE parameters TTIME, FRFREQ, and FRINT. Use of the NDE relationships between grain angle and the variable TTIME, given in Table 7.2, yielded a relationship between predicted and actual MOR with an SEE of 1007 psi and an r^2 value of 90.2 percent. For grain angle predicted by Eq. 6.4, using the NDE parameter FRFREQ and the relationships of grain angle and moisture content with MOR, correlation of predicted and actual MOR resulted in an r^2 of 81.2 percent iwth an SEE of 1396 psi.

A simplified approach in the NDE of pole strength would be the direct correlation between strength and NDE parameters. This is because the first approach used requires knowledge of parallel to grain strength, which is the desired parameter for poles. The best results, based on the SEE, were obtained using a third-order polynomial with the variable TTIME (Eq. 6.7). Prediction of MOR from this method yielded an SEE of 1642 psi and an r^2 of 87.2 percent. A straightline relationship with the NDE variable FRFREQ and MOR, Eq. 6.5, resulted in an SEE of 1642 psi and an r^2 of 74.4 percent. Use of Eq. 6.7 for MOR prediction with the variable TTIME resulted in negative strength predictions at large grain angles, clearly an unacceptable method.

8.3 RECOMMENDATION FOR FURTHER RESEARCH

Since the density of the material in this investigation was closely controlled, it was not included in the data analysis. However, density strongly influences the strength and stiffness of clear wood. It is known that material density also influences

propagation velocity through the material. Since density of the wood often requires destructive sampling, it is often unknown. This decreases the value of velocity measurements for NDE purposes when material density is highly variable. Further testing should be conducted to determine if the other NDE variables studied, such as FRFREQ, are also dependent upon density.

Since velocity is fundamentally related to material behavior further use of the spectral analysis procedures seem warranted. Specifically, the phase information available from the cross-spectral density function can provide velocity information as a function of frequency. This may provide more insight into the material characteristics and strength than information obtained from velocity of the fastest wave only, as is traditionally done.

Specimens for this research were clear material of small size. The next obvious step is to extend the information obtained to full-size members. An important consideration would be the influence of knots and the grain deviation around knots, which often are the controlling factors in the strength of structural wood members. The relationwhips of the NDE parameters FRFREQ and FRINT with global grain angle were significant. If the presence of localized cross grain could be determined, it could be useful in predicting failure location on strength.

8.4 APPLICATIONS OF RESULTS TO A POLE NDE TECHNIQUE

Prediction of the strength of utility poles to determine the need for their removal from an active line, appears most promising if testing is conducted across the grain. The only significant relationship with wieght loss from decay, a prime consideration of the

pole user, was obtained for 90 degree oriented specimens. However, a fundamental problem in prediction of pole strength with testing perpendicular to the grain is that bending of the poles causes stress in the longitudinal direction. For this research, the wave propagation direction coincided with the direction of stress application during destructive testing. Serious thought must be given to this aspect of the NDE procedure. Pole failure often occurs at knots and knot clusters which have not been investigated as to their influence on the wave propagation spectral properties. Additionally, poles are roughly circular in cross section while the specimens for this research were rectangular. It is expected that specimen geometry influences the wave propagation characteristics.

Although prediction of MOE was not emphasized in the data analysis of this research, the relationships between the NDE parameters and MOE appear similar for MOE prediction as for MOR perdiction. Further work needs to be done on the influence of decay on the NDE variables with closer control of the decay process and measurement of weight loss, possibly by use of conditioning specimens to constant moisture contents before and after exposure to decay.

Several topics need to be developed and investigated before a successful NDE of wood poles with stress wave spectral analysis procedures would be commercially feasible. Testing must be able to include the regions of the pole where failure is most likely to occur, which must include a section of the pole above groundline. The encouraging information obtained from this exploratory work is that the condition of wood does influence the spectral characteristics of the stress waves. In short, many problems still remain unsolved for

NDE of wood pole strength, but the basic premise and method appear viable.

LITERATURE CITED

1. Achenbach, J. D. 1980. Direct and inverse methods for scattering by cracks at high frequencies. Proceedings of the DARPA/AFML Review of Progress in Quantitative NDE. 5th ed. Thousand Oaks, California. pp. 367-376.

2. Adler, L. and Lewis, D. K. 1980. Diffraction of ultrasonic waves by elliptical cracks in metals. Proceedings of the DARPA/AFML Review of Progress in Quantitative NDE. 5th ed. Thousand Oaks, California. pp. 377-383.

3. Becker, H. 1967. Möglichkeiten der Anwendung von Ultraschall bei der Untersuchung von Holz und Holzspanplatten. Holzforschüng. Vol. 25(5):135-145. English Summary.

4. Bendat, J. S., and Piersol, A. G. 1971. Random Data: Analysis and Measurement Procedures. Wiley-Intersceince. New York. 407 p.

5. Bertholf, L. D. 1965. Use of elementary stress wave theory for prediction of dynamic strain in wood. Washington State Institute of Technology. Bulletin 291. Washington State University.

6. Bodig, J., and Jayne, B. 1982. Mechanics of Wood and Wood Composites. Van Nostrand Reinhold Co. New York. 712 p.

7. Boyce, J. S. 1961. Forest Pathology. 3rd ed. McGraw-Hill Book Co. New York. 572 p.

8. Breeze, J. E., and Nilberg, R. H. 1971. Predicting by sonic measurements the strength of logs and poles having internal decay. Forest Prod. J. Vol. 21(5):39-43.

9. Carlson, H. 1980. Machine stress rated lumber: A look at its past, present, and future. Automation in Housing and Systems Building News. July.

10. Cartwright, K., et al. 1931. The effect of progressive decay by Trametes Serialis Fr. on the mechanical strength of the wood of Stika spruce. Great Britain Dept. Sci. Ind. Res., For. Prod. Res. Bull. No. 11.

11. Comben, A. J. 1964. The effect of low temperatures on the strength and elastic properties of lumber. J. Inst. Wood Sci. Vol. 13:42-55.

12. Courteau, R. W. 1967. Propagation and attenuation of elastic waves in wood. M.S. Thesis. Washington State University, Pullman, Washington. 126 p.

13. Detroit Edison Power and Light. 1979. Sonic pole test: Cuts cost of inspection/treatment by 83 percent. Electric Light and Power News. July.

14. Diller, J. D., and Koch, E. J. 1959. Weight losses of 40 wood species exposed to destructive fungi. Forest Prod. J. Vol. 9(9): 298-302.

15. Dunlop, J. I. 1978. Damping loss in wood at mid-kilohertz frequencies. Wood Sci. and Tech. Vol. 12(1):49-62.

16. Dunlop, J. I. 1980. Testing of particleboard by acoustic techniques. Wood Sci. and Tech. Vol. 14(1):69-78.

17. Dunlop, J. I. 1981. Testing of poles by acoustic pulse method. Wood Sci. and Tech. Vol. 15(4):301-310.

18. El-Osta, N. L. M., et al. 1979. Prediction of modulus of rupture from modulus of elasticity for some Egyptian hardwoods. Wood and Fiber. Vol. 11(3):147-154.

19. EPRI. 1981. Probability-based design of wood transmission structures, Vol. 1: Strength and Stiffness of Wood Utility Poles. EPRI EL-2040. Vol. 1. Project 1352-1. Final Report. September 1981. pp. 1-5.

20. Galligan, W., and Courteau, R. W. 1965. Measurement of elasticity of lumber with longitudinal stress waves and the piezoelectric effect of wood. Proceedings of 2nd Symposium on Nondestructive Testing of Wood. Washington State University. pp. 223-244.

21. Gerhards, C. C. 1975. Stress wave speed and MOE of sweetgum ranging from 150 to 15 percent M.C. Forest Prod. J. Vol. 25(4): 51-57.

22. Gerhards, C. C. 1979. Comparison of two nondestructive instruments for measuring pulse transit time in wood. Wood Science. Vol. 11(1):13-16.

23. Gerhards, C. C. 1980. Effect of cross grain on stress waves in lumber. USDA For. Prod. Lab. Research Paper 368. 9 p.

24. Grahm, R.D. and Helsing, G.G. 1979. Wood pole maintenance manual: Inspection and supplemental treatment of Douglas-fir and western redcedar poles. Forest Research Laboratory, Oregon State University, Research Bulletin 24.

25. Hartley, C. 1958. Evaluation of wood decay in experimental work. USDA For. Prod. Lab. Mimeo. No. 2119.

26. Hayford, D. T., et al. 1977. The correlation of ultrasonic attenuation and shear strength in graphite-polyimide composites. J. of Comp. Mat. Vol. 11(10):429-44.

27. Hearmon, R. F. S. 1965. The assessment of wood properties by vibrations and high frequency acoustic waves. Proceedings of 2nd Symposium on Nondestructive Testing of Wood. Washington State University. pp. 49-67.

28. Hearmon, R. F. S. 1966. Theory of the vibration testing of wood. Forest Prod. J. Vol. 16(8):29-40.

29. Henningsson, B., et al. 1975. Soft rot in salt treated electricity poles from the years 1940-1954. The Swedish Wood Preservation Institute. Meddelanden Reports Nr. 117.

30. Hoffmeyer, P. 1975. Mechanical properties of soft rot decayed Scots pine with special reference to wooden poles. Särtryck ur Svenska Träskyddinstitutets Meddelande Nr. 117.

31. Hoyle, R. J. 1961. A nondestructive test for stiffness of structural lumber. Forest Prod. J. Vol. 11(6):251-254.

32. Hoyle, R. J. 1968. Background to machine stress rating. Forest Prod. J. Vol. 18(4):87-97.

33. James, W. L. 1961. Effect of temperature and moisture content on internal friction and speed of sound in Douglas-fir. Forest Prod. J. Vol. 11(9):383-390.

34. James Electronics Co. The James V-meter. Product information sheet. Chicago, Illinois.

35. Jensen, L. C. 1965. Sonic detection of internal decay in wood poles. Proceedings of 2nd Symposium on Nondestructive Testing of Wood. Washington State University. pp. 207-221.

36. Kaiserlik, J. H., and Pellerin, R. F. 1977. Stress wave attenuation as an indicator of lumber strength. Forest Prod. J. Vol. 27(6):39-43.

37. Kaiserlik, J. H. 1978. Nondestructive testing to predict effect of degradation on wood: A critical assessment. USDA For. Prod. Lab. Gen. Tech. Report 119.

38. Kaplan, W. 1981. Advanced Mathematics for Engineers. Addison-Wesley Publishing Co. Reading, Massachusetts. 929 p.

39. Kennedy, R. W. 1958. Strength retention in wood decayed to small weight losses. Forest Prod. J. Vol. 8(10):308-314.

40. Kolsky, H. 1963. Stress Waves in Solids. Dover Publications, Inc. New York. 213 p.

41. Konarski, B., and Wazny, J. 1977. Zusammenhang zweischen der ultraschallgeschwindigkeit und der mechanischen eigenschaften pilzbefallen holzes. Holz als roh und Werkstoff. Vol. 35(9): 341-345. English Abstract.

42. Kramer, P. R. 1964. Correlation of bending strength and stiffness of southern pine. Forest Prod. J. Vol. 14(10):495-496.

43. Lee, I. D. G. 1958. A nondestructive method for measuring the elastic anisotropy of wood using an ultrasonic pulse technique. Journal of Inst. Wd. Sci. Vol. 1(1):43-57.

44. Logan, J. D. 1980. Machine stress rating capacity triples over past three years. Forest Industries. Vol. 107(1):48-49.

45. Lord, A. E. 1972. Ultrasonic wave propagation in metal-matrix components. J. of Comp. Mat. Vol. 6(4):278-285.

46. Mann, R. W., Baum, G. A., and Hakeger, C. C. 1979. Elastic wave propagation in paper. Tappi Vol. 62(8):115-118.

47. Metriguard Co. The Model 3300 E-tester. Product information sheet. Pullman, Washington.

48. Metriguard Co. The Model 3031 Stress Wave Timer. Product information sheet. Pullman, Washington.

49. Miklowitz. 1978. The Theory of Elastic Waves and Waveguides. North Holland Publishing Co. Amsterdam, Holland. 618 p.

50. Miller, B. D., Taylor, F. L., and Popeck, R. A. 1965. A sonic method for detecting decay in wood poles. Proceedings of the American Wood-Preservers' Association. 61st ed. St. Louis, Missouri. pp. 109-115.

51. Miller, D. G. 1962. Selection efficiencies of nondestructive strength tests. Forest Prod. J. Vol. 12(8):358-362.

52. Miller, D. G. 1964. Effect of tolerance on selection efficiency of nondestructive strength tests of wood. Forest Prod. J. Vol. 14(4):179-183.

53. Miller, D. G. 1968. Nondestructive testing of joists by a vibrational technique. Forest Prod. J. Vol. 18(2):25-28.

54. Moon, F. C. 1972. Wave surfaces due to impact on anisotropic plates. J. of Comp. Mat. Vol. 6(1):62-79.

55. Muhlheren, K., Bodig, J., and Goodman, J. 1980. Simulation of wood pole bending strength. Structural Research Report No. 33. Colorado State University.

56. Newland, D. E. 1975. An Introduction to Random Vibrations and Spectral Analysis. Longman Group Limited. London. 285 p.

57. O'Halloran, M. E., Bodig, J., and Bowden, D. C. 1972. Non-destructive parameters of lodgepole pine dimension lumber in bending. Forest Prod. J. Vol. 22(2):84-96.

58. Oved, Y., Luttwak, G. E., and Rosenburg, Z. 1978. Shock wave propagation in layered composites. J. of Comp. Mat. Vol. 12(1): 84-96.

59. Pain, H. J. 1976. The Physics of Vibrations and Waves. 2nd ed. John Wiley and Sons, Ltd. New York. 357 p.

60. Panshin, A. J., and de Zeeuw, C. 1970. Textbook of Wood Technology, Vol. I. 3rd ed. McGraw-Hill Book Co. New York. 705 p.

61. Pellerin, R. F. 1965. A vibrational approach to nondestructive testing of structural lumber. Forest Prod. J. Vol. 15(3):93-101.

62. Pellerin, R. F. 1976. Nondestructive evaluation of wood and wood products. Proceedings of XVI IUFRO World Congress. Norway. Vol. 5. pp. 184-189.

63. Pentoney, R. E. 1955. Effect of moisture content and grain angle on the internal friction of wood. Composite Wood. Vol. 2:131-136.

64. Reinhart, J. S. 1975. Stress Transients in Solids. Hyper Dynamics. P.O. Box 392. Santa Fe, New Mexico. 230 p.

65. Scheffer, T. C. 1936. Progressive effects of polyporous versicollor on the physical and chemical properties of red gum sapwood. USDA Tech. Bull. No. 527.

66. Sellevold, E. J., et al. 1975. Low temperature internal friction and dynamic modulus for beech wood. Wood and Fiber. Vol. 7(3):162-169.

67. Shaw, A. D. 1974. Sonic vibration technique for rot detection in wood poles. IEEE Transactions on Instrumentation and Measurement. Vol. IM-23, No. 3:240-244.

68. Shaw, A. D. 1978. Banpass filter comparator for confirming the absence of serious voids in wood poles. IEEE Transactions on Instrumentation and Measurement. Vol. IM-27, No. 3:273-276.

69. Shigo, A. L., Shortle, W. C., and Ochrymowych, J. 1977. Detection of active decay at groundline in utility poles. U.S. Forest Service General Technical Report NE-35, Northeastern Experiment Station, Upper Darby, Pennsylvania.

70. Southwest Research Institute. 1973. Nondestructive testing: A survey. NASA Doc. SP-5113. 282 p.

71. Taylor, J. A. 1978. Pole maintenance--its needs and its effectiveness. Proceedings of the American Wood-Preservers Association, McLean, Virginia. pp. 128-141.

72. Thompson, W. T. 1981. Theory of Vibrations with Applications. 2nd ed. Prentice-Hall, Inc. Englewood Cliffs, New Jersey. 220 p.

73. Tittmann, B. R., Elsley, R., and Paton, N. 1980. Measurements of ultrasonic scattering from bulk flaws of complex shape. Prceedings of the DARPA/AFML Review of Progress in Quantitative NDE. 5th ed. Thousand Oaks, California. pp. 359-366.

74. U.S. Department of Agriculture. 1974. Wood Handbook. Agriculture Handbook No. 72, Superintendent of Documents, Washington, D.C.

75. Varley, E. ed. 1976. Propagation of Shock Waves in Solids. Amer. Soc. of Mech. Eng. The Applied Mechanics Conference. Salt Lake City, Utah. AMD-Vol. 17. 114 p.

76. Wang, S., Suchland, O., and Hart, J. H. 1980. Dynamic test for evaluating decay in wood. Forest Prod. J. Vol. 30(7):35-36.

77. Wanngard, F. F. 1966. Resistance of wood to chemical degradation. Forest Prod. J. Vol. 16(2):53-64.

78. Wasley, R. J. 1978. Stress Wave Propagation in Solids, An Introduction. Marcel-Dekker, Inc. New York. 279 p.

79. Wilcox, W. W. 1965. Fundamental characteristics of wood decay indicated by a sequential microscopical analysis. Forest Prod. J. Vol. 15(7):255-259.

80. Wilcox, W. W. 1978. Review of literature on the effects of early stages of decay on wood strength. Wood and Fiber. Vol. 9(4):252-257.

81. Wood-SLIMP. 1975. Theoretical and practical base for the pilodyn wood tester.

82. Zabel, R. A., Kenders, A. M., and Lombard, F. F. 1980. Fungi associated with decay in treated Douglas-fir transmission poles in the Northeastern United States. Forest Prod. J. Vol. 30(4): 51-56.

83. Zener, C. 1956. Elasticity and Anelasticity of Metals. University of Chicago Press. Chicago, Illinois. 254 p.

APPENDICES

APPENDIX A

LISTING OF ACRONYMS FOR NDE PARAMETERS

NDE Acronym	Description of NDE set I parameters	Units
FRAMP	Maximum amplitude of the amplitude response spectrum.	(Unitless)
FRFREQ	Frequency at which the amplitude response function reaches a maximum value (FRAMP).	(Hz)
FRINT	Maximum value of the integrated amplitude response spectrum.	(Unitless)
TTIME	Time required for stress wave to travel between the two accelerometers on the wood.	(μsec)

NDE Acronym	Description of NDE set II parameters	Units
ENGAMP	Maximum amplitude of the energy spectral density function of the stress wave response in wood.	$(100g^2s/Hz)$
ENGFAMP	For GAMC study specimens, the ENGAMP value of the front accelerometer on the wood.	"
ENG1AMP	For GAMC study specimens, the ENGAMP value of the back accelerometer, recorded concurrently with the front accelerometer.	"
ENG2AMP	For GAMC study specimens, the ENGAMP value of the back accelerometer, recorded concurrently with the impact.	"
ENGINP	Maximum value of the energy spectral density function of the impact to the wood.	"
ENGINT	Total energy content of the impact to the wood.	$(100g^2s)$
INTENG	Total energy content of the stress wave response in the wood.	"
INTFENG	For GAMC study specimens, the INTENG value of the front accelerometer on the wood.	"
INT1ENG	For GAMC study specimens, the INTENG value of the back accelerometer recorded concurrently with the front accelerometer response.	"
INT2ENG	For GAMC study specimens, the INTENG value of the back accelerometer recorded concurrently with the impact.	"
NENGFAMP	The ENGFAMP value normalized to the impact through division by the corresponding ENGINP value.	(unitless)
NENG2AMP	The ENG2AMP value normalized to the impact through division by the corresponding ENGINP value.	"
NINTFENG	The INTEFENT value normalized to the impact through division by the corresponding ENGINP value.	"
NINT2ENG	The INT2ENG value normalized to the impact through division by the corresponding ENGINP value.	"

NDE Acronym	Description of NDE set II parameters	Units
RENGAMP	The ratio of maximum energy spectral densities, i.e., ENGFAMP divided by ENG1AMP.	"
RINTENG	The ratio of total energy content values of the front and back accelerometers, i.e., INTFENG divided by INT1ENG.	"

NDE Acronym	Description of NDE set III parameters	Units
ENGAMPPD	For DEC study specimens, the ENGAMP value of the accelerometer on the wood before exposure to decay.	($100g^2s/Hz$)
ENGAMPD	For DEC study specimens, the ENGAMP value after specimen exposure to decay.	"
ENGINPD	For DEC study specimens, the ENGINP value of the impact before specimen exposure to decay.	"
ENGIND	For DEC study specimens, the ENGINP value of the impact after specimen exposure to decay.	"
ENGINTPD	For DEC study specimens, the ENGINT value before specimen exposure to decay.	($100g^2s$)
ENGINTD	For DEC study specimens, the ENGINT value after specimen exposure to decay.	"
INTENGPD	For DEC study specimens, the INTENG value of the specimen before exposure to decay.	"
INTENGD	For DEC study specimens, the INTENG value of the specimen after exposure to decay.	"
NENGAMPPD	The ENGAMPPD value normalized to the impact through division by the corresponding ENGINPD value.	(unitless)
NNENGAMPPD	The ENGAMPPD value normalized to the impace through division by the corresponding ENGINTPD value.	"
NENGAMPD	The ENGAMPD value normalized to the impact through division by the corresponding ENGINPD value.	"
NNENGAMPD	The ENGAMPD value normalized to the impact through division by the corresponding ENGINTD value.	"
RENGAMPD	The ratio of decayed to undecayed maximum normalized energy spectral densities, i.e., NENGAMPD divided by NENGAMPPD.	"
RRENGAMPD	The ratio of decayed to undecayed maximum normalized energy spectral densities, i.e., NNENGAMPD divided by NNENGAMPPD.	"

NDE Acronym	Description of NDE set III parameters	Units
NINTENGPD	The INTENGPD value normalized to the impact through division by the corresponding ENGINPD value.	(unitless)
NNINTENGPD	The INTENGPD value normalized to the impact through division by the correpsonding ENGINTPD value.	"
NINTENGD	The INTENGD value normalized to the impact through division by the corresponding ENGIND value.	"
NNINTENGD	The INTENGD value normalized to the impact through division by the corresponding ENGINTD value.	"
RINTENGD	The ratio of decayed to undecayed normalized total energy content values, i.e., NINTENGD divided by NINTENGPD.	"
RRINTENGD	The ratio of decayed to undecayed normalized total energy content values, i.e., NNINTENGD divided by NNINTENGPD.	"

SPEC. NO.	FRFREQ[1/] (Hz)	FRAMP[2/]	FRINT[3/]	TIME[4/] (μsec)
00-1	4875.0	3.878±	2372.4	62.0
00-2	5000.0	1.1975	1658.2	50.0
00-3	3850.0	3.7788	1984.0	61.0
00-4	3825.0	2.9551	1791.9	54.0
00-5	3675.0	3.2159	1681.1	54.0
00-6	3675.0	4.3972	1811.9	53.0
03-1	2650.0	1.2103	1004.1	66.0
03-2	3800.0	2.0238	1505.5	57.0
03-3	3625.0	1.3184	1464.1	48.0
03-4	3750.0	2.7043	1905.9	53.0
03-5	4000.0	2.3989	1717.7	55.0
03-6	3925.0	3.0916	1774.9	50.0
03-7	3825.0	3.0440	1788.6	49.0
06-1	2575.0	1.3445	937.6	78.0
06-2	3525.0	2.7196	1474.4	64.0
06-3	3975.0	3.5354	1754.1	53.0
06-4	3900.0	4.3042	2033.7	57.0
06-6	3675.0	3.8268	1659.2	48.0
06-7	4875.0	1.5966	2021.7	44.0
10-2	3350.0	3.0977	1529.6	72.0
10-3	3425.0	2.0924	1484.0	68.0
10-4	3625.0	4.1530	1798.1	67.0
10-5	4425.0	4.6234	2555.6	48.0
10-6	3150.0	2.9537	1346.7	66.0
10-7	4150.0	2.5334	2361.7	48.0
15-1	3550.0	1.4286	1346.3	90.0
15-2	3225.0	1.5936	1320.6	81.0
15-3	3675.0	2.9337	1675.6	65.0
15-4	4700.0	3.8724	2226.7	64.0
15-5	3625.0	4.7681	1803.0	68.0
15-6	2900.0	3.4473	1661.5	62.0
15-7	3225.0	2.8362	1511.5	61.0

SPEC. NO.	FRFREQ (Hz)	FRAMP (unitless)	FRINT (unitless)	TIME (μsec)
20-1	2425.0	2.0863	1183.5	97.0
20-2	2450.0	2.8509	1304.1	92.0
20-3	2550.0	4.1389	1401.1	82.0
20-4	2325.0	4.2109	1292.1	94.0
20-5	2825.0	3.5214	1418.1	89.0
20-6	3100.0	3.9596	1580.7	74.0
20-7	2950.0	3.8597	1621.3	72.0
30-1	3475.0	1.9126	693.9	166.0
30-2	1625.0	3.4778	799.4	154.0
30-3	1825.0	3.0812	979.2	125.0
30-4	2025.0	3.1778	1075.5	119.0
30-5	1975.0	2.8918	1023.8	122.0
30-6	2200.0	5.3103	1297.4	102.0
60-2	900.0	3.3652	436.6	352.0
60-3	875.0	2.3212	429.8	340.0
60-4	900.0	3.5687	477.0	297.0
60-5	1125.0	6.1051	670.2	270.0
60-6	1050.0	5.0637	646.1	272.0
60-7	1075.0	5.7934	682.1	254.0
90-1	775.0	2.2832	310.0	442.0
90-2	800.0	2.6808	370.8	370.0
90-3	825.0	2.6022	406.4	325.0
90-4	850.0	4.1836	454.5	343.0
90-5	900.0	2.8896	446.9	314.0
90-6	900.0	4.7036	495.8	311.0
90-7	1100.0	6.1612	637.3	234.0

APPENDIX B

FREQUENCY RESPONSE FUNCTION VALUES FRFREQ[1/], FRAMP[2/], FRINT[3/], AND TRANSIT TIME VALUES TTIME[4/] FOR GRAIN ANGLE-MOISTURE CONTENT STUDY SPECIMENS

Specimen Number Notation: xx-0

xx = nominal grain angle
0 = moisture content group

[1/] FRFREQ - Frequency at which the amplitude response function reaches a maximum value.

[2/] FRAMP - Maximum amplitude of the amplitude response function.

[3/] FRINT - Maximum value of the integrated amplitude response spectrum.

[4/] TTIME - Time required for the stress wave to travel between the two accelerometers on the wood specimen.

SPEC. NO.	ENGAMP[1] ($100g^2s/Hz$)	INTFENG[2] ($100g^2s$)	ENG1AMP[3] ($100g^2s/Hz$)	INT1ENG[4] ($100g^2s$)
0-1	1.7167	28.296	3.0940	37.169
3-1	1.9023	39.755	2.2180	42.320
6-1	1.8297	29.915	1.5337	39.724
15-1	2.5889	44.735	3.2910	55.756
20-1	3.7776	64.728	3.4738	71.167
30-1	3.9649	72.820	5.3234	79.452
90-1	4.5354	71.569	6.7298	91.072
0-2	1.6014	22.418	1.4617	26.116
3-2	2.3794	26.101	2.1064	33.802
6-2	2.5014	30.166	2.2715	31.528
10-2	3.2067	41.898	2.6876	40.428
15-2	2.5330	30.582	1.9401	31.910
20-2	2.5789	40.100	2.2943	38.214
30-2	4.9310	63.808	4.1738	54.117
60-2	2.8728	39.156	4.1599	41.611
90-2	2.7992	41.142	2.9924	38.029
0-3	3.5981	39.937	2.4457	33.228
3-3	2.0199	29.804	4.3638	47.361
6-3	4.1306	38.717	1.5845	26.252
10-3	3.3333	34.662	2.0424	31.263
15-3	3.5920	34.434	1.9646	27.598
20-3	2.4582	48.134	3.6155	55.188
30-3	2.5778	50.230	3.8558	57.791
60-3	3.0106	44.020	2.9621	38.694
90-3	2.5028	36.219	2.7555	34.221
0-4	1.9408	28.080	3.3876	42.000
3-4	2.3953	34.414	4.2205	48.756
6-4	4.1068	43.453	3.3004	35.849
10-4	4.6351	37.380	2.9546	32.265
15-4	1.4923	27.397	3.6458	38.711
20-4	3.3256	50.392	3.2983	51.975
30-4	2.3278	42.828	2.3050	43.293
60-4	3.9028	47.554	3.4776	41.256
90-4	3.4517	47.560	5.0952	51.984
0-5	4.8232	44.624	3.0808	47.271
3-5	2.7158	29.349	3.2725	42.086
10-5	2.1937	25.564	2.3687	31.443
15-5	2.4164	29.259	2.5011	30.739
20-5	3.2763	57.301	5.3093	60.905
30-5	3.0395	49.095	2.7934	48.625
60-5	4.8892	54.074	6.3491	67.752
90-5	3.4479	52.107	2.5557	43.736

SPEC. NO.	ENGAMP ($100g^2s/Hz$)	INTFENG ($100g^2s$)	ENG1AMP ($100g^2s/Hz$)	INT1ENG ($100g^2s$)
0-6	3.5862	38.650	2.1441	30.407
3-6	3.8425	47.976	3.2134	53.067
6-6	5.0521	42.889	2.4395	28.270
10-6	4.2913	43.299	2.3994	38.307
15-6	2.7368	50.413	2.1083	46.415
20-6	5.1415	51.474	4.2868	52.044
30-6	7.8249	99.285	7.0703	94.685
60-6	6.9644	71.493	6.9559	69.441
90-6	6.1996	69.700	5.0607	57.398
3-7	3.7124	32.768	1.6271	27.507
6-7	3.1598	28.773	2.4049	30.550
10-7	1.6703	30.510	3.6509	43.964
15-7	3.5359	42.380	2.1286	39.057
20-7	3.2887	57.741	3.5063	63.107
60-7	6.4070	68.851	6.6731	68.783
90-7	7.6182	81.425	9.9664	96.243

APPENDIX C

ENERGY SPECTRUM VALUES ENGAMP[1/], INTFENG[2/], ENG1AMP[3/] AND INT1ENG[4/] FOR GRAIN ANGLE-MOISTURE CONTENT STUDY SPECIMENS

[1/] ENGAMP - Maximum amplitude of the energy spectral density function of the stress wave response in wood, measured at the front accelerometer.

[2/] INTFENG - Total energy content of the stress wave in the wood specimen, measured at the front accelerometer.

[3/] ENG1AMP - The ENGAMP value, except measured at the back accelerometer using accelerometer arrangement one.

[4/] INT1ENG - Total energy content of the stress wave in the wood specimen, measured at the back accelerometer using accelerometer arrangement one.

APPENDIX D

ENERGY SPECTRUM VALUES ENG2AMP[1/], INT2ENG[2/], ENGINP[3/] AND ENGINT[4/] FOR GRAIN ANGLE-MOISTURE STUDY SPECIMENS

1/ ENG2AMP - Maximum amplitude of the energy spectral density function of stress wave measured at the back accelerometer using accelerometer arrangement two.

2/ INT2ENG - Total energy content of the stress wave measured at the back accelerometer using accelerometer arrangement two.

3/ ENGINP - Maximum amplitude of the energy spectral density function of the impact to the wood specimen.

4/ ENGINT - Total energy content of the impact to the wood.

SPEC. NO.	ENG2AMP ($100g^2Hz$)	INT2ENG ($100g^2s$)	ENGINP ($100g^2/Hz$)	ENGINT ($110g^2s$)
0-1	3.2420	38.193	1.9346	82.291
3-1	1.9120	60.177	3.5957	140.010
6-1	1.6630	41.606	3.7040	131.460
15-1	3.4487	58.763	3.8345	138.890
20-1	3.4345	70.242	4.4999	157.600
30-1	5.2366	79.928	4.3743	146.940
90-1	6.9721	92.659	3.4783	116.210
0-2	1.4117	26.591	2.3714	80.237
3-2	1.9903	31.895	2.3969	76.896
6-2	1.9757	23.937	2.0261	63.690
10-2	1.6113	37.859	2.7049	89.828
15-2	1.8001	30.073	2.3623	77.713
20-2	2.3639	35.956	2.5278	77.118
30-2	4.6077	59.416	2.2731	75.089
60-2	3.8835	38.208	1.7043	43.655
90-2	3.1754	39.651	1.5095	51.658
0-3	2.4029	32.761	2.7012	80.101
3-3	4.2799	47.337	3.4584	102.540
6-3	1.5252	25.856	2.4530	80.418
10-3	1.9864	29.083	2.5282	78.938
15-3	2.1303	32.837	2.4705	80.260
20-3	3.5613	50.333	2.2228	73.495
30-3	4.1685	63.023	2.4599	77.781
60-3	2.9738	39.551	1.7389	52.803
90-3	2.9089	35.858	1.6511	48.101
0-4	3.3755	41.565	2.6006	94.908
3-4	4.0383	46.493	2.8749	93.222
6-4	3.4158	34.721	2.2531	77.507
10-4	2.8738	30.995	2.3862	63.686
15-4	3.6166	36.678	2.4852	68.438
20-4	3.6277	55.862	2.8118	76.572
30-4	2.9224	53.383	2.2293	67.847
60-4	3.7041	43.976	1.5315	57.533
90-4	5.1606	54.981	1.6702	61.668
0-5	2.9101	44.483	2.9008	85.003
3-5	3.4429	44.193	2.9416	92.189
10-5	2.2633	31.135	3.5423	80.868
15-5	2.2961	30.679	2.3276	65.681
20-5	5.3596	61.871	2.3712	82.329
30-5	2.7620	48.351	2.4180	70.768
60-5	5.7497	57.106	2.2895	57.037
90-5	2.4127	40.188	1.6457	54.840

SPEC. NO.	ENG2AMP ($100g^2Hz$)	INT2ENG ($100g^2s$)	ENGINP ($100g^2/Hz$)	ENGINT ($110g^2s$)
0-6	2.2082	30.698	2.3154	68.960
3-6	3.3251	52.646	3.5298	116.050
6-6	2.3407	28.480	2.2113	59.358
10-6	2.3550	40.300	2.4031	79.928
15-6	2.0210	45.370	2.5148	88.551
20-6	4.3716	51.531	3.6777	101.270
30-6	7.1473	95.501	3.1289	99.644
60-6	7.1361	71.148	1.9825	62.775
90-6	5.1584	58.591	1.8958	66.605
3-7	1.6489	28.295	2.2418	65.666
6-7	2.4939	32.503	2.3839	76.382
10-7	3.5824	40.162	2.5340	83.385
15-7	2.2222	45.517	2.5828	87.265
20-7	3.5470	65.803	2.5690	91.937
60-7	6.5861	67.852	1.9382	58.443
90-7	9.8314	95.798	2.3103	77.427

APPENDIX E

ENERGY SPECTRUM VALUES ENGINPD[1/], ENGIND[2/], ENGINTPD[3/], AND ENGINTD[4/] FOR DECAY STUDY SPECIMENS

Specimen Number Notation: xoo

x = nominal grain angle in tens of degrees
oo = sequence number

[1/] ENGINPD - The maximum value of the energy spectral density function of the impact to the wood specimen before exposure to decay.

[2/] ENGIND - The maximum value of the energy spectral density function of the impact to the wood specimen after exposure to decay.

[3/] ENGINTPD - Total energy content of the impact to the specimen before exposure to decay..

[4/] ENGINTD - Total energy content of the impact to the specimen after exposure to decay.

SPEC. NO.	ENGINPD ($100g^2/Hz$)	ENGIND ($100g^2s/Hz$)	ENGINTPD ($100g^2s$)	ENGINTD ($100g^2s$)
001	26.2	ND*	34.3	ND
002	22.2	ND	30.6	ND
003	7.6	10.2	8.1	9.4
004	13.6	15.8	20.0	11.8
005	11.2	17.0	11.1	21.3
006	10.4	15.4	12.4	12.7
007	12.6	20.1	19.0	18.1
008	12.0	32.4	18.5	21.7
009	15.6	17.7	17.2	13.2
010	11.2	14.8	15.1	10.8
011	13.3	21.1	19.3	16.1
012	15.4	15.8	22.7	16.0
013	16.9	14.6	18.3	15.0
014	12.4	7.0	13.8	8.9
015	8.8	7.5	11.9	8.8
016	7.9	11.3	7.6	11.1
017	7.3	10.8	8.4	10.1
018	13.6	15.2	20.7	16.0
019	12.3	9.1	17.7	9.0
020	15.5	14.8	18.6	14.1
201	21.2	ND	28.3	ND
202	10.2	18.3	14.0	19.0
204	11.8	24.0	15.7	29.7
205	11.6	19.0	12.1	12.4
206	12.0	52.8	16.8	29.9
207	14.6	15.3	16.2	12.4
208	11.9	10.1	14.3	9.3
209	15.0	9.0	14.7	10.3
210	5.7	6.5	8.4	8.2
211	11.4	12.2	14.4	11.1
212	10.4	10.3	12.4	10.7
213	12.0	9.6	16.4	9.2
901	10.7	ND	12.1	ND
902	10.3	ND	12.6	ND
903	8.0	10.5	7.8	10.1
905	6.5	11.9	8.7	13.7
906	10.4	6.5	8.6	4.8
907	10.2	17.6	10.3	12.3
908	6.7	21.1	7.9	14.3
909	8.8	6.4	8.5	4.9
910	9.9	8.3	11.7	4.6
911	5.6	7.7	7.1	6.9
912	7.1	6.8	8.8	5.3
913	8.8	3.6	6.9	4.0
915	7.0	5.1	7.5	4.5
917	6.6	7.2	7.9	4.6
918	10.0	4.5	9.1	4.4
919	8.3	7.2	9.9	5.1

*ND - Not exposed to decay.

APPENDIX F

ENERGY SPECTRUM VALUES ENGAMPPD[1/], ENGAMPD[2/], INTENGPD[3/], AND INTENGD[4/] DECAY STUDY SPECIMENS

[1/] ENGAMPD - Maximum amplitude of the energy spectral density function of the stress wave in the wood specimen before exposure to decay.

[2/] ENGAMPD - Maximum amplitude of the energy spectral density function of the stress wave in the wood specimen after exposure to decay.

[3/] INTENGPD - Total energy content of the stress wave in the wood specimen before exposure to decay.

[4/] INTNEGD - Total energy content of the stress wave in the wood specimen after exposure to decay.

SPEC. NO.	ENGINPD ($100g^2/Hz$)	ENGIND ($100g^2s/Hz$)	ENGINTPD ($100g^2s$)	ENGINTD ($100g^2s$)
001	7.7	ND*	2.4	ND
002	9.6	ND	2.3	ND
003	2.8	9.3	0.7	1.4
004	16.6	7.8	2.8	1.3
005	10.9	5.5	1.3	2.3
006	8.6	9.0	1.2	1.4
007	16.1	8.4	2.6	1.7
008	4.6	11.5	1.4	1.9
009	20.0	6.4	2.2	1.2
010	22.8	8.4	2.7	2.7
011	20.5	5.1	2.8	1.1
012	6.5	6.5	1.6	1.4
013	5.9	2.3	1.5	1.0
014	15.0	4.0	1.8	1.0
015	8.9	4.5	1.5	0.8
016	6.2	2.9	0.8	0.8
017	5.6	11.0	0.9	1.4
018	11.5	14.3	2.2	2.3
019	2.9	6.3	1.4	1.0
020	18.7	16.6	2.5	1.7
201	38.2	ND	9.2	ND
202	8.6	11.8	3.1	4.2
204	18.3	23.2	4.7	8.0
205	4.8	20.9	1.8	4.4
206	9.9	26.1	3.6	6.9
207	28.3	8.1	6.5	1.8
208	15.3	9.7	3.0	1.9
209	8.4	4.6	1.7	1.9
210	5.0	2.7	1.4	1.3
211	10.2	13.0	3.1	3.4
212	23.1	10.2	3.0	2.6
213	15.3	5.4	4.4	1.6
901	35.4	ND	6.2	ND
902	59.0	ND	7.4	ND
903	34.9	46.5	6.0	6.3
905	16.3	90.2	2.9	8.3
906	25.2	17.2	3.1	2.4
907	18.9	21.7	3.2	4.0
908	23.5	38.9	3.6	5.9
909	16.6	7.2	2.8	1.6
910	42.2	13.2	4.4	1.6
911	11.1	22.7	3.5	3.9
912	28.3	17.5	5.5	2.6
913	12.1	9.9	2.2	1.9
915	15.1	16.4	2.0	2.1
917	28.0	10.9	4.3	1.6
918	20.3	8.7	3.7	1.3
919	25.8	7.6	3.8	1.2

*ND - Not exposed to decay.

APPENDIX G

FREQUENCY RESPONSE FUNCTION VALUES FRFREQ[1/] AND FRINT[2/] FOR DECAY STUDY SPECIMENS AFTER EXPOSURE TO DECAY

[1/] FRFREQ - Frequency at which the amplitude response function reaches a maximum value.

[2/] FRINT - Maximum value of the integrated amplitude response spectrum.

SPEC. NO.	FRFREQ (Hz)	FRINT (unitless)
001	4100.0	1580.6
002	3825.0	1312.6
003	5000.0	1267.6
004	4100.0	1517.6
005	3225.0	1129.5
006	4275.0	1733.6
007	3875.0	1464.0
008	4300.0	1486.2
009	3975.0	1510.0
010	3050.0	1192.4
011	3975.0	1500.2
012	3675.0	1373.7
013	4375.0	1503.6
014	5000.0	1575.1
015	475.0	1368.5
016	450.0	1512.2
017	350.0	1121.9
018	4375.0	1576.1
019	3700.0	1219.1
020	4500.0	1509.2
201	2500.0	1103.6
202	2600.0	1089.5
203	350.0	807.1
204	2525.0	1082.2
205	2700.0	1385.2
206	3075.0	1367.0
207	2550.0	1166.2
208	3125.0	1449.3
209	2600.0	1254.2
210	2425.0	1218.9
211	2525.0	1041.1
212	2550.0	1341.2
213	2425.0	1804.2
901	800.0	285.5
902	775.0	304.6
903	1375.0	386.7
905	775.0	287.6
906	1525.0	466.5
907	5000.0	392.5
908	775.0	265.8
909	1875.0	272.2
910	800.0	414.7
911	1425.0	286.9
912	5000.0	516.5
913	1425.0	489.1
915	800.0	272.4
917	1475.0	307.6
918	750.0	307.6
919	3125.0	403.3

APPENDIX H

SUMMARY OF MATERIAL PROPERTIES FOR GRAIN ANGLE-MOISTURE CONTENT STUDY SPECIMENS

SPEC. NO.	SG	GRAIN ANGLE (deg)	MC (%)	MOE (ksi)	MOR (psi)	COMMENTS
00-1	0.42	3	91	1260	6590	
00-2	0.37	2	63	1260	6040	
00-3	0.43	2	34	1260	6360	
00-4	0.43	3	22	1530	8250	
00-5	0.38	3	26	1210	6650	
00-6	0.42	4	16	1310	9380	
00-7	0.39	3	7	1730	12590	INVALID NDE
03-1	0.39	4	82	1200	6160	
03-2	0.38	3	49	1310	6190	
03-3	0.45	4	17	1580	8790	
03-4	0.37	3	30	1270	5910	
03-5	0.45	4	26	1380	7400	
03-6	0.43	4	16	1660	10500	
03-7	0.37	2	7	1570	12320	
06-1	0.42	7	166	1290	6440	
06-2	0.41	8	37	1150	5920	
06-3	0.46	8	19	1610	10130	
06-4	0.43	6	19	135	8550	
06-5	0.43	6	17	1670	9700	INVALID NDE
06-6	0.43	8	15	1890	10020	
06-7	0.45	7	7	1650	12290	
10-1	0.40	14	100	910	5030	
10-2	0.41	11	41	800	5910	
10-3	0.40	12	30	950	6010	
10-4	0.40	10	23	910	5680	
10-5	0.44	10	16	1240	8320	
10-6	0.43	13	16	930	6420	
10-7	0.42	12	7	1140	7330	
15-1	0.43	15	86	660	4500	
15-2	0.40	14	48	650	4660	
15-3	0.40	11	27	820	6080	
15-4	0.43	14	18	790	5840	
15-5	0.41	12	20	930	6690	
15-6	0.42	14	16	810	6010	
15-7	0.45	14	7	930	6280	

SPEC. NO.	SG	GRAIN ANGLE (deg)	MC (%)	MOE (ksi)	MOR (psi)	COMMENTS
20-1	0.42	20	113	600	4440	
20-2	0.42	18	32	500	4120	
20-3	0.40	20	23	400	3520	
20-4	0.41	21	20	410	3530	
20-5	0.42	21	17	350	3560	
20-6	0.41	18	16	710	5065	
20-7	0.42	19	7	730	5350	
30-1	0.40	31	166	210	2090	
30-2	0.40	29	52	150	2650	
30-3	0.38	29	30	170	2140	
30-4	0.40	28	24	210	2250	
30-5	0.38	28	27	190	2300	
30-6	0.40	28	15	290	3180	
30-7	0.40	27	7	360	3420	INVALID NDE
60-1	0.40	61	164	40	730	INVALID NDE
60-2	0.38	63	49	40	570	
60-3	0.39	62	32	30	310	
60-4	0.40	62	22	30	430	
60-5	0.42	59	15	60	960	
60-6	0.40	61	15	60	1140	
60-7	0.42	63	7	70	590	
90-1	0.40	89	160	30	530	
90-2	0.40	88	44	20	510	
90-3	0.41	88	25	30	490	
90-4	0.41	88	21	30	550	
90-5	0.43	88	17	30	740	
90-6	0.34	88	15	30	600	
90-7	0.41	90	7	50	1000	

APPENDIX I

SUMMARY OF MATERIAL PROPERTIES FOR DECAY STUDY SPECIMENS

SPEC. NO.	SG	GRAIN ANGLE (deg)	MC (%)	MOE (ksi)	MOR (psi)	Wt. LOSS (%)	COMMENTS
001	0.55	2	88	2550	11210	ND*	
002	0.55	3	91	2610	12320	ND	
003	0.55	5	69	2330	10320	4	
004	0.54	5	68	2170	9420	4	
005	0.54	3	70	2220	11450	1	
006	0.54	2	67	2090	10610	1	
007	0.53	2	81	1910	10650	3	
008	0.52	2	84	1130	9630	3	
009	0.54	2	63	2450	11180	1	
010	0.54	2	62	2170	10900	1	
011	0.53	3	95	1760	9720	WG**	
012	0.54	2	87	2190	10040	WG	
013	0.54	3	78	1910	9570	WG	
014	0.54	3	65	2210	10020	WG	
015	0.52	2	88	2190	9970	0	
016	0.53	2	84	1880	10170	WG	
017	0.53	2	71	2240	10780	WG	
018	0.54	2	64	2120	10680	WG	
019	0.53	2	103	2110	9340	WG	
020	0.54	4	94	1990	9580	WG	
201	0.54	18	96	640	4580	ND	
202	0.54	19	93	640	4430	4	
203	0.52	19	77	720	4710	5	
204	0.52	20	82	490	4950	WG	
205	0.52	18	67	520	4450	WG	
206	0.53	17	79	660	4840	WG	
207	0.53	19	76	830	5270	WG	
208	0.55	18	72	1580	8890	WG	
209	0.55	20	80	680	4360	WG	
210	0.54	18	85	520	4220	WG	
211	0.53	19	77	590	4570	3	
212	0.55	19	72	620	4300	2	
213	0.54	19	94	720	4330	2	
901	0.54	90	113	40	750	ND	
902	0.56	90	114	40	740	ND	
903	0.55	90	94	40	710	WG	
904							SPECIMEN BROKE
905	0.54	90	101	30	640	1	
906	0.53	90	98	30	660	1	
907	0.53	90	109	40	480	4	
908	0.52	90	105	20	425	4	
909	0.51	90	104	30	530	2	
910	0.51	90	107	30	510	2	
911	0.55	90	100	40	550	2	
912	0.54	90	103	40	530	2	
913	0.54	90	88	40	550	1	
914	0.53	90	99				SPECIMEN BROKE

* ND = not decayed
** WG = weight gained

SPEC. NO.	SG	GRAIN ANGLE (deg)	MC (%)	MOE (ksi)	MOR (psi)	Wt. LOSS (%)	COMMENTS
915	0.44	90	133	30	540	5	SAPWOOD
916							SPECIMEN BROKE
917	0.53	90	90	30	360	4	
918	0.52	90	93	20	250	4	
919	0.51	90	105	30	300	9	
920							SPECIMEN BROKE

APPENDIX J

REGRESSION ANALYSIS STATISTICS

Table J-1. Summary of parabolic regression statistics for prediction of moisture content at various grain angles.

Group Designation	Mean Grain Angle (degrees)	NDE Variable: TTIME r^2 (%)	TTIME SEE (%)	TTIME Significance* Level	FFREQ r^2 (%)	FFREQ SEE (%)	FFREQ Significance Level	FRINT r^2 (%)	FRINT SEE (%)	FRINT Significance Level
CGA1	2.6	37.4	24.8	N.S.	68.3	17.7	N.S.	74.1	16.0	5
CGA2	4.1	99.4	3.2	N.S.	99.0	4.1	2.5	95.8	8.3	N.S.
CGA3	7.2	98.4	10.0	0.5	98.5	9.4	0.5	99.4	6.3	0.1
CGA4	11.2	73.5	6.3	N.S.	32.5	10.1	N.S.	37.5	9.7	N.S.
CGA5	14.1	98.7	5.4	N.S.	56.1	31.1	N.S.	64.1	28.1	N.S.
CGA6	19.5	62.4	27.3	N.S.	22.8	39.1	N.S.	85.4	17.0	2.5
CGA7	28.9	90.3	16.2	N.S.	99.6	3.1	0.1	91.6	15.1	N.S.
CGA8	61.9	93.1	5.1	N.S.	58.7	12.5	N.S.	74.9	9.8	N.S.
CGA9	88.3	98.3	8.7	0.1	68.2	37.0	N.S.	88.6	22.2	2.5

*N.S. - Not significant at the 5 percent level.
5 - Significant at the 5 percent level.
2.5 - Significant at the 2.5 percent level.
0.5 - Significant at the 0.5 percent level.
0.1 - Significant at the 0.1 percent level.

Table J-2. Summary of regression statistics for prediction of MOR at various grain angles.

Group Designation	Mean Grain Angle (degrees)	NDE Parameters FRAMP		FRFREQ		FRINT		TTIME	
		r^2 (%)	SEE (psi)	r^2 (%)	SEE (psi)	r^2 (%)	SEE (psi)	r^2 (%)	SEE (psi)
CGA1	2.6	3.3	2295	6.1	2261	0.3	2330	22.9	2049
CGA2	4.1	39.2	1528	46.3	1437	58.7	1260	69.3	1086
CGA3	7.2	12.9	890	68.2	538	72.0	506	77.6	451
CGA4	11.2	0.8	2697	69.4	1497	51.2	1891	78.2	1264
CGA5	14.1	73.8	484	0.1	945	30.4	789	95.7	197
CGA6	19.5	1.3	825	41.3	634	35.2	669	41.1	637
CGA7	28.9	86.9	168	8.1	444	38.3	364	22.6	408
CGA8	61.9	52.7	245	59.1	228	53.8	243	33.5	291
CGA9	88.3	56.2	133	90.7	61	72.2	106	58.5	129

Table J-3. Summary of regression statistics for prediction of MOE at various grain angles.

Group Designation	Mean Grain Angle (degrees)	NDE Parameters FRAMP		FRFREQ		FRINT		TTIME	
		r^2 (%)	SEE (ksi)	r^2 (%)	SEE (ksi)	r^2 (%)	SEE (ksi)	r^2 (%)	SEE (ksi)
CGA1	2.6	0.1	148	7.7	142	1.9	146	19.6	132
CGA2	4.1	0.1	220	42.1	167	23.7	192	70.8	119
CGA3	7.2	0.2	214	50.5	151	31.0	178	47.0	156
CGA4	11.2	5.6	159	69.0	91	74.3	83	84.8	64
CGA5	14.1	46.7	98	0.3	134	13.2	125	77.8	63
CGA6	19.5	1.8	167	30.7	140	25.8	147	34.5	136
CGA7	28.9	38.4	43	11.2	51	47.0	39	31.9	45
CGA8	61.9	85.1	7.4	85.8	7.2	89.4	6	64.8	11
CGA9	88.3	60.8	6	79.4	4.5	66.5	6	47.7	7.1

Table J-4. Summary of measured MOE and E_d values obtained from Eq. 2.4 for all GAMC specimens.

Spec. No.	MOE (ksi)	E_d (ksi)	Spec. No.	MOE (ksi)	E_d (ksi)
00-1	1260	1022	20-1	600	418
00-2	1260	1385	20-2	500	464
00-3	1260	1081	20-3	400	557
00-4	1530	1380	20-4	410	434
00-5	1210	1219	20-5	350	496
00-6	1310	1399	20-6	710	701
00-7	1730	1725	20-7	730	758
03-1	1200	838	30-1	210	136
03-2	1310	1094	30-2	150	158
03-3	1580	1828	30-3	170	228
03-4	1270	1233	30-4	210	264
03-5	1380	1392	30-5	190	239
03-6	1660	1609	30-6	290	360
03-7	1570	1442	30-7	360	600
06-1	1290	646	60-1	40	21
06-2	1150	937	60-2	40	29
06-3	1610	1532	60-3	30	32
06-4	1350	1238	60-4	30	42
06-5	1670	1609	60-5	60	54
06-6	1390	1746	60-6	60	51
06-7	1650	2175	60-7	70	61
10-1	910	473	90-1	30	19
10-2	800	740	90-2	20	27
10-3	950	809	90-3	30	36
10-4	910	834	90-4	30	33
10-5	1240	1787	90-5	30	41
10-6	930	924	90-6	30	33
10-7	1140	1706	90-7	50	70
15-1	660	497			
15-2	650	570			
15-3	820	886			
15-4	790	982			
15-5	930	830			
15-6	810	1022			
15-7	930	1132			

APPENDIX K

SUMMARY OF MEASURED AND PREDICTED MOR VALUES

Table K. Comparison of actual and predicted MOR values for GAMC specimens.

Spec. No.	MOR_{act} [1]	MOR_{pred1} [2]	MOR_{pred2} [3]	MOR_{pred3} [4]	MOR_{pred4} [5]	MOR_{pred5} [6]	MOR_{pred6} [7]	MOR_{pred7} [8]
00-1	6590	6255	6255	5043	5516	5735	6975	9454
00-2	6040	6362	6362	6111	6111	6450	8316	9730
00-3	6360	6362	5283	5283	5283	6255	7081	7195
00-4	8250	7247	6111	6639	6111	6383	7852	7140
00-5	6650	6255	5043	5735	5936	5936	7852	6809
00-6	9380	8824	7429	8565	7249	8269	7966	6809
03-1	6160	6111	3657	4800	5283	2763	6561	4549
03-2	6190	6255	5283	5516	5735	5735	7516	7084
03-3	8790	8506	6991	8506	7330	4762	8554	6699
03-4	5910	6255	5043	5936	5739	6255	7966	6974
03-5	7400	6111	5283	5735	5936	5936	7739	7525
03-6	10500	8824	7602	8824	7602	7945	8316	7360
03-7	12320	12813	10548	12283	10049	10548	8434	7140
06-1	6440	5516	3456	3657	4800	2234	5415	4384
06-2	5920	5283	5043	4800	5043	4800	6766	6478
06-3	10130	6816	6816	7673	6814	6816	7966	7470
06-4	8550	7409	6816	7121	6501	6816	7416	7305
06-6	10020	7884	7517	9155	7884	7517	8554	6809
06-7	12290	11034	12586	12813	10548	11034	9044	9454
10-2	5910	4558	4800	4320	5043	5735	5971	6092
10-3	6010	4320	5043	4558	4800	4800	6360	6258
10-4	5680	5350	5623	5079	5079	6154	6460	6699
10-5	8320	6892	7945	8824	7602	6892	8554	8462
10-6	6420	5856	6538	6892	5856	3935	6561	5652
10-7	7330	8560	10548	12283	10049	8560	8554	7856
15-1	4500	3657	5043	2920	4090	6255	4405	6533
15-2	4660	3868	4800	3456	4558	5283	5150	5817
15-3	6080	4558	5043	4800	5043	5743	6663	6809
15-4	5840	5151	7959	6411	6083	5962	6766	9069
15-5	6690	5361	6269	5659	5161	6866	6360	6699
15-6	6010	5533	6192	7249	6192	7249	6975	5100
15-7	6280	7637	9546	10548	8088	7207	7081	5817

Table K. Comparison of actual and predicted MOR values for GAMC specimens (continued).

Spec. No.	MOR_{act} [1]	MOR_{pred1} [2]	MOR_{pred2} [3]	MOR_{pred3} [4]	MOR_{pred4} [5]	MOR_{pred5} [6]	MOR_{pred6} [7]	MOR_{pred7} [8]
20-1	4440	2763	3088	2617	3657	4800	3876	4053
20-2	4120	3088	3088	2920	3457	3456	4249	4108
20-3	3520	3073	3846	3846	3846	4070	5063	4329
20-4	3530	3234	3416	3416	3611	3611	4097	3833
20-5	3560	3798	5639	4249	4016	4498	4484	4935
20-6	5065	4595	6538	5856	5226	6192	5781	5541
20-7	5350	5722	8560	8560	6417	8560	5971	5211
30-1	2090	1602	5043	1023	1675	1023	681	6368
30-2	2650	1753	1129	1169	1836	1413	1006	2290
30-3	2140	1753	1472	1675	2234	1535	2167	2731
30-4	2250	1969	2065	1969	2168	1796	2481	3171
30-5	2300	1836	1836	1836	2353	1753	2321	3061
30-6	3180	2697	3465	3465	3654	3465	3524	3557
60-2	570	642	545	532	559	576	1084	691
60-3	310	652	538	538	542	559	1039	636
60-4	430	749	626	648	636	621	670	691
60-5	960	1005	937	872	884	923	385	1187
60-6	1140	969	872	872	884	896	405	1022
90-1	530	520	522	520	520	532	242	1077
90-2	510	521	525	527	542	538	-389	416
90-3	490	539	548	564	548	542	1073	471
90-4	550	618	632	635	619	625	939	526
90-5	740	710	743	755	738	714	1054	581
90-6	600	760	796	809	791	781	842	691
90-7	1000	1000	1197	1300	1097	1035	814	691
							123	1132

[1] MOR_{act} - MOR value of specimen determine from destructive flexure test.

[2] MOR_{pred1} - Predicted MOR value of specimen utilizing Hankinson's formula, Eq. 2.7, and moisture content correction, Eq. 7.1. Specimen grain angle and moisture content values used are measured.

[3] MOR_{pred2} - Predicted MOR value of specimen utilizing Hankinson's formula, Eq. 2.7, and moisture content content correction, Eq. 7.1. Specimen grain angle was predicted using Eq. 6.3. Measured moisture content was used.

[4] MOR_{pred3} - Predicted MOR value of specimen utilizing Hankinson's formula, Eq. 2.7, and moisture content correction, Eq. 7.1. Specimen grain angle was predicted using Eq. 6.4. Measured moisture content was used.

[5] MOR_{pred4} - Predicted MOR value of specimen utilizing Hankinson's formula, Eq. 2.7, and moisture content correction, Eq. 7.1. Measured moisture content was used. Based on the moisture content, the appropriate equation in Table 7.2 involving NDE variable TTIME was used to predict specimen grain angle.

[6] MOR_{pred5} - Predicted MOR value of specimen utilizing Hankinson's formula, Eq. 2.7, and moisture content correction, Eq. 7.1. Measured moisture content was used. Based on the moisture content, the appropriate equation in Table 7.2 involving the NDE variable FRINT was used to predict specimen grain angle.

[7] MOR_{pred6} - Predicted MOR value of specimen using Eq. 6.5 and the NDE varible FRFREQ.

[8] MOR_{pred7} - Predicted MOR value of specimen using Eq. 6.7 and the NDE variable TTIME.